ULTRA-FAST PHOTON AND ELECTRON BEAM DIAGNOSTICS FOR FREE ELECTRON LASERS

Xiaoling Yan

A thesis submitted in partial fulfilment of
the requirements of the University of
Abertay Dundee for the degree of
Doctor of Philosophy

16 June 2003

ULTRA-FAST PHOTON AND ELECTRON BEAM DIAGNOSTICS FOR FREE ELECTRON LASERS

Xiaoling Yan

A thesis submitted in partial fulfilment of the requirements of
the University of Abertay Dundee for the degree of
Doctor of Philosophy

This research programme was carried out in collaboration with
the FOM Instituut voor Plasmafysica "Rijnhuizen",
3430 BE Nieuwegein, The Netherlands.

16 June 2003

I certify that this thesis is a true and accurate version of the thesis approved by the external examiners.

Signe[redacted] Date....7-7-03.....

Declaration

I hereby declare that while registered as a candidate for the degree for which this thesis is presented I have not been a candidate for any other award. I further declare that, except where stated, the work in this thesis is original and was performed by myself.

Signed..  ..(Xiaoling Yan) Date..16-06-2003

Acknowledgements

To acknowledge everyone who contributed to this thesis in some manner is clearly impossible, but a major debt is owed my supervisors Prof. Dr. Allan Gillespie and Dr. Allan MacLeod. I want to thank them not only for advice and encouragement throughout this period but also for getting me interested in Optics and Free Electron Lasers in the first place.

Although I was a student at a UK university, I spent most of my time working at a laboratory in The Netherlands – the FOM Instituut voor Plasmafysica, "Rijnhuizen" at Nieuwegein – and I had the great opportunity to work with many excellent scientists at the FELIX facility there, namely Dr. Lex van der Meer, Dr. Dick Oepts and Dr Guido Knippels. They helped me invaluably in analysing results, understanding the physics and planning further experiments. In particular I must single out Guido, who was acting as a daily supervisor while I was working at FELIX. I also want to thank the technicians at FELIX group. Their friendly and co-operative spirit made my visiting at FOM "Rijnhuizen" a lot of pleasure.

Finally, my husband, Tielun, offered encouragement and exercised great patience throughout my study. So also did other family members: my parents and parents-in-law, brothers and sisters. I would like to thank my father and mother for their continuing support and appreciation of the choices that I have made. To all these wonderful people I am pleased to express my gratitude.

Abstract

Characterisation of the ultra-short optical pulses produced by infrared free-electron lasers (FELs) is an important task, not only for the further development of free electron lasers and their theory, but also for their operation as a research tool. The setting up and optimisation of the FEL requires effective and reliable diagnostics tools. This thesis presents techniques for the measurement of sub-picosecond optical and electron pulses. A range of techniques is developed that allows measurements of the electric field of both optical pulses and electron bunches to be made with an accuracy of better than 100 fs. These techniques have been used to obtain the first complete electric-field characterisation of ultra-short pulses from a far-infrared FEL; to study the formation of single-sided exponential optical pulses in two FELs; and to obtain the longitudinal profile of electron bunches, both by probing the near-field transition radiation and by directly sensing the Coulomb field of the electron bunches.

Although the techniques described are not truly single-shot – requiring measurements averaged over a period of a few microseconds – ways in which they could be extended to provide single-shot capability are discussed.

Chapter 1 General Introduction

1.1 Introduction

The free-electron laser (FEL) is a special member of the laser family, in which coherent radiation is produced as a result of oscillation of free electrons, instead of electrons that are bound in atoms, molecules or crystal. Madey and his co-workers at Stanford university demonstrated the first operation of a FEL in 1975 [1][2]. In the following twenty or so years, FELs have been proved to be valuable and versatile scientific tools, by virtue of their continuous and easily tuneable wavelength range, high optical power and short pulses. The first FEL user facility in Europe was the Free-Electron Laser for Infra-red eXperiments, FELIX [3], at Nieuwegein in The Netherlands, followed closely by the Collaboration pour un Laser Infrarouge à Orsay, CLIO, at the Université de Paris Sud. User facilities in the USA include the free electron laser at the Jefferson laboratory (JLab) and the Stanford Picosecond FEL Centre etc. A comprehensive survey of present facilities is given in references [4] and [5]. Appendix 1 summarises these data, showing operational FEL (user) facilities with the wavelength ranges accessible at each at the time of writing.

In this chapter, the basic principles of operation of a free-electron laser (FEL) are introduced in sufficient depth, in order to serve as a background for understanding the remainder of the thesis. Section 1.2 describes the amplification mechanism. Section 1.3 covers the short pulse effects that are very important in FELs operating with large slippage. Since the thesis is mainly concerned with results taken at FELIX facility, an FEL that operates in the large slippage regime, a brief description of the FELIX facility is presented in section 1.4, including the layout and the general performance. The ultra-fast high time-resolution diagnostic of the longitudinal profile of the FEL pulse and electron beam is central to this thesis. An outline of the work covered in the remainder of the thesis is given in section 1.5.

1.2 FEL principles

The principle of free-electron laser is based on the interaction between a relativistic electron beam and a spatially periodic magnetic field, the so-called undulator. The undulator may comprise an array of permanent magnets of alternating polarity – a planar undulator – or may, as is frequently the case in a helical undulator, be provided by currents in suitably constructed coils. A typical planar undulator configuration is illustrated in

Figure 1-1. In the undulator, the electrons perform a transverse wiggling motion in one plane due to the Lorentz force. The acceleration associated with this motion causes the electrons to emit dipole radiation, which is essentially synchrotron radiation. However, the presence of the spatially periodic magnetic field of the undulator narrows the broadband spectrum of the radiation significantly. The resonance condition may be expressed in terms of the radiation wavelength, λ_0, the electron energy, γmc^2, and the undulator parameters as

$$\lambda_0 = \frac{\lambda_u}{2\gamma^2}(1+K^2) \qquad \textbf{Equation 1-1}$$

where λ_u is the period of the undulator field and K is a dimensionless parameter proportional to the magnetic field amplitude. Typically K is of the order of unity and $\gamma^2 >> 1$ for the highly relativistic electron beam. The spectrum width of the spontaneous emission is determined by the number N_u of the undulator periods: $\Delta\lambda/\lambda = 1/N_u$. This spontaneous emission is captured in an optical resonator, and the stored optical field induces newly injected electrons to radiate coherently. In this way, high-power laser output is produced.

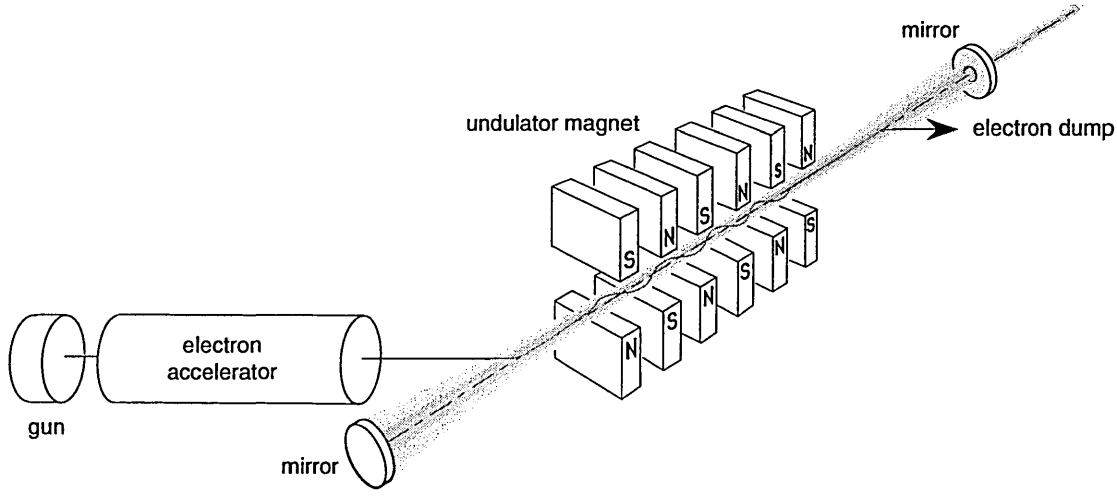

Figure 1-1 *Schematic layout of the FEL oscillator. A relativistic electron beam is injected into a spatially periodic magnetic field produced in the undulator. The magnetic field forces the electrons to perform a 'wiggling' motion that causes the electrons to radiate. This radiation is captured in an optical cavity and amplified on successive passes through the undulator in the presence of the gain medium of freshly injected electrons [4, 6].*

The gain mechanism can be understood by transforming to the rest frame of the electrons [7]. The undulator field transforms in this frame into electromagnetic wave propagating towards the electrons, and gives

rise to a Compton-backscattered wave that appears in the laboratory frame with a Doppler upshift. In the electron frame, the scattered wave and the original undulator wave combine to form a standing wave pattern. Enhanced stimulated scattering occurs due to the formation of a density grating in the electron distribution under the influence of the ponderomotive force associated with this standing wave. Actually the wavelength of the resulting radiation is slightly larger than the resonance wavelength given in equation 1-1. In the so-called low-gain Compton regime, the gain is proportional to the current of the electron beam. At higher currents the gain increases nonlinearly. The latter regime is often attained at relatively low electron energies, corresponding to wavelengths in the sub-millimeter region.

As seen from equation 1-1, the wavelength is determined by macroscopic parameters, rather than by microscopic properties of the gain medium. This striking difference with other lasers has the consequence that an FEL can in principle be operated at any wavelength by a suitable choice of the parameters in equation 1-1. Another useful feature of FEL is the high output power that is possible because the electron beam can carry high power without dissipating unused energy in the laser cavity.

1.3 Short pulse effects

This section introduces concepts and mechanisms that are particularly important for FELs, such as FELIX, that operate with a combination of short electron bunch lengths and long optical wavelengths. FELIX was the first FEL to be operated under these conditions and two new modes of operation have been observed as a consequence: the so-called limit-cycle regime [8] [9] and the superradiant regime [10].

Most FELs that operate in the infrared part of the spectrum use a RF-linac to provide the electron beam. RF-linac produces a pulsed electron beam, consisting of electron bunches with a typical duration of a few picoseconds. These bunches are produced at the frequency of the accelerating potential which may typically be in the range from 10 MHz to several GHz. Furthermore, few RF-linacs can operate continuously so that the electron bunches are produced in bursts lasting for a few tens of microseconds. The resulting optical radiation exhibits the same structure: the picosecond-long optical pulses are called *micropulses* and the train of micropulses is called a *macropulse* (see Figure 1-2). Super-conducting RF-linac can, however, provide an almost continuous train of micropulses – i.e. CW operation.

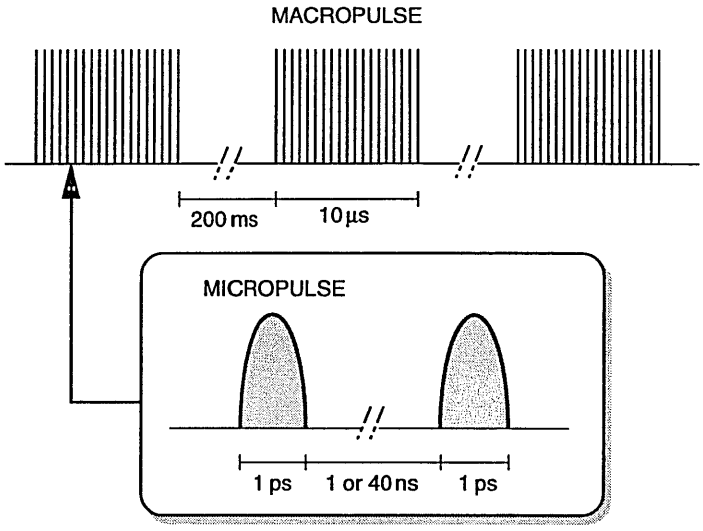

Figure 1-2 *Typical time structure of the electron beam provided by the RF-linac at FELIX. The optical pulse structure is basically the same as the electron beam pulse structure.*

1.3.1 Slippage

Whether an electron pulse is considered short depends on the scale with which the length is measured. The slippage distance L_s gives the most important length scale in relation to short-pulse effects. Slippage refers to the fact that the electrons fall behind the optical field that they generate, because their velocity must be less than the speed of light and because the electrons follow an undulating path. The distance that the electrons slip behind the radiation is constrained by the resonance condition (Eq. 1-1) to be one radiation wavelength in the time taken to traverse one undulator period. In each undulator period the radiation moves ahead of the electrons by one radiation wavelength, so that on an undulator of N_u periods the slippage length will be given by $L_s = N_u \lambda$. The phenomenon of slippage has the consequence that each individual electron interacts with a portion of the radiation field of length L_s; while each position in the propagating field is in turn influenced by electrons in a length L_s of the electron beam.

The ratio of the slippage length to the electron bunch length σ_e - which is the variance associated with the longitudinal electron distribution – is known as the slippage parameter, or longitudinal coupling parameter $\mu_c = N_u \lambda / \sigma_e$ and is a measure of the importance of short pulse effects. When $\mu_c < 1$, a large part of the optical pulse develops as if the electron beam were continuous. Only at the beginning and end of the optical pulse are there regions where electrons and radiation are not in contact for the entire transit through the

undulator: the front of the optical pulse interacts with electrons only at the beginning of the undulator, before the radiation escapes the electrons due to slippage; and the rear of the optical pulse is produced by the electrons at the rear of the electron bunch as they near the end of the undulator. As soon as the slippage length becomes comparable with the electron bunch length, transient effects at the beginning and end of the pulses can become important.

The slippage length is not always the most appropriate parameter to use to characterise short pulse effects. For example, in a high-gain single-pass device the radiation field reaches saturation before the end of the undulator and therefore the full slippage length is not an appropriate parameter to use. In that case the co-operation length [11] is an appropriate parameter. In a low-gain oscillator configuration, such as at FELIX, the optical pulses are stored in a resonator or cavity formed by mirrors at either end of the undulator, and amplified by fresh electron pulses on successive round trips in the cavity. In this case the end effects can accumulate and become observable even in cases where the slippage length is considerably less than the bunch length. Co-operation length is also an important concept when considering the evolution of short, superradiant optical pulses in a free-electron laser oscillator [10][12].

1.3.2 Lethargy

The effect of short electron pulses on the gain in successive round trips is illustrated qualitatively in Figure 1-3, which shows the relative positions of the electron and optical pulses at the entrance and exit of the undulator for three successive round trips. At the top of the figure an electron pulse and an optical pulse are shown at the entrance to the undulator. As they pass through the undulator, the optical pulse advances by the slippage length relative to the electron pulse and, at the same time experiences gain. Note that the leading part of the optical pulse shows relatively little gain because it loses contact with the electrons in the first part of the undulator. This effect is not simply due to slippage. In an FEL the gain depends strongly on the position in the undulator. In the first part of the undulator, the electrons are bunched under the influence of the radiation field, with little contribution to the gain. Towards the end of the undulator, the bunched electrons effectively emit radiation, which adds coherently to the stored radiation field in the optical cavity. This position-dependent gain results in the optical pulse growing mainly at its trailing edge while its leading edge loses contact with the electrons and experiences no gain, thereby reducing the *group velocity* of the optical pulse. The simplified description of the effect of slippage given in the previous section is therefore no longer valid. Although the phase

of velocity of the optical wave still exceeds the electron speed, the envelope of the optical pulse is changed by the position-dependent gain regime such that its maximum slips back with respect to the electron pulse.

In the next round trip, shown in the middle part of the figure, the optical pulse at the entrance to the undulator is shown with a slightly reduced intensity because of cavity losses. As a result, in successive round trips, the front of the optical pulse decays more and more while a peak grows at the rear. Note, however, that the growth of the rear of the pulse is restricted because for most of the passage down the undulator the electrons are interacting with the low intensity field at the front of the pulse. This effect is known as laser lethargy and results in the pulse growing slowly or not at all [[13]]. Lethargy is important during the build up of the optical field but is not important when saturation has been reached: at saturation the rear of the pulse cannot grow because of the reduced gain and therefore the group velocity of the optical pulse returns to c and the optical pulse shape remains constant.

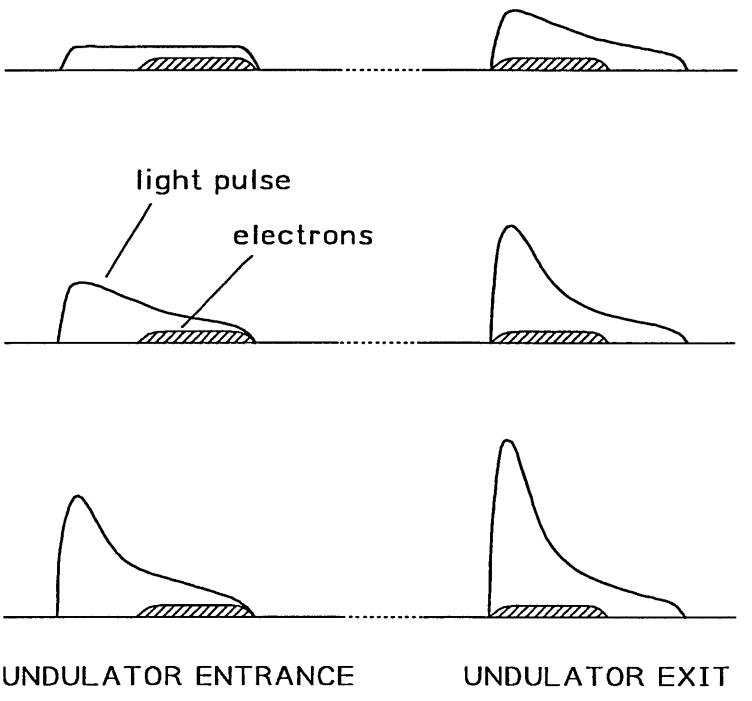

Figure 1-3 *Illustration of the effect of slippage on the growth of the optical pulse. The relative positions of an electron bunch and an optical pulse are shown at the entrance and exit of the undulator in a situation where the optical cavity has been adjusted for* ***perfect synchronism*** *between the circulating optical pulse and the newly arriving electron bunches. Successive round trips are shown from top to bottom. The leading part of the optical pulse does not grow because it interacts with the electrons only in the first part of the undulator where the gain is low because the electrons are not yet bunched.*

1.3.3 Cavity desynchronisation

The lack of gain at the leading edge of the optical pulse described in the previous section results in the slow build-up of optical power. This can be compensated by a slight shortening of the cavity length – usually termed cavity desynchronisation. Instead of arranging that the round trip time of the optical pulse exactly matches the repetition rate of the electron bunches—i.e. the optical round trip time is an integer multiple of the repetition rate, which is the case for a synchronised cavity—the cavity length is reduced by a small amount δL from its synchronous value. The optical pulse then arrives at the entrance of the undulator for its next round trip slightly ahead of the electron pulse, as illustrated in Figure 1-4. In successive round trips, the part of the optical pulse, which experienced little gain, is moved ahead of the electrons so that the electrons experience the larger optical field from the rear of the optical pulse at the beginning of the undulator. The optical pulse can then grow without the maximum shifting continuously backwards. The combination of a reduced group velocity and a shorter optical cavity leads to a effective synchronism between the optical and electron pulses, and the optical pulse can develop into a stable shape and grows uniformly to saturation.

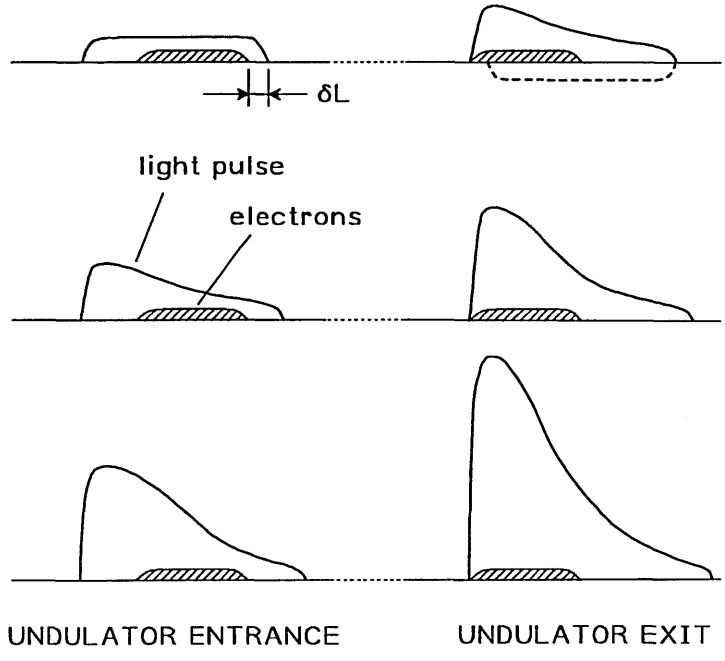

Figure 1-4 *Illustration of the effect of cavity desynchronism on the growth of the optical pulse. As previously, the relative positions of an electron bunch and an optical pulse are shown at the entrance and exit of the undulator and successive round trips are shown from top to bottom. The optical pulse can continue to grow without shifting backwards because the electron pulse experiences a higher optical field, producing efficient bunching, at the start of the undulator.*

1.4 The Free-Electron Laser for Infrared eXperiments (FELIX)

FELIX has been designed as a versatile source of radiation in the infrared and far-infrared spectral regions, for the applications by scientific users around the world. At the time of writing the wavelength range extends from 5 μm to 300 μm. To cover this range, the instrument comprises two branches working at different electron beam energies. The long wavelengths (16 μm – 300 μm) are provided by FEL-1, while the short wavelengths (5 μm – 35 μm) are covered by FEL-2. FEL-1, which was originally designed to lase in the range 16 μm – 110 μm, was upgraded in 1998 by the installation of a waveguide inside the undulator that extended its operating range to its present long-wavelength limit of 300 μm. A schematic layout of the machine is given in Figure 1-5.

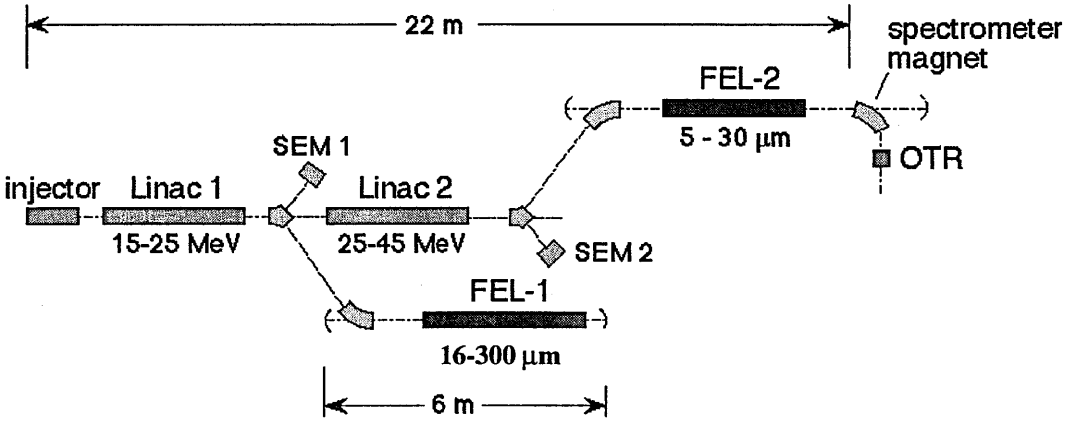

Figure 1-5. *The basic layout of the Free Electron Laser for Infrared eXperiments (FELIX). Two separate FEL sections are used to cover the wavelength range from 5-300 μm. The positions of the electron-beam diagnostics discussed in chapter 2 are indicated: SEM 1 and SEM 2 are secondary emission monitors and OTR is an optical transition radiation monitor.*

1.4.1 The electron beam

The electron beam injector consist of a thermionic triode electron gun, that is modulated at 1 GHz to generate electron bunches with 1 ns separation. The electron bunches contain approximately a total charge of 200 pC and are roughly 200 ps long. To inject these bunches into the 3-GHz travelling wave linear accelerator, the bunch duration is shortened by a 1-GHz pre-buncher and a 3-GHz buncher section. The 1-GHz pre-buncher

induces a velocity modulation on the electron bunch by the application of a rapidly varying electric field. The velocity modulation is such that the leading electrons slow down while the trailing electrons speed up. This velocity modulation results in a compressed bunch duration of about 40 ps at the end of the drift section between the pre-buncher and the buncher. In the 3-GHz buncher a similar procedure is applied in 14 separate RF cavities, resulting into the bunch duration of 6 ps that is desired for injection into the first linac. The electron energy at the entrance to linac-1 is roughly 3.8 MeV so that the bunches are no longer strongly influenced by space charge effects any more. These electrons are further accelerated in two 3-GHz travelling wave linear accelerators (linac-1 and linac-2) to energies of 14-25 MeV and 25-45 MeV respectively. Behind each linac, the electron beam can be bent into an FEL resonator, by using a chicane in the beam line. A chicane contains three quadrupole magnets between two dipoles. This bending section is close to achromatic but has a slight non-isochronicity of about 0.2 ps/%. Therefore the bunch length can be even further compressed in this section by applying an appropriate energy distribution for the bunch when it enters the chicane. Table 1-1 gives an overview of the electron beam parameters at FELIX.

***Table 1-1** Electron beam parameters at FELIX*

Beam energy	14 – 46 MeV
Energy spread (rms)	0.2%
Normalised emittance	50π mm mrad
Bunch length (rms)	0.4 – 0.6 mm
Bunch charge	140 – 200 pC
Microbunch spacing	1 ns or 40 ns
Macropulse duration	≤ 10 μs
Macropulse repetition rate	≤ 5 Hz

As indicated in *Table 1-1*, the electron bunch can be separated either by 1 ns or 40 ns. This is achieved by an additional modulation of 25 MHz at the electron gun, superimposed on the 1 GHz modulation. Note that when set to 40 ns, there is only one optical pulse circulating in the cavity, which is useful for the users to study fast phenomena with relaxation times greater than 1 ns.

1.4.2 The FEL undulator and optical cavity

FEL-1 and FEL-2 have identical undulator sections consisting of two rows of samarium-cobalt permanent magnets forming 38 periods of length 65 mm. The distance between the rows can be varied to change the K value of the undulator and thereby alter the wavelength of the laser radiation over a time scale of a few tens of seconds. The maximum value of K, which corresponds to the longest wavelength radiation, is obtained when the gap size is at the minimum determined by the size of the electron beam vacuum tube. Table 1-2 lists the important parameters for the undulator and optical cavity.

Table 1-2 *The important parameters for the undulator and optical cavity at FELIX*

	FEL-1	FEL-2
Cavity length	6.0 m	6.15 m
Rayleigh length	1.2 m	1.2 m
Curvature of upstream mirror	3.0 m	2.783 m
Curvature of downstream mirror	4.0 m	4.0 m
Aperture radius	1.5 mm	1.0 mm
Cavity round trip loss	5 – 15%	5 – 10%
Mirror reflectivity at 10.6 μm	> 98%	> 98 %
Mirror radii	25 mm	25 mm
Vacuum tube width	27.0 mm	16.7 mm
Undulator period	65 mm	65 mm
Number of undulator periods	38	38
Undulator strength (K)	< 1.3	< 1.9

In each FEL, the cavity consists of two gold-coated copper mirrors placed at opposite ends of the undulator. The measured cavity round-trip losses are shown in Figure 1-6. At the downstream end of the undulator the electrons are bent out of the optical cavity. In FEL-1 the electrons are simply dumped, but in FEL-2 the bending magnet was designed as a magnetic spectrometer. The total cavity length is 6 m, with the undulator positioned asymmetrically towards the downstream end. The curvature of the mirrors gives the optical beam a waist near the centre of the undulator and a Rayleigh length of 1.2 m. The downstream mirror is held in a

solid gimbal mount carried by a precision translation stage, coupled to the vacuum system by bellows. Angular and longitudinal adjustments are made with motorised micrometers and the distance between the cavity mirrors is actively controlled to within 0.5 μm by a Hewlett-Packard laser interferometer system. A fraction of the optical radiation generated in the FEL cavity is coupled out through a hole in the upstream mirror and is guided in an evacuated transport system from the accelerator vault to the user stations in the experimental area. The optical beam line is evacuated to prevent absorption, and separated from the linac vacuum system by diamond windows at the Brewster angle.

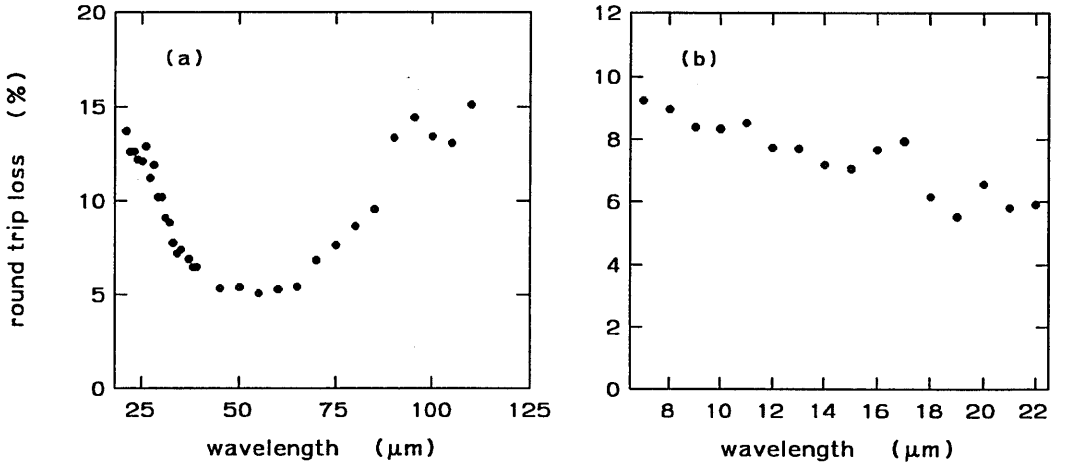

Figure 1-6. *The measured round-trip loss in FEL-1 (a) and FEL-2 (b). The losses are estimated from the ringdown time of the radiation coupled out through the aperture in the upstream mirror. The losses in FEL-1 increase at short wavelengths due to the formation of high-order transverse modes and at long wavelengths due to clipping of the optical field by the electron-beam vacuum tube in the undulator.*

1.4.3 Performance

Saturated laser output is achieved over the wavelength range 5–300 μm. The wavelength can be changed relatively rapidly by means of altering the undulator field strength: a variation of a factor of two in FEL-1 and of three in FEL-2 may be obtained in a matter of minutes. When a larger wavelength change is required, a change in beam energy or even a move to the other FEL may be necessary, which takes around 30 minutes. The output power as measured directly behind the laser is shown below as a function of the radiation wavelength. Figure 1-7 gives the micropulse energy during the saturated part of the macropulse, as obtained for six different settings of the electron energy ranging from 14.8 to 46.5 MeV. At each electron energy, only the undulator field

strength was varied. In practice, the FEL output can be optimised at any particular wavelength by adjusting the accelerator settings for that case. The power available in the user stations is typically a factor of two smaller due to losses in the 30-m long transport system. The macropulse power is given by the micropulse energy multiplied by the repetition frequency. The overall average power is equal to the product of the macropulse power and the duty cycle, which ranges up to 0.01%. This results in a maximum average power in the user stations of 0.5 W.

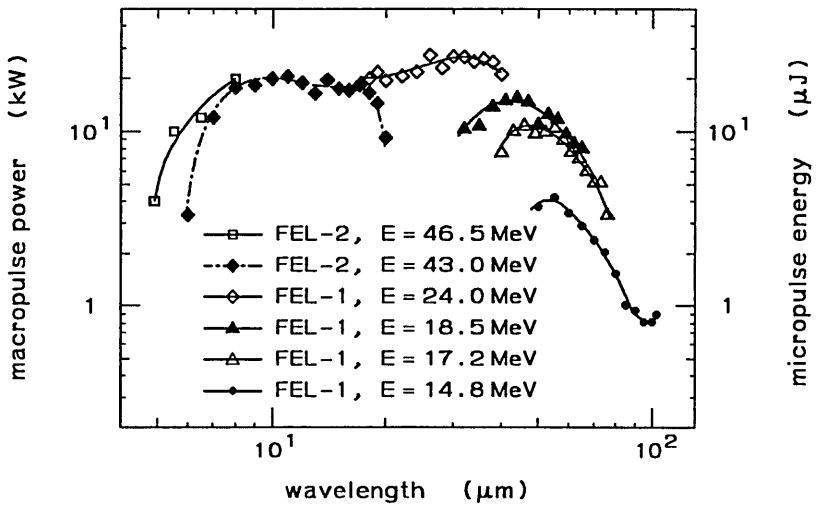

Figure 1-7 *Saturated macropulse power and micropulse energy as a function of the radiation wavelength. Results are shown for various values of the electron beam energy. At each electron energy, the wavelength is varied via adjustment of the undulator field strength.*

The micropulse duration may be tuned over roughly an order of magnitude by adjustment of the cavity desynchronism. Sub picosecond pulses have been achieved over a wide range of wavelengths and pulses as short as 200 fs have been measured leading to peak optical powers in the region of tens of MW. The combination of these high electric fields and short pulse duration make FELIX suitable for the study of non-linear phenomena and fast relaxation processes. In Figure 1-8 the optical pulse duration (a) and the width of the optical power spectrum (b) are shown for a wavelength of 24.5 μm as a function of the cavity desynchronism. In Figure 1-8 (c) the time-bandwidth product is plotted, showing that it close to the Fourier transform limit – the theoretical time-bandwidth product is 0.31 for a $\mathrm{sech}^2 t$ -shaped pulse. Similar performance is found at other wavelengths [14].

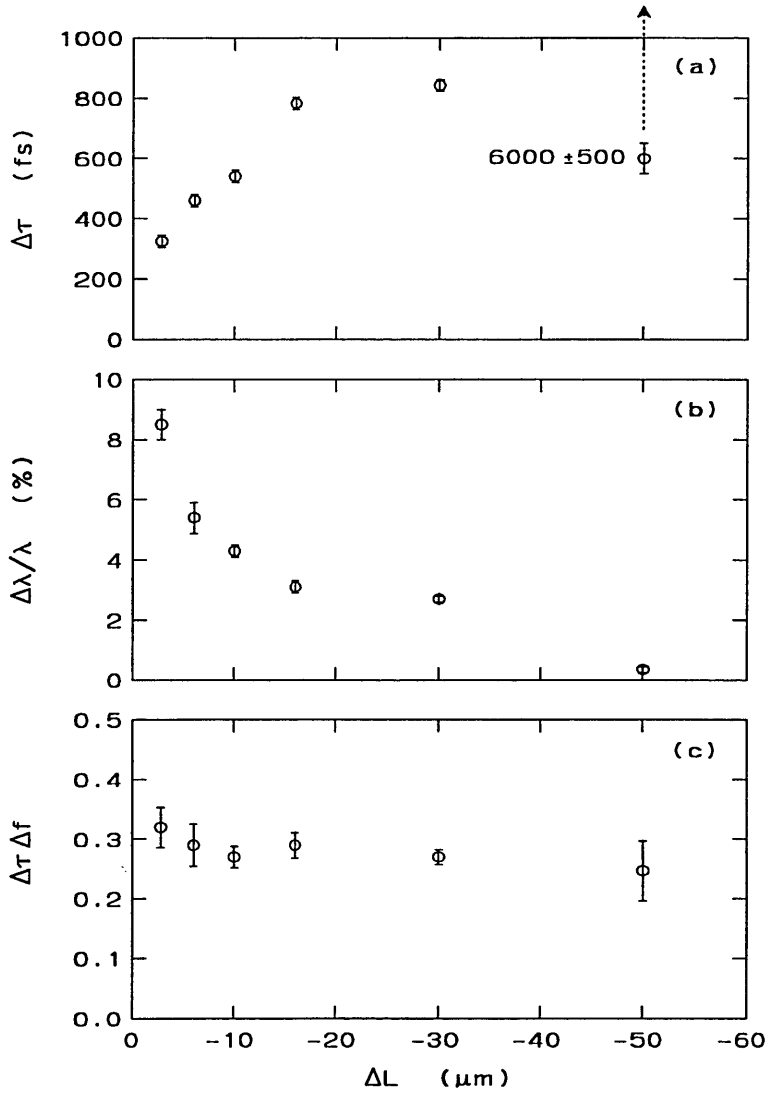

Figure 1-8 *Measured optical pulse duration (a), spectral width (b), and time-bandwidth product (c) as a function of cavity desynchronisation at a laser wavelength of 24.5 μm. All measurements are taken at the FWHM. The deduced time-bandwidth product is close to 0.31, the theoretical value for a* $\mathrm{sech}^2(t)$ *-shaped pulse.*

1.5 Motivation and Outline of this thesis

Characterisation of the ultra-short optical pulses produced by (far-) mid-infrared free-electron lasers (FELs) is an important task, not only for the further development of free electron lasers and their theory, but also for their operation as a research tool. Scientists who use FEL beam in their experiments, rely on the knowledge of the optical pulse length and even of its shape in order to interpret their experimental results correctly. Unfortunately, the sub-picosecond time scale is beyond the range of standard techniques, new methods have to be developed to monitor pulses as short as a few optical cycles.

The aim of this thesis is to study ultra-fast diagnostic techniques for subpicosecond optical and electron pulses. In the earlier section of this chapter, an introduction to basic FEL physics and to the FELIX free-electron laser facility has been presented. Chapter 2 describes the first diagnostic technique, the so called differential optical gating technique, which measures the intensity of the infrared optical pulse and its time derivative simultaneously with an unsynchronised ultrashort Ti:Sapphire laser, using a sum-frequency generation in a $AgGaS_2$ crystal as the gating mechanism. The FEL pulse shape is then reconstructed with a time resolution of the order of 100 fs. Chapter 2 also presents the study of synchronisation between the Ti:S laser pulses and the FEL pulses.

As the differential optical gating technique has ambiguity in reconstruction of the pulse shape at its peak position, where the derivative is zero, we introduce a new diagnostic method — an electro optical detection technique, in Chapter 3. The electro-optical detection technique based on the Pockels effect has been studied, both theoretically and experimentally. Intrinsically the electro optical sampling is a cross correlation technique, which we can use with subpicosecond resolution, because the synchronisation between the Ti:S laser pulses and the FEL pulses turns out to be rather good. Two types of configuration of detection are demonstrated. The efficiency of electro-optical detection in an electro-optical crystal of ZnTe has been studied, and an unexpected orientation dependence of the ZnTe crystal is explained in Chapter 3.

Using the electro-optical detection technique as a powerful diagnostic tool for sub-picosecond optical pulses, we are able to study the FEL physics systematically. Chapter 4 covers the generation and complete electrical-field characterisation of FEL pulses at FELIX. A further discussion of formation of low time-bandwidth product, single-sided exponential optical pulses in FEL oscillator is given in Chapter 5. Accurately measuring the synchronous length of the FEL optical cavity becomes more important, as at FELIX, it was found that extremely short optical pulses can be produced when the cavity is set close to perfect synchronism. Using the electro optical sampling technique, accurate measurement of the cavity synchronism of the waveguide far-infrared FEL is obtained with a precision of 1 micron and the measurement results are verified by theoretical model and calculation in chapter 6.

Many applications based on relativistic electron bunches require an accurate measurement of the peak current. For this, the duration and possibly the shape of the electron bunch have to be measured. Free Electron Lasers (FELs) are important devices that use high-peak current electron bunches. Considerable effort has been

made to extend the operating wavelength range into the XUV and soft X-ray part of the spectrum. Crucial for the success of these projects is the demonstration of self-amplified spontaneous emission (SASE) at short wavelengths. An important parameter in these experiments is of course the length and shape of the driving electron bunch, therefore precise measurement of the longitudinal electron beam profile is important for the successful operation of X-ray FELs. In Chapter 7, we demonstrate that the transverse electric field profiles associated with relativistic electron pulses can also be measured non-destructively with a sub-picosecond resolution using the electro-optical sampling technique. Recent work at FELIX has shown that the electro-optical sampling technique can be developed into a direct single-shot measurement of electron bunch profile, and an account of this new technique and its preliminary test results is given in the last chapter of this thesis [15].

1.6 References

[1] L.R. Elias, W.M. Fairbank, J.M.J. Madey, H.A. Schwettman and T.I. Smith, *Phys. Rev. Lett*, **36**, 717-720 (1976).

[2] D.A.G. Deacon, L.R. Elias, J.M.J. Madey, G.J. Ramian, H.A. Schwettman and T.I. Smith, *Phys. Rev. Lett.*, **38**, 892-894 (1977).

[3] D. Oepts, A.F.G. van der Meer et al., Infrared Phys. Tech., **36**, 297-308 (1995).

[4] W.B. Colson, etc. *Phys. Res. A* **407**, 26-29 (1998).

[5] W.B. Colson, http://www.physics.nps.navy.mil/table1.pdf ,
G. Ramian, http://sbfel3.ucsb.edu/www/fel_table.html

[6] G. Dattoli and A. Renieri, *Laser Handbook Vol. 4*, edited by M. L. Stitch and M. Bass, North-Holland, Amsterdam, 1-133 (1985).

[7] T.C. Marshall, Free-Electron Lasers, MacMillan, New York (1985).

[8] D. A. Jaroszynski, R. J. Bakker, A. F. G. van der Meer, D. Oepts and P.W. van Amersfoort, *Phys. Rev. Lett.*, vol **70**, 3412-3415 (1993).

[9] R. J. Bakker, G. M. H. Knippels, A. F. G van der Meer, D. Oepts, and P. W. van Amersfoort, *Phys. Rev. E*, **48**, R3256-R3258 (1993).

[10] D. A. Jaroszynski, P. Chaix, N. Piovella et. al, *Phys. Rev. Lett.*, vol **78**, 1699-1702 (1997).

[11] R Bonifacio, B.W.J. McNeil and P. Pierini, *Phys. Rev. A*,vol **40**, 4467-4475 (1989).

[12] N. Piovella, P. Chaix, G. Shvets and D.A. Jaroszynski, *Phys. Rev. E*, vol **52**, 5470-5486 (1995).

[13] H. Al-Abawi, F. A. Hopf, G.T. Moore and M.O. Scully, *Opt. Commun.*, vol **30**, 235-238 (1979).

[14] G.M.H. Knippels etc. *Phys.Rev. Lett.* **75**, 1755-1758 (1995)

[15] I. Wilke, A.M. MacLeod, W.A. Gillespie etc. *Phys. Rev. Lett.*, vol **88**, 124801 (2002).

Chapter 2 Differential optical gating measurement of FEL pulse shape

Abstract

This chapter presents measurements of the temporal pulse shapes of the FEL obtained from FELIX, using a differential optical gating technique with a 10-fs Ti:Sapphire laser, and sum-frequency generation in a $AgGaS_2$ crystal as the gating mechanism. By employing a differential technique to simultaneously measure the intensity of the infrared optical pulse and its time derivative, we have reconstructed the mid-infrared pulse shape with a time resolution of the order of 100 fs. Further study of synchronisation between the Ti:S laser and the FEL at FELIX encouraged us to use other diagnostic techniques, described later in this thesis, as the jitter measured in our experiment turns out to be only about 400 fs rms over a scanning time of 2 minutes, and < 100 fs over a rapid scanning time of 10 μs (length of one typical FEL macropulse at FELIX).

2.1 Introduction

Characterisation of the ultrashort optical produced by free-electron lasers (FELs) is important both for the further development of the FEL and for its operation as a research tool. Conventional streak cameras can only achieve picosecond resolution and do not work in infrared (IR). The development of ultrafast lasers has led to the development of advanced methods to characterise the temporal profile of the short optical pulses. In order to measure pulses shorter than the response time of the conventional detector, a non-linear optical gating technique can be employed. The most common method is to use the optical pulse itself as the gating pulse. The autocorrelation can provide a clean measurement of optical pulse length, but it is not practical in some cases, either because the peak power of the optical pulse is too low, or because suitable non-linear crystals are not available at longer wavelengths. Furthermore, autocorrelation methods suffer from the drawback that the pulse shape is difficult to resolve. In these instances, it is possible to characterise the optical pulse shape by employing a cross correlation technique using an ultrafast optical pulse from an external laser source as the gating, and then the measurement resolution is determined by the length of the gate pulse. In practice, it is often difficult to achieve good (subpicosecond) synchronisation between the two lasers, therefore the data must be obtained in a single shot measurement with arrays of fast, sensitive long-wavelength detectors. Recently, a simple technique called differential optical gating (DOG) has been developed, in which these synchronisation problems are considerably avoided [1].

2.2 Differential Optical Gating Technique

Using the differential optical gating technique, one can obtain detailed optical pulse shape information via optical gating with unsynchronised laser pulse trains. The principle of this technique is to measure simultaneously the intensity of the sample pulse and its time derivative by cross-correlating it with two pulses (one is delayed with respect to another) from an external ultrafast laser. Provided the time delay between the two pulses is known, each two-pulse measurement allows the FEL pulse intensity $I(t_0)$ and its time derivative dI/dt to be calculated at the time of measurement, t_0, which is in principle unknown because of the presumed jitter between the two lasers. Subsequent measurements produce further pairs $\{I,\ dI/dt\}$ at different times, t. These accumulate —either as the result of jitter or by altering the delay between the two lasers — to provide a map of dI/dt as a function of I, i.e.

$$\frac{dI}{dt} = f(I) \qquad \textbf{Equation 2-1}$$

One can recover time information of $I(t)$ by integrating this equation directly,

$$\int_{I_0}^{I_1} \frac{dI}{f(I)} = \int_{t(I_0)}^{t(I_1)} dt = t(I_1) - t(I_0) \qquad \textbf{Equation 2-2}$$

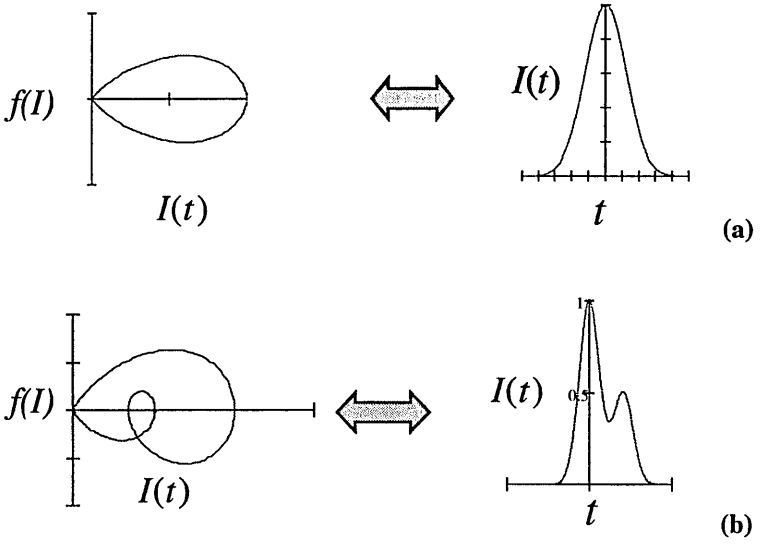

Figure 2-1. *Illustration of the principle of Differential Optical Gating (DOG) technique. The left side shows the accumulated map of the pulse intensity I(t) and its time derivative f(t), while the right side gives the time information of the pulse by integration. Here (a) presents a simple pulse and (b) shows one with a subpulse.*

In order to obtain an umambiguous reconstruction of the optical pulse shape, it is clear that (1) $f(I)$ can not be zero, and (2) $f(I)$ must be single valued within a given quadrant of $\{I, dI/dt\}$ space. This requirement will raise problems even for a very simple pulse shape, which has a zero in the derivative at the pulse maximum. Therefore, using Equation 2-2, one can reconstruct the leading and trailing edge separately, but some uncertainty remains at the peak of the intensity profile of the pulse. However, it is possible to eliminate the uncertainty by making an additional measurement using the same method, which will be discussed later in this chapter.

2.3 The gate pulse from Ti:Sapphire laser system

Ultrashort Ti:Sapphire lasers have been widely used in cross-correlation measurements. In the differential optical gating technique, a femto-second laser is employed as the gate pulse. Table 2-1gives the general parameters of this Ti:Sapphire laser system (Femto Source Pro, Femto Lasers, Vienna, Austria). Figure 2-2 gives the 10-fs fringe-resolved autocorrelation function of the Ti:Sapphire pulse used in our differential optical gating measurement.

Table 2-1: *parameters of the Ti:Sapphire femto-second Laser*

Central wavelength	800 nm
Repetition rate	100 MHz
Pulse duration	≤ 12 fs
Spectral width	≥ 75 nm
Pulse jitter	< 400 fs (rms)
Peak power	> 400 KW
Averaged power	> 300 mW

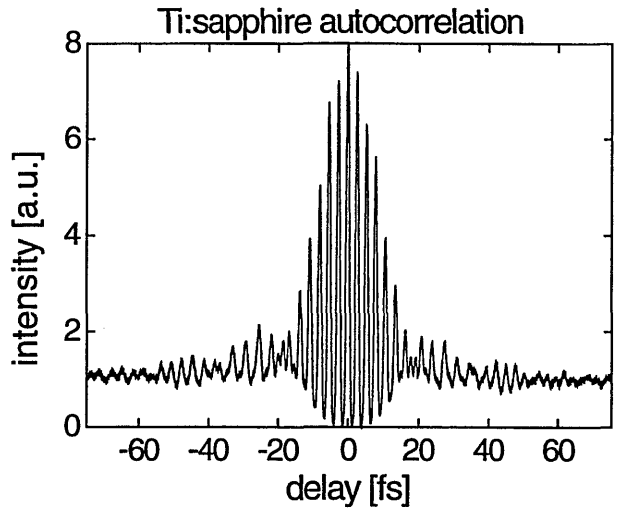

Figure 2-2 *Autocorrelation function of the Ti:Sapphire pulse*

2.4 Differential Optical Gating measurement at FELIX

Figure 2-3 gives the experimental set-up for the DOG measurement at FELIX. The DOG measurements were made at an FEL wavelength of 9 μm using the sum-frequency generated by the FEL radiation and the 800 nm radiation from the Ti:Sapphire laser in a $AgGaS_2$ crystal (Type-I phase matching, MolTech, Berlin, Germany). In this set-up, the source and the gating beam are split into equal parts and guided into two separate arms. In each arm, both the source and the gate pulse trains are focused and overlapped in a non-linear 100-μm thick $AgGaS_2$ crystal to produce photons at the sum frequency of the source and the gate beams. This signal is passed through a polariser to block the Ti:S radiation and then detected using a silicon photodiode. The two arms are identical except that one arm is delayed using an optical delay line, which provides a small time delay T_d. Since the Ti:Sapphire pulse is much shorter than the FEL pulse, the signal measured at each arm is proportional to the intensity of the FEL pulse. The time derivative is not measured directly, instead, one can approximate the derivative from the difference between two intensities spaced closely in time. The time delay T_d must be chosen carefully to provide a sufficiently large difference on the slowly varying parts while maintaining adequate temporal resolution on the rapidly varying parts of the FEL pulse shape.

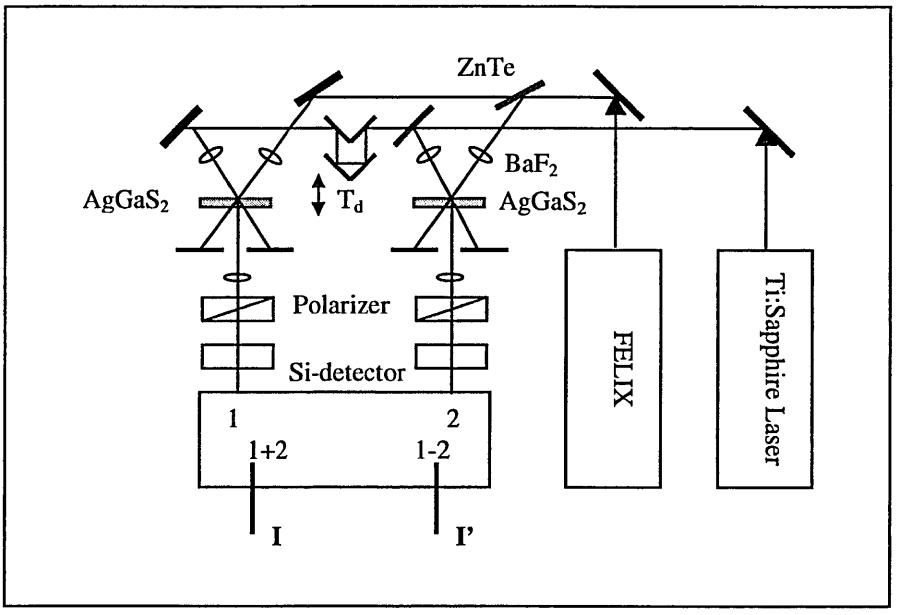

Figure 2-3. *Experimental setup of differential optical gating measurement*

An automated data acquisition program was written to collect and store the intensity and its derivative of FEL pulse for each shot. After collecting several thousand data pairs, one accumulates a density map in the {I, dI/dt} space. Since there are always some intensity fluctuations, pulse shape fluctuations, and noise due to difference in response between two arms, the curve of the measurement *f(I)* will results in a finite width. Using a density map display and counting all the measured data, one can fit the data with a curve which is through the centre of the intensity distribution, therefore reconstructs the time information of the FEL pulse shape. However, these fluctuations and noises will limit the time resolution of the pulse shape during the reconstruction process.

We have studied the FEL optical pulse shape in two important regimes of operation. First, when the laser cavity is detuned away from perfect synchronism, relatively long FEL pulses are generated. A typical DOG picture is shown in Figure 2-4(A), the data exhibit a strong asymmetry about the *I* axis. The function *f(I)* is obtained from this density map by tracing a line which follows the centre of the intensity distribution curve. Then the pulse shape is reconstructed using equation 2-2, the *f(I)* curve is integrated separately for the rising and trailing edges of the pulse. To join the two regions, we take advantage that the density map indicates the relative amount of time spent in a given part of the curve *f(I)*. In another word, higher density indicates a slower varying part of the pulse. It is possible to eliminate the uncertainty at the peak of pulse by making an additional measurement at a larger time delay T_d, which is of the order of the pulse length, thus one can correlate the peak of the pulse to the wings. By tuning the

delay time T_d to a minimum value at which the *f(I)* curve is a straight line with a slope of 1, then T_d corresponds to the full pulse width. The reconstructed pulse shape is indicated in Figure 2-4(B). The leading edge fits well to an exponential, whereas the trailing edge is fitted by a Gaussian. These results are taken at the early part of the macropulse, before the formation of a subpulse sets in. Similar pulse shapes were observed at the Stanford FEL [1]. The reconstructed pulse is also in good agreement with separate measurements of the intensity autocorrelation function (1.33 ps fwhm) [2] and the optical spectrum (time-bandwidth product of 0.35). Under certain conditions (at an intermediate cavity detuning length, where a dynamic balance between the laser lethargy and saturation of optical power is reached), the formation of subpulses, which have a clear signature in the DOG data, is seen. An example is given in Figure 2-5 (A), with a reconstructed micropulse shape shown in (B).

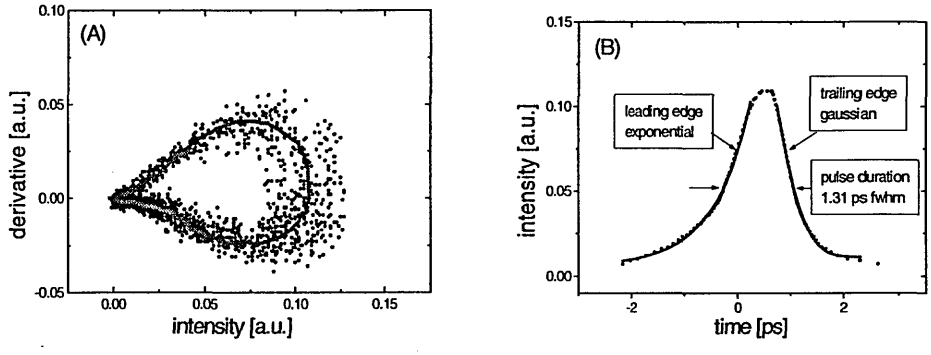

Figure 2-4 *Raw DOG data (A) and reconstructed FEL pulse (B) for ΔL=-22μm, λ=9μm.*

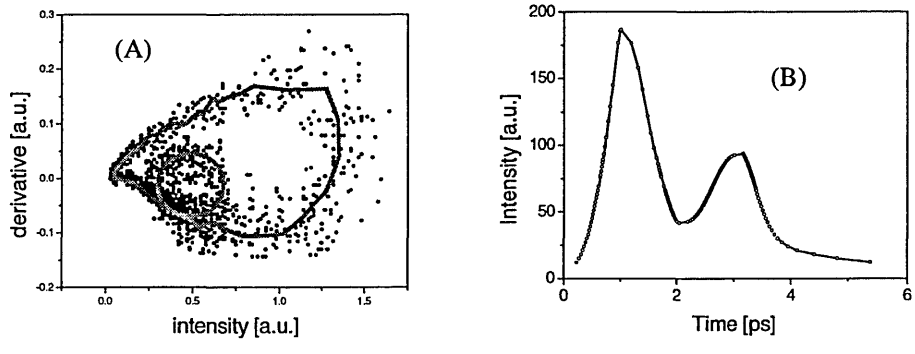

Figure 2-5 *(A) DOG data with a subloop, indicating the formation of subpulses on the trailing edge. (B) Reconstruction of the FEL pulse.*

In a second series of measurements we focused on the shortest possible FEL pulses to demonstrate the improved time-resolution of approximately 100 fs that we obtained. The data presented here represent the first high-resolution pulse shape measurements of these ultrashort FEL pulses, and provided a basis for more stringent tests of FEL theory in this operating regime than were previously possible. The DOG data shown in Figure 2-6 correspond to an FEL pulse of approximately 200 fs fwhm in duration. Although our current time resolution is perhaps still not good enough to resolve the details of the pulse shape fully, we have fitted it for illustration purposes with the first supermode [3], which is an analytic expression for the FEL pulse shape at small values for the cavity detuning:

$$|A_1(\xi)|^2 \approx (3\sqrt{3}/\pi^2\nu)\, exp(\sqrt{3}\,(2/\nu)^{1/3}\,(\xi-1))\sin^2(\pi\xi) \qquad \textbf{Equation 2-3}$$

In this formula, $\nu = 2\Delta L/(L_s\gamma)$ is the normalised cavity detuning length, ΔL is the cavity detuning length, $L_s = N_u\lambda$ is the slippage length (N_u=38 is the number of undulator periods at FELIX, λ is the wavelength of FEL optical radiation), γ is the normalised gain parameter ($\gamma \approx 1.5$ to 2 in FELIX FEL), and $\xi = (ct - z)/L_s$ is the position within the optical pulse in units of the slippage length L_s. Our fit yields a value for ν=0.036±0.002, whereas the calculated value yields ν = 0.03.

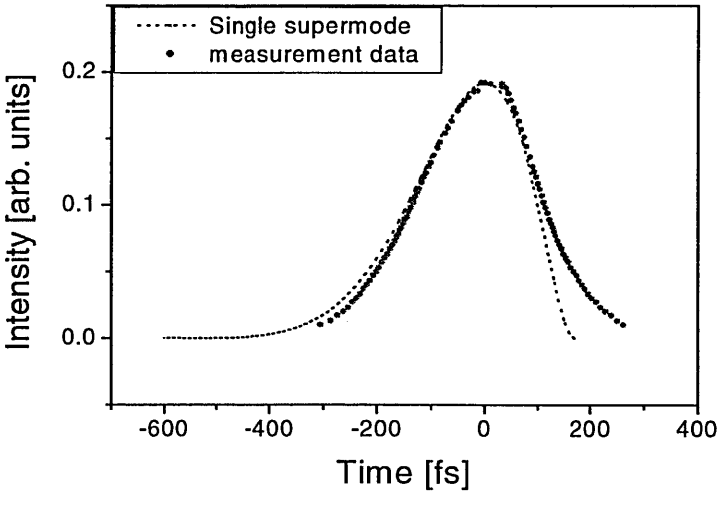

Figure 2-6 *Reconstruction of a short FEL pulse taken at ΔL=-10μm and λ=9μm. The dotted line corresponds to the first supermode (see text).*

2.5 Pros and Cons of DOG

Differential optical gating is a simple method for measuring the shape of an optical pulse using an unsynchronised ultrafast laser (poor synchronisation is not an issue for the DOG technique, even no synchronisation is required between the probe laser and the optical pulse). It can be used for the study of a low intensity source throughout a broad range of wavelengths, by using a range of gating mechanisms, like sum-frequency generation, Kerr or Pockels effects, photo-induced plasma absorption etc. A temporal resolution of the order of 100 fs has been achieved with the DOG technique. The time resolution of this technique is determined by the gate pulse width (~10fs), optical or electrical noise, and dispersive optics and focusing geometry, it can be improved further by optimising the design of the focussing optics for the Ti:Sapphire laser and using thinner, less dispersive, sum-frequency mixing crystals. The cons of the DOG technique are also obvious: it has ambiguity in reconstruction process where the derivative is zero, it requires repetitive constant pulse shape in order to accumulate data of $\{I(t), dI/dt\}$ over a few minutes, and it has difficulty in resolve multiple (sub) pulses which frequently occur in practice. Furthermore, it requires repetitive pulse traces that is reproducible, both in terms of amplitude and shape for both the beam under investigation and the gate beam.

2.6 Sub-picosecond synchronisation of Ti:Sapphire laser to FELIX

In this section, we will discuss the synchronisation between the FEL from FELIX and the Ti:Sapphire laser. Previous attempts to synchronise a different FEL with a regenerative mode-locked Ti: Sapphire laser have led to several picoseconds of jitter [4]. In such circumstances, the DOG technique becomes a good choice for measuring the sub-picosecond optical pulse shape with an unsynchronised ultra-fast pulsed laser. At FELIX, the implementation of a good optical and electronic synchronisation loop has allowed the first successful synchronisation of a Kerr-lens mode-locked 10-fs Ti:Sapphire laser system to an FEL at FELIX with a jitter of sub-picosecond scale. This synchronisation scheme, which was developed concurrently with the DOG measurements has meant that other methods can be used to provide even more accurate measurements of the FEL pulse length.

A schematic layout of the feedback loop is given in Figure 2-7 [5]. The Ti:Sapphire laser is pumped by 5 W of 532 nm from an intra-cavity frequency-doubled Nd:YVO_4 laser (Millenia V, Spectra Physics, Mountain View, CA USA), and employs so-called 'chirped-mirror' technology to achieve reliable and stable production of the ultrashort optical pulses [6]. See Table2-1 for its general parameters. The cavity of this Ti:S laser is modified by mounting a tiny (5 mm diameter, 1 mm thick) high-reflector in the short arm of the cavity on a PZT with 10 μm

range. This piezo-controlled mirror is used for active cavity stabilisation. A fast Si-photodiode (-3 dB at 1.5 GHz) is used to monitor the 100-MHz optical pulse train. The 1 GHz component of this signal and a reference signal of the 1 GHz clock of the FEL are combined in a double-balanced mixer, the output of which serves as the error signal for driving the PZT. The unity-gain bandwidth of the loop is 1 kHz, determined primarily by the PZT drive electronics and the loop filter. The use of the 10^{th} harmonic of the 100-MHz roundtrip frequency in the feedback loop provides better locking because of the reduced influence of amplitude-to-phase-noise in the loop [7].

When the FEL and the Ti:Sapphire laser are frequency-locked to each other, the temporal overlap is found by simply scanning an RF-phase-shifter. Type-I sum-frequency generation in a 100-μm thick $AgGaS_2$ crystal (MolTech, Berlin, Germany) has been used at an FEL wavelength of 9 μm to measure the degree of jitter that is left between the two lasers in a direct optical cross-correlation experiment. The sum-frequency is detected through a calcite polarizer that blocks the Ti:Sapphire background (see Figure 2-7). The infrared FEL pulse duration was similarly measured with a CdTe-based autocorrelator to be 435 fs fwhm in duration (see trace (a) in Figure 2-8). The duration of the Ti:Sapphire laser pulses was measured separately with an autocorrelator close to the $AgGaS_2$ sample and was found to be 10 fs fwhm (see trace (b) in Figure 2-8). In Figure 2-8 trace (c), a delay line was scanned to vary the optical delay between the two laser pulses, and individual data points correspond to a fifty-shot-averaged measurement over successive macropulses. The jitter from the cross-correlation signal can thus be estimated to be 400 fs rms (~900 fs fwhm, assuming uncorrelated Gaussian noise). The achieved degree of synchronisation is present over many minutes and the resulting system performs well compared to other commercially available systems that allow locking of a Ti:Sapphire laser to an external clock. For example Spectra-Physics and Coherent typically specify a jitter of less than 3 ps rms (~6 ps fwhm) on a 60-second time scale or shorter for table-top-systems. In our case the FEL is located 40 meter away from the Ti:Sapphire laser, and the excellent synchronisation achieved demonstrates the intrinsically stable cavity design of the Ti:Sapphire laser, as well as the tight locking of the FEL to its 1 GHz clock. The large separation between the lasers leads to a slow thermal drift in synchronisation of about 1 ps per half-hour.

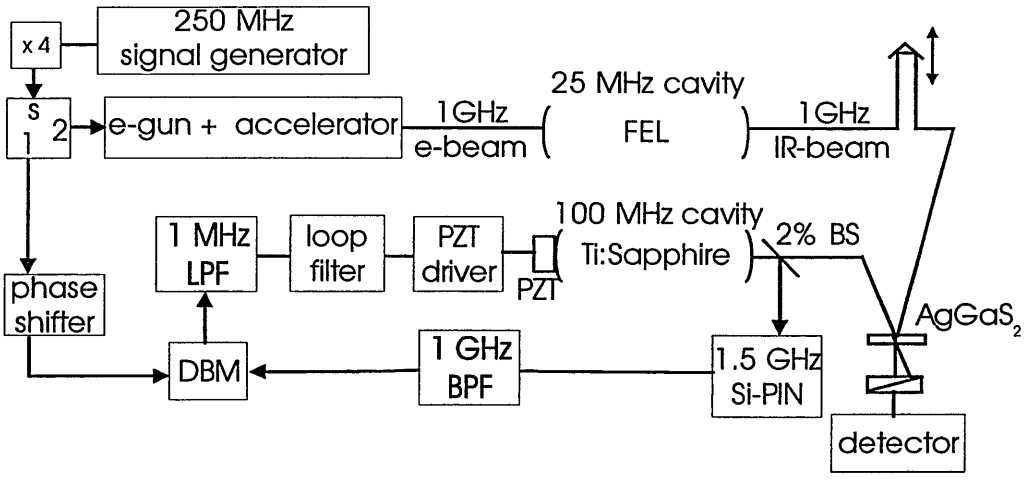

Figure 2-7 *Schematic layout of synchronisation electronics and optics. An ultra-stable rf-clock (SMG 801.0001.52, Rohde & Schwarz, Munich, Germany) running at 250 MHz is multiplied by four to yield 1 GHz. An rf-splitter splits the 1 GHz signal in two. One arm serves as the reference clock input for the double-balanced mixer (DBM), while the other part drives the electron gun and accelerating structures. A fast 1.5GHz silicon-diode detects the 100 MHz Ti:Sapphire pulse train and filters out the 1 GHz component, which is mixed with the 1 GHz clock in the double-balanced mixer to yield the phase difference. After passing through a 1-MHz low-pass filter and a loop filter (unity gain at 1 kHz) the error signal is send to a PZT-driver to adjust the cavity length. A phase shifter is used to control temporal overlap. i.e. to remove the constant time delay present in the system after locking the feedback loop.*

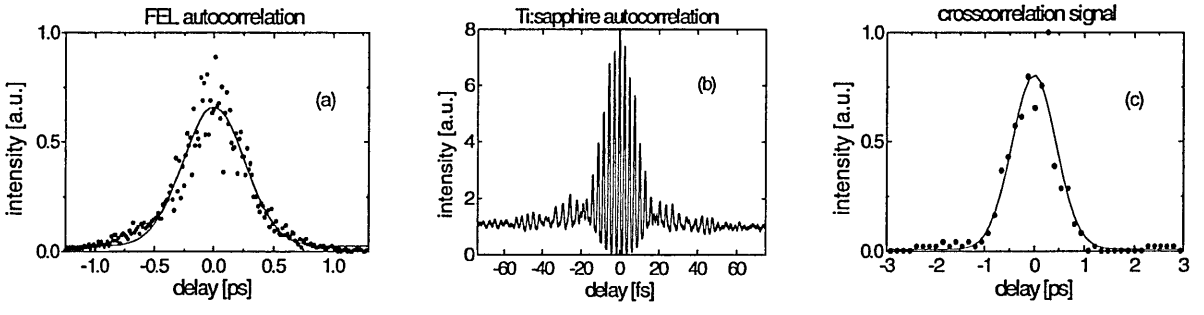

Figure 2-8 *Trace (a) shows the background-free autocorrelation measurement of the 435-fs FEL pulse with a purpose-built autocorrelator based on CdTe, and trace (b) gives the 10-fs fringe-resolved autocorrelation function of the Ti:Sapphire pulse. Trace (c) shows the measured optical cross-correlation between the FEL running at 9 μm and the Ti:Sapphire laser at 800 nm in a 100-μm thick $AgGaS_2$ crystal. The derived jitter is 400 fs rms (~900 fs fwhm). The scan took approximately two minutes to record) [[2]].*

Although we demonstrated the synchronisation of the Ti:Sapphire laser to the FEL at an infrared wavelength of 9 μm, this is only limited by the availability of suitable sum-frequency mixing crystals (and has been verified between 7 and 13 μm wavelength with the same $AgGaS_2$ crystals). The synchronisation is present over the whole FELIX wavelength (4.2-300 μm) range since we directly locked to the FEL's internal RF-clock. Furthermore, we also are able to synchronise the Ti:Sapphire laser to FELIX when it runs at 25 or 50 MHz repetition rate instead of 1 GHz. This is achieved with a slight modification of the feedback loop so that first locking to the 25/50 MHz is obtained, before the 1 GHz lock is activated. Identical synchronisation performance is observed in these modes since the 25/50 MHz signals are just necessary in the beginning to select the appropriate 1 GHz cycle, but do not influence the loop characteristics (the 25/50 MHz signal can even be removed, once locking is obtained).

2.7 Conclusion

The optical pulses of infrared FELs can be strongly asymmetric, especially when the cavity is desynchronised. Differential Optical Gating (DOG) with an external femto-second laser has proved to be a useful technique for studying these asymmetric pulses. We have measured the pulse length of a mid-infrared FEL using the differential optical gating technique, with an unsynchronised ultrafast (10 fs) Ti:Sapphire laser as the gate pulses. The measurements were made at wavelengths between 8 and 9 μm, with a temporal resolution of the order of 100 fs. The FEL optical pulses generated in two important regimes of operation are studied. One is the ultrashort FEL pulse (about 250 fs) generated near zero cavity desynchronism, while another measurement gives the formation of optical subpulses, when the cavity is detuned from perfect synchronism.

By further studying the synchronisation between Ti:S laser and the FEL at FELIX, we achieved a small jitter between these two laser systems (400 *fs* rms over a scanning time of 2 minutes, and <100 *fs* over a rapid scanning time of 10 μs). This good synchronisation makes it possible to choose a more straightforward technique to measure the FEL and electron pulse shape, and this new method is called electro optical sampling (EOS) technique, which will be further discussed in details in the following chapters.

2.8 References

[1] C.W. Rella, G.M.H. Knippels, D.V. Palanker, T.I. Smith, H.A. Schwettman, the proceedings of the 19th Int. FEL. Conf., Beijing, China, 1997.

[2] G.M.H. Knippels etc. Opt. Lett. 1754 (1998).

[3] N. Piovella P. Chaix , G. Shvets, D. Jaroszynski, Phys. Rev. **E 52**, 5470-5486 (1995).

[4] R.J. Stanley, R.L. Swent, T.I. Smith, Opt. Commun. **115**, 87-92 (1995).

[5] G.M.H. Knippels et al., Opt. Lett. **23**, 1754 (1998).

[6] L. Xu, G. Tempea, A. Poppe, M. Lenzner, C. Spielmann, F. Krausz, A. Stingl, K. Ferencz, Appl Phys. B **65**, 151-159 (1997).

[7] D. von der Linde, Appl. Phys. B **39**, 201-217 (1986).

Chapter 3 Angular Dependence of Electro-Optic Sampling in ZnTe

Abstract

This chapter gives a general introduction to the electro optical sampling technique. The orientation dependence of electro-optic sampling in a crystal of ZnTe<110> is obtained in a series of experiments; calculations of the transverse electro-optic modulation in ZnTe<110> are presented. With a probe beam normally incident upon the (110) plane of a crystal of ZnTe, the maximum efficiency of electro-optical detection can be obtained by making the polarisation of the probe beam parallel or perpendicular to that of the THz beam.

3.1 Introduction

Over the last decade, there has been an increasing interest in the generation and detection of electro-magnetic pulses with frequencies in the Tera-hertz regime. For the detection of freely propagating electro-magnetic pulses in the sub-picosecond time domain, several techniques have been developed. These include the method of optically gated photoconductive antennas [1], interferometric techniques using a bolometer as a detector [2], and electro-optic (EO) detection [3,4,5]. Although both the amplitude and phase information can be obtained with photoconductive dipole antennae, the limitation of these detectors is the resonant behavior of their Hertzian dipole structure, therefore the signal waveform is not a simple cross-correlation of the incoming terahertz pulse and the optical gating pulse. Furthermore, these antennae are insensitive to frequencies above 5 THz. Far-infrared interferometry can provide information about the temporal profile of the THz pulses, but the phase information is lost.

An alternative method [4] , called electro-optic sampling (or detection), has been developed for the complete characterization of the THz pluses. Electro-optic sampling technique is based on the linear electro-optic effect (also known as Pockels effect) [6]: when an electric field is applied to an electro-optic crystal, it induces birefringence. The birefringence can then be probed by a synchronised ultra-short Ti:Sapphire (Ti:S) laser pulse. The induced birefringence causes the initially linearly polarised optical probe beam to acquire a phase difference between its polarisation components parallel and perpendicular to the induced optical axis of the sensor crystal, and therefore the probe beam will become elliptically polarised. The degree of ellipticity can be measured by using suitable polarisation optics. By scanning the delay between the Ti:S pulse train and the THz pulse train, a cross-correlation of the incident electric field of the THz pulse is obtained. Note that with this electro-optic detection technique, an asymmetric pulse

shape can be measured with sub-picosecond time resolution and without time-reversal ambiguity. Furthermore, information about the electric field, including its sign, is obtained in contrast with most other techniques that yield only information on the intensity. Another advantage of this technique is a nearly flat frequency response of certain (low dispersion) EO sensor crystals in the THz regime [7]. It has been demonstrated that frequencies up to 37 THz can be measured with this technique [8].

As most of terahertz generation and detection experiments employ an ultra fast Ti:S laser to generate and also to detect the THz pulses, the Ti:Sapphire pulses are therefore naturally synchronised with the THz beam. In our case, the Ti:S laser and FEL laser are completely independent laser systems, an external synchronisation loop with a small jitter is required in order to use this EO sampling technique to measure the FEL pulse shape. Fortunately, as described in chapter 2, the Ti:S laser is well synchronised to the FEL laser with a small jitter of 400 fs rms over two minutes, enabling us to adopt this technique to measure the FEL pulse shape at long IR wavelength where the pulse length is much longer than 400 fs. For the electro-optical measurement with the rapid scanning technique, which will be discussed in chapter 4, the jitter is <100fs over 10 μs (the typical length of an FEL macropulse at FELIX).

3.2 Experimental setup for EO sampling

Figure 3-1 illustrates the experimental setup for the detection of THz pulses, using free-space electro-optic sampling technique. In this experiments, the THz beam is produced by the FELIX [9]. We use the FEL beam in the wavelength range of 40-220 μm for the electro-optic sampling experiments and especially at 150 μm, where the phase velocity of the THz beam matches the group velocity of the optical probing pulse, which results in a large interaction length and a good time resolution. An ultrashort Ti:Sapphire (Ti:S) laser (FemtoSource Pro, Femtolasers, Vienna), producing 12 fs pulses with a repetition rate of 100 MHz at 800 nm, is used as the probe beam. The collinear THz beam and the optical probe beam are normally incident on the (110) face of a 0.5-mm-thick crystal of ZnTe (from Uni-export, U.K.). ZnTe has been employed as the primary sensor material for free-space electro-optic sampling in many experiments, since it has a large figure-of-merit of 51.7 pm/V, a small group velocity mismatch of 1.1 ps/mm [10], a broadband detection capability (from 82 MHz to 37THz) [11]. Figure 3-2 gives the measured transmittance patterns of EO sampling crystals: ZnTe <110> and GaP <110>. It can be seen clearly that ZnTe crystal has a broad transmission band, and GaP can be adopted as an EO sensor in the spectral range where ZnTe has no transmission of light at wavelength between 40 μm (wave number 250 cm^{-1}) and 67 μm (wave number 150 cm^{-1}),

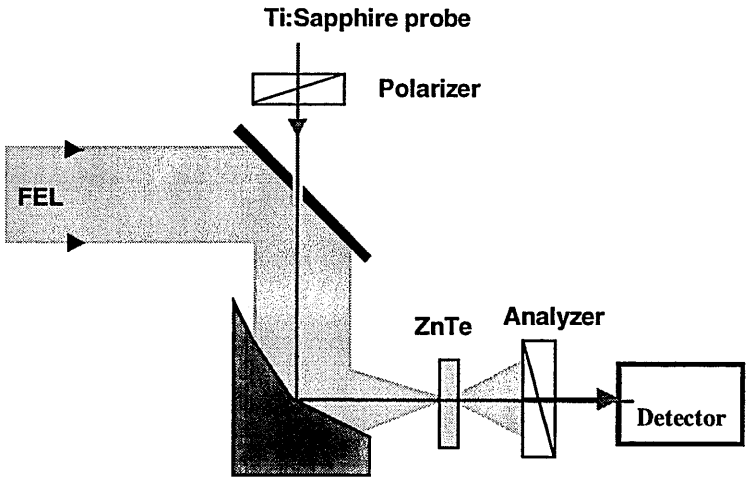

Figure 3-1 *Schematic of the electro-optic detection setup.*

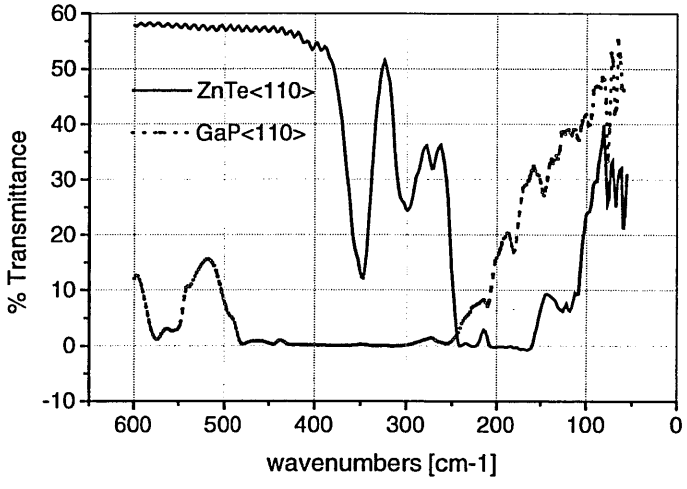

Figure 3-2 *Spectral transmittance of EO sensor crystals: ZnTe <110> and GaP <110>. Solid curve gives the transmittance pattern of ZnTe <110>, while dotted line gives the transmittance of GaP <110>.*

With the crystal between crossed polarisers, we rotated it in its (110) plane, and observed an approximately six-fold symmetry in the transmitted intensity versus the rotation angles (see Figure 3-3). It is not immediately clear that this result should be expected for the cubic ZnTe crystal rotated around a two-fold symmetry axis. Therefore the EO effect for collinear (110) incidence was calculated with arbitrary angles for the polarisation and the crystal c-axis.

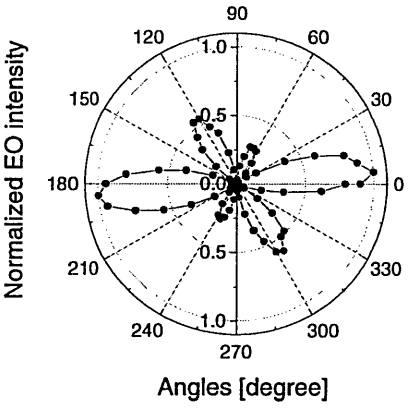

Figure 3-3 *Observed transmitted probe laser intensity vs. rotation angle of a ZnTe <110> crystal between crossed polarisers, in the field of a 150-μm-wavelength FEL pulse.*

3.3 Theory of EO Sampling in ZnTe

We define a laboratory co-ordinate system with *x, y, z* along the crystal's symmetry axes *a, b, c* as shown in Figure 3-4. The direction and the polarisation of the probe beam and THz beam in the ZnTe crystal are also shown in Figure 3-4.

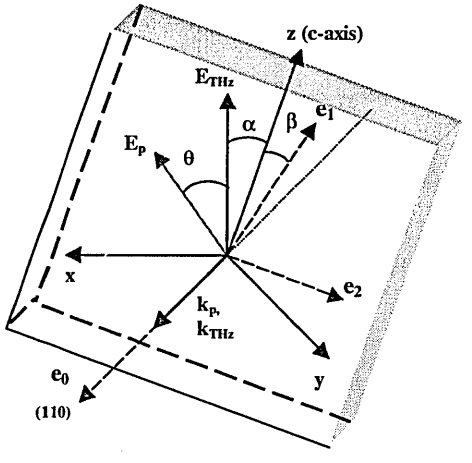

Figure 3-4 *Laboratory co-ordinate system with (x, y, z) defined along the crystal's symmetry axes of a, b and c.* E_{THz} *and* E_p *indicate the polarisation direction of the THz beam and the probe beam.* k_p *and* k_{THz} *give the propagating direction of the THz beam and the probe beam. The new principal axes of the indicatrix ellipsoid due to the applied external THz electric field is presented by (* $\vec{e}_0, \vec{e}_1, \vec{e}_2$ *).*

Provided the THz beam has its polarisation direction in the (110) plane but with an angle α to the z-axis, then in the presence of the applied electric-field (E_x, E_y, E_z) of the THz pulses, the indicatrix for the cubic ZnTe crystal is given by

$$M = \begin{bmatrix} 1/n_0^2 & r_{41}E_z & r_{41}E_y \\ r_{41}E_z & 1/n_0^2 & r_{41}E_x \\ r_{41}E_y & r_{41}E_x & 1/n_0^2 \end{bmatrix} \qquad \textbf{Equation 3-1}$$

Where r_{41} is the electro-optic coefficient of the crystal, n_0 is the refractive index of the crystal without applied electric field, and E_0 is the amplitude of the applied field,

$$E_x = \frac{\sqrt{2}}{2}E_0 \sin\alpha,\ E_y = \frac{-\sqrt{2}}{2}E_0 \sin\alpha,\ E_z = E_0 \cos\alpha \qquad \textbf{Equation 3-2}$$

The eigenvalues of matrix **M**, giving the new refractive index of the crystal, are

$$\begin{bmatrix} \nu_0 \\ \nu_1 \\ \nu_2 \end{bmatrix} = \begin{bmatrix} \frac{1}{n_0^2} + r_{41}E_0 \cos\alpha \\ \frac{1}{n_0^2} + \frac{1}{2}r_{41}E_0\left[\sqrt{4 - 3\cos^2\alpha} - \cos\alpha\right] \\ \frac{1}{n_0^2} - \frac{1}{2}r_{41}E_0\left[\sqrt{4 - 3\cos^2\alpha} + \cos\alpha\right] \end{bmatrix} \qquad \textbf{Equation 3-3}$$

Accordingly, the eigenvectors $(\vec{e}_0, \vec{e}_1, \vec{e}_2)$, representing the new principle axes of the indicatrix ellipsoid due to the applied external THz electric field are given by:

$$\vec{e}_0 = \frac{1}{\sqrt{2}}\begin{pmatrix} 1 \\ 1 \\ 0 \end{pmatrix},\ \vec{e}_1 = \frac{1}{\sqrt{2 + A^2}}\begin{pmatrix} 1 \\ -1 \\ A \end{pmatrix},\ \vec{e}_2 = \frac{1}{\sqrt{2 + B^2}}\begin{pmatrix} 1 \\ -1 \\ B \end{pmatrix} \qquad \textbf{Equation 3-4}$$

with

$$A = \frac{\sqrt{4 - 3\cos^2\alpha} + \cos\alpha}{\sqrt{2}\sin\alpha},\ B = \frac{-\sqrt{4 - 3\cos^2\alpha} + \cos\alpha}{\sqrt{2}\sin\alpha} \qquad \textbf{Equation 3-5}$$

The eigenvector $\vec{e}_0$ is perpendicular to the (110) plane, but $\vec{e}_1$ and $\vec{e}_2$ lie in the (110) plane (in the naturally curved face plane of the crystal). The new principal axes are determined only by the angle and not the strength of the applied electric field, and $\vec{e}_1$ makes an angle β to the z-axis, where

$$\cos(\beta)=\sqrt{\frac{\sqrt{4-3\cos^2(\alpha)}+\cos(\alpha)}{2\sqrt{4-3\cos^2(\alpha)}}}\times \text{sign}[\sin(\alpha)] \qquad \textbf{Equation 3-6}$$

Note that $sign[\sin(\alpha)]=1$ if $0\le\alpha\le\pi$, or $sign[\sin(\alpha)]=-1$ if $\pi\le\alpha\le 2\pi$. In Figure 3-5, β_1 and β_2 are the calculated results based on equation 2-6 when $\alpha_1=[0,\pi]$ and $\alpha_1=[\pi,2\pi]$, respectively. We find that $\beta\approx\frac{1}{2}\alpha$, which is plotted as the solid line in Figure 3-5.

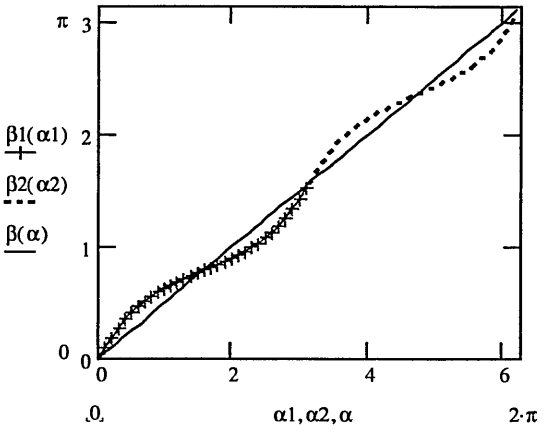

Figure 3-5 *the new principal axis $\vec{e}_1$ induced by the applied THz field is determined by the orientation of the applied THz field and the crystal symmetric axis c. β_1 and β_2 are the calculated results based on equation (6) when $\alpha_1=[0,\pi]$ and $\alpha_2=[\pi,2\pi]$, respectively. Here, β is the fitted curve and $\beta=\alpha/2$.*

The crystal acts as a waveplate with phase retardation given by Eq. 3-7, where L is the length of the crystal.

$$\Delta\varphi = 2\pi\frac{L\Delta n}{\lambda} = \frac{2\pi L}{\lambda}\frac{n_0^3}{2}(v_1-v_2) = \pi\frac{L}{\lambda}n_0^3 r_{41}E_0\sqrt{4-3\cos^2(\alpha)} = C\sqrt{4-3\cos^2(\alpha)} \qquad \textbf{Equation 3-7}$$

For ZnTe with L = 0.5 mm, n_0= 2.85, r_{41}= 4 pV/m, and at λ=150 μm, we have $C=\pi\frac{L}{\lambda}n_0^3 r_{41}E_0=0.182\times10^{-6}E_0$, with E_0 in V/m. When the crystal is rotated between fixed crossed polarisers and in a fixed external E-field, the induced waveplate effectively rotates over $\alpha+\beta\approx 3\alpha/2$, while the phase retardation varies between C and $2C$. If the crystal is rotated by 2π, then effectively the angle between the applied E-field and the new principle axis ($\vec{e}_1$) of the crystal will be 3π. As the crystal acts like a waveplate, it repeats its maximum transmission for a rotation of the $\vec{e}_1$ axis over $\pi/2$. This occurs for a rotation of the crystal over $\pi/3$, giving rise to the six-fold transmission pattern. Furthermore,

since the maximum phase retardation varies between C and $2C$, one will expect an amplitude modulation on the six-fold pattern.

3.4 Rotating the crystal

The intensity of the EO signal depends on many factors: the intensity of the applied E-field given by C, the relative orientation of the field and the crystal given by α, and the angle between the direction of the linear polarizer and the polarisation direction of the E-field given by θ. Intensity transmission of the probe beam through a polarizer/ waveplate/ analyser combination is given by:

$$I(C,\alpha,\beta,\theta) = D^2(C,\alpha,\beta,\theta) \qquad \textbf{Equation 3-8}$$

where

$$D(C,\alpha,\beta,\theta) = \frac{1}{\sqrt{2}}\sin[2(\theta-(\alpha+\beta))]\times\sqrt{1-\cos(\Delta\varphi)} \qquad \textbf{Equation 3-9}$$

Since $\beta = \alpha/2$, then

$$D(C,\alpha,\theta) = \sin(2\theta-3\alpha)\times\sin(\frac{\Delta\varphi}{2}) \qquad \textbf{Equation 3-10}$$

Therefore one can clearly see here that the electro-optical effect induced by Terahertz radiation strongly depends on the following factors: Firstly, the refraction index n of the crystal, its electro-optical coefficient r_{41} and the amplitude of the electrical filed of the THz beam. As $C = \pi\frac{L}{\lambda}n_0{}^3 r_{41}E_0$, when $C \le 2.0$, those factors will mainly determine the amplitude of the electro-optical signal, but not the shapes of the curve (six-fold pattern) of the orientation dependence of the THz detection efficiency.

Figure 3-6 shows results of the calculated transmitted intensity of the probe laser while the ZnTe crystal is rotated between the crossed polarisers. An external electric field is applied parallel to the probe polarisation direction, with increasing field strength for the diagrams (a) to (c), so that the parameter C equals 0.1, 1.0, and 2.0, respectively. The latter corresponds to field strength of 11 MV/m and a 0.5-mm-thick ZnTe crystal. Such field strengths have been attained in an FEL pulse of 5 μJ in 10 ps focused to a 1.5-mm-diameter spot. If C is big enough to make the phase retardation larger than 90^0, then the pattern becomes more complicated.

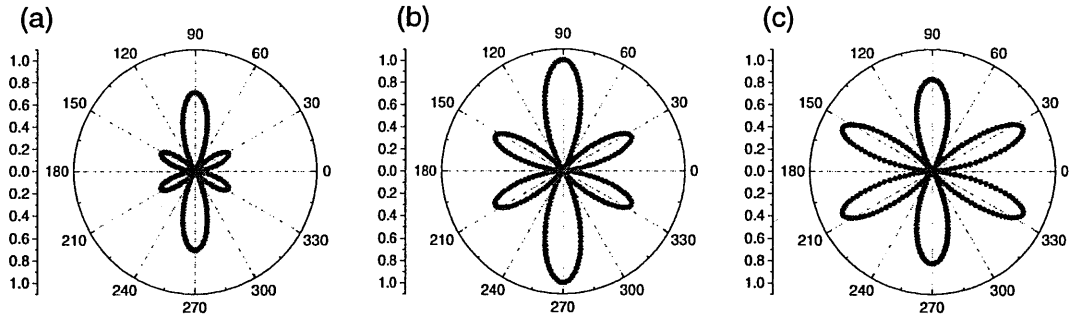

Figure 3-6 *Variation of the transmitted intensity of the EO signal while the crystal is rotated between crossed polarizers. An electric field is applied parallel to the polarization direction of the probe beam, with field strength increasing for the diagrams (a) C=0.1 (E_{fel}=0.55 MV/m), (b) C=1.0 (E_{fel}= 5.5 MV/m) and (c) C=2.0 (E_{fel}=11MV/m) respectively.*

Secondly, the angle between the direction of the linear polarizer (or the polarisation of the probing Ti:S laser) and the polarisation direction of the E-field of the THz beam, which is defined by θ. From equation 3-7 and equation 3-10, we know there is no difference between the intensity of the electro-optical signals measured at $\theta=0^0$ and $\theta=90^0$. While using a balanced detector, which gives signals proportional to the electrical field, we will expect to get signals at the detector with a phase difference of 90 degrees. Figure 3-7 shows the calculated results, where in (a) to (c) the electric field of FEL is set to be perpendicular, at 45 degrees and parallel to the polarisation of the probe beam.

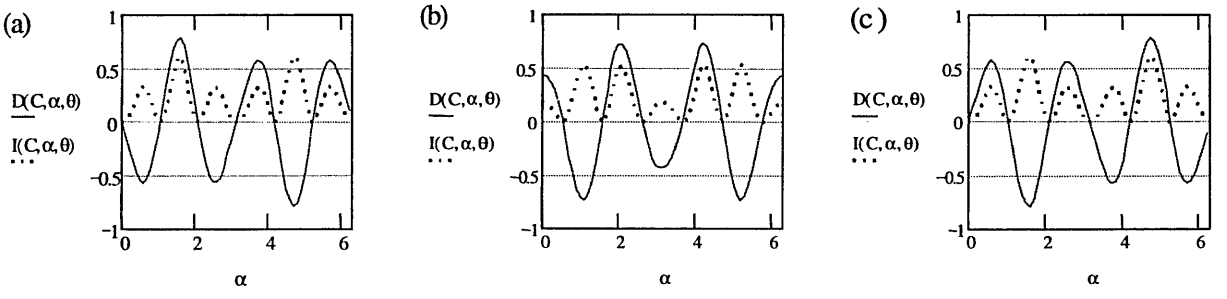

Figure 3-7 *Transmitted intensity of the EO signal vs. rotation angle for three polarisation settings of the FEL field. The polarisation direction of the electric field of FEL is (a) parallel (θ=0), (b) at 45 degrees (θ=π/4) and (c) perpendicular (θ=π/2) to the polarisation of the probe beam.*

Further investigations of equation 3-7 and equation 3-10 show that rotating the angle of the polarizer to the THz E-field can also change the ratio between the six-folded peaks. If $\theta \neq k\pi/4$ (k=0,±1,...), then the ratio varies accordingly. Figure 3-8 shows the calculation results for the experiment shown in Figure 3-3, which responds to an angle of $\theta=107.2^0$.

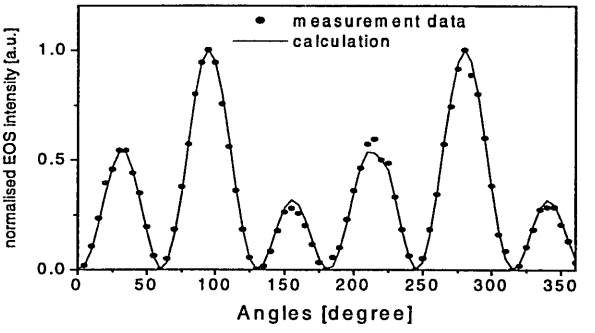

Figure 3-8 *Calculated transmission pattern corresponding to experimental observed pattern of Fig. 2-2. The angle between the E_0 field and the probe polarisation is set equal to 107.2^0.*

3.5 Conclusion

In conclusion, we observed a six-fold symmetry in the transmitted intensity of the electro-optic signal versus the rotation angle of the sensor ZnTe <110>. Calculations for the transmission of the EO signal agreed with experimental results obtained at 150-μm wavelength. The optimal angles for the maximum EO sampling signal are the following: The electric field direction of the THz beam is applied in the crystal <110> plane with an angle $\alpha=\pi/2+k\pi$ (k=0,±1,..) to the principal axis *c* of the crystal, while the probe beam should be linearly polarised by the polarizer whose preferred direction is at an angle $\theta=k\pi/2$ (k=0,±1,..) to the polarisation direction of the applied E-field.

One should note that this six-fold orientation dependency of electro-optical signal is valid for all THz frequencies. From Eq. 3-7 and Eq.3-10, one can see that the frequency dependent values of refractive index and the electro-optical coefficient r_{41} of ZnTe crystal only determine amplitude of the measured electro-optical signal, but not the shape of the curve of the angle dependence of the THz detection efficiency. Although we did the measurement and calculation for ZnTe, the calculations apply to the crystal of the same structure (eg. other zincblende crystals, such as GaP). The similar results were also presented in Dr. P. Planken's paper [12], but our work had been done independently and in fact preceded to his paper.

3.6 Reference:

[1] P.R. Smith, D.H. Auston and M.C. Nuss, IEEE J. Quantum Electron. **24**, 255 (1988).

[2] B.I. Greene, J.F. Federici etc. Appl. Phys. Lett. **59,** 893 (1991).

[3] A. Nahata etc. Appl. Phys. Lett. **68**, 150 (1996).

[4] Q. Wu and X. C. Zhang, Appl. Phys. Lett. **67,** 3523 (1995).

[5] P. Uhd Jepsen etc. Phys. Rev. E **53**, R3052 (1996)

[6] C.C. Davis, *Lasers and electro-optics: fundamentals and engineering* (Cambridge University Press, 1996), p. 472.

[7] K.P. Cheung and D.H. Auston,, Infrared Phys. **26**, 23 (1985).

[8] A. Leitenstorfer, S. Hunsche, J. Shah, M.C. Nuss, Appl. Phys. Lett. **74**, 1516 (1999).

[9] D. Oepts, A.F.G. van der Meer and P.W. van Amersfoort, Infrared Phys. Technol. **36**, 297 (1995).

[10] Q. Wu and X.-C. Zhang, Appl. Phys. Lett. **68**, 1604 (1996).

[11] Q. Wu, M. Litz, and X.C. Zhang, Appl. Phys. Lett. **68**, 2924 (1996).

[12] P.C.M. Planken, H-K. Nienhuys, H.J. Bakker, W.T. Wenckebach, J. Opt. Soc. Am. B, Vol. **18** Issue 3, 313 (2001)

Chapter 4 Generation and complete electric-field characterisation of intense ultra-short tuneable far-infrared laser pulses

Abstract

Intense, rapidly tuneable, picosecond laser pulses have been generated in the far infrared from 30 to 250 μm, a range not well covered by other sources. The transform-limited, diffraction-limited pulses have energies of up to 17 μJ, peak power of more than 1 MW, a length of only 18 optical periods, and focused intensities of 0.1 GW/cm^2. Measurements of both the optical field amplitude and the phase have been performed at 150 μm with electro-optical detection technique probing the field induced birefringence in ZnTe with an actively synchronised ultra-short Ti:Sapphire laser. The shortest optical pulse observed at 150 μm has a length of only 18 optical field cycles at FWHM of its intensity profile.

4.1 Introduction

Free-electron lasers are well established as a versatile source of high-intensity rapidly tuneable laser radiation in wavelength ranges where other laser sources are scarce. In particular, the mid-to-far-infrared part of the spectrum (3-1000 μm) can conveniently be covered by FELs because of the rather modest requirements on the accelerator that provides the electron beam. This has led to the development of several international infrared FEL facilities that serve a broad range of scientific users [1,2,3,4,5,6,7,8]. FELs produce high pulse energies in transform-limited pulses of variable bandwidth, in strong contrast to the weak broadband Terahertz (THz) radiation sources [9] that are pumped by Ti:Sapphire (Ti:S) femto-second laser systems.

A key feature of the new FEL, constructed at the Free-Electron Laser for Infrared eXperiments facility FELIX [10], is that it operates at long wavelengths (30-250 μm) with short electron pulses (0.3 mm rms.). A characteristic parameter is the longitudinal decoupling parameter μ_c, which is the ratio between the slippage distance L_s ($L_s = N_u\lambda$, where N_u is the number of undulator periods, and λ is the laser wavelength) and the (rms) electron bunch length σ_e. In our case, μ_c ranges from 4-30, while the largest value used in other FELs is $\mu_c \approx 2.2$. The slippage distance is the difference between the distances travelled by an electron and an optical wavefront, respectively, during the electron's transit through the undulator. It is also the range over which transients due to

the electron pulse edges influence the optical pulse. The operation of a short-pulse, large-slippage FEL oscillator is sensitive to the synchronism between the optical pulses circulating in the laser cavity and the injected electron pulses. The cavity detuning ΔL, i.e. the difference between the actual cavity length and the synchronous length for which the round-trip time of the optical wave exactly matches the electron repetition interval, is an important parameter in the FEL interaction dynamics (see chapter 1 for details). The formation of the optical pulses in an FEL with large μ_c is a delicate balance between desynchronism, gain, and saturation. It is possible to generate optical pulses that are much shorter than L_s and therefore contain only a few cycles of the optical field. The laser behaviour at short optical pulse lengths and high intra-cavity powers has been demonstrated to scale according to superradiant scaling laws [11], related to the 'spiking' mode of operation that is observed for values of μ_c smaller than unity [12].

The design of the large-slippage free-electron laser has been reported elsewhere [13]. A one-dimensional waveguide is used to reduce the diffraction losses at long wavelengths. Some machine parameters are summarised in Table 4-1. This chapter describes the characterisation of the optical output of the newly build FEL, such as small-signal gain, cavity losses, pulse energy, beam quality, and focuses on the complete characterisation of the electric field amplitude and phase of the picosecond FEL IR pulses.

Table 4-1 *Parameters for the long-wavelength FELIX laser*

Electron energy	12-25 MeV
Peak current	50 A
Undulator Period	65 mm
Number of periods	38
Normalised vector potential	1.9 (rms,max)
Optical cavity length	6 m
Waveguide width	10 mm

4.2 FEL Pulse energy and gain

In Figure 4-1 (a) the measured pulse energy is shown as a function of the laser wavelength. The picosecond pulses (micropulses) arrive in a burst 5-10 μs long (macropulse) with a micropulse spacing of 1 ns (1 GHz repetition rate). The macropulses are repeated at 10 Hz, leading to an average power of a few hundred

milliwatts. Typically, 50-70% of the measured pulse energy is available for experiments since the beam has to be transported through an evacuated transport system containing up to 30 metal mirrors to the user area. In Figure 4-1 (b) the measured gross gain (solid dots) is plotted together with the calculated [13] gross gain (open dots) and is seen to agree fairly well. The solid triangles in Figure 4-1 (b) represent the measured roundtrip loss whereas the estimated roundtrip loss due to out-coupling through the hole in one of the end mirrors is indicated by a solid square. The roundtrip loss is calculated from an exponential fit to the ring-down at the end of the macropulse. For a reason that is not yet well understood the cavity loss increases more rapidly with wavelength than anticipated from calculations (no data points are given at longer wavelengths since the detector employed was not fast enough to measure cavity losses in excess of 16%). This is probably the cause of the rapid drop in the out-coupled pulse energy above 120 μm. Transverse beam size measurements have been performed, see Figure 4-1 (c), at 150-μm wavelength with a 2x2 inch pyro-electric array (LBA200, Spiricon). All measurements yield a clean symmetric beam profile and show diffraction-limited beam quality ($M^2 < 1.1$) [14].

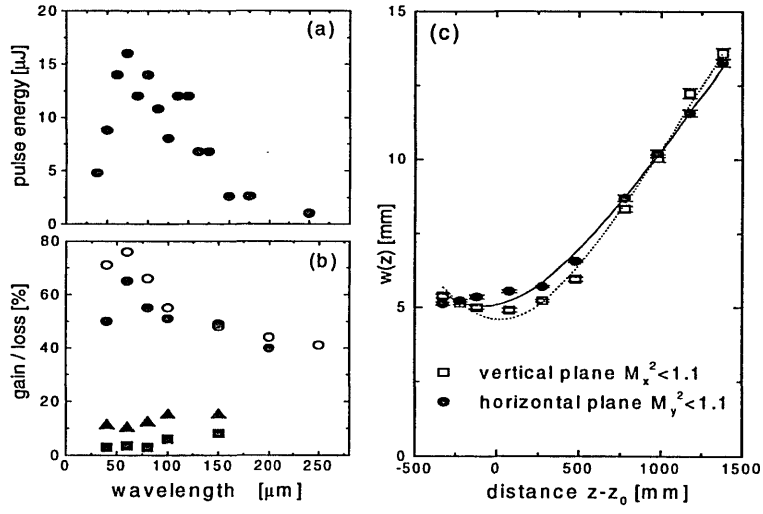

Figure 4-1. *The measured optical pulse energy versus wavelength at the outcoupler is shown in (a). The measured gross gain (solid dots) and calculated gain [13] (open dots) are shown in (b). The triangles are the measured cavity roundtrip loss, whereas the squares correspond to the estimated contribution of the out-coupling to the roundtrip loss. Fig. (c) shows the Gaussian spot size variation at 150-μm wavelength when the laser beam is weakly focussed for both the horizontal (solid dots) and vertical plane (open squares). The fits (solid line for the horizontal plane and dotted line for the vertical plane) indicate a diffraction-limited beam.*

4.3 FEL Pulse duration and shape

4.3.1 Two types of detector

To study the optical pulse duration and shape we adapted a cross-correlation technique frequently used to characterise other THz sources [15]. The technique probes the electric-field-induced birefringence in a linear electro-optic (EO) crystal with a laser at visible (or near-infrared) frequencies. ZnTe is an ideal EO-crystal because of its good optical properties at the probing Ti:S frequency as well as at THz frequencies. The set-up used in our experiment is shown schematically in Figure 4-2. The Ti:Sapphire laser, producing 3-nJ, 10-fs pulses at 100 MHz repetition rate (Femto Source Pro, Femto Lasers, Vienna), is actively synchronised to the FEL optical output and the total jitter between the two lasers is approx. 1 ps FWHM over a time scale of several minutes [16]. A polariser set the polarisation direction of the Ti:Sapphire laser by 90° with respect to the polarisation direction of the FEL laser. Both the Ti:Sapphire laser and the FEL laser normally incident into the (110) plane of a 500-μm thick ZnTe crystal (Uni-export, UK). The crystal is rotated such that its <001> axis is along the polarisation direction of the FEL laser. The FEL-induced birefringence in the EO-crystal causes a phase difference between the polarisation components of the propagating Ti:Sapphire pulse parallel and perpendicular to the new principle O-axis of the EO-crystal. This acquired phase difference $\Delta\varphi$ is proportional to the FEL's electric field strength E_{Fel} in the crystal*,

$$\Delta\varphi = \pi \frac{L}{\lambda} n_0^3 r_{41} E_{Fel} \sqrt{4 - 3\cos^2(\alpha)} \qquad \textbf{Equation 4-1}$$

where $L = 50\mu m$ is the thickness of the crystal, n_0= 2.85 is the original refractive index of the crystal, $r_{41} = 4pV/m$ is the electro-optical coefficient of ZnTe crystal, and $\lambda = 150\mu m$ is the wavelength of the incident FEL beam which has its polarisation direction in the (110) plane but with an angle α=0 to the <001> axis of the crystal. The phase retardation experienced by the Ti:Sapphire laser in the crystal causes its radiation to become elliptically polarised.

As shown in the experimental setup of the electro-optical detection, we can choose two different configurations of detection. Type (a) detector consists of a second polarizer and a fast silicon photodiode, and type (b) detector includes a quarter waveplate, a Wollaston prism and a balanced detector. From chapter 3 we know that the electro-optical signal passing through a combination of polariser/crystal/ analyser is denoted as:

* See chapter 3 for more information.

$$I_{EOS} \propto \sin^2(\frac{\Delta\varphi}{2}) \propto (\Delta\varphi)^2 \propto E_{Fel}^2 \propto P_{Fel} \qquad \textbf{Equation 4-2}$$

Therefore, for small phase retardation the intensity of the Ti:Sapphire radiation emerging from the second polarizer is proportional to the square of the electric field, i.e. the intensity of the FEL pulse, and this has been verified by power dependence measurements (see Figure 4-3). The intensity profile can be measured, with a temporal resolution limited by the jitter of 1 ps FWHM (400*fs* rms), by varying the optical delay between the Ti:Sapphire pulse and the FEL micropulse.

It is well known [15] that a more sensitive measurement of the EO-effect can be performed if the second polariser is replaced by the combination of a ¼-λ waveplate and a polarising beam splitter as shown in Figure 4-2 (b). The EO-signal can then be detected on two separate Si-diodes and the ¼-λ waveplate provides an optical bias so that the response of each diode for small phase retardation is proportional to the electric field strength instead of the intensity (see Figure 4-3).

$$I_{EOS-1} \propto \sin^2(\frac{\Delta\varphi}{2}+\frac{\pi}{4}) \propto \sin(\Delta\varphi) \propto E_{fel} \propto \sqrt{P_{fel}} \qquad \textbf{Equation 4-3}$$

$$I_{EOS-2} \propto \cos^2(\frac{\Delta\varphi}{2}+\frac{\pi}{4}) \propto \sin(\Delta\varphi) \propto E_{fel} \propto \sqrt{P_{fel}}$$

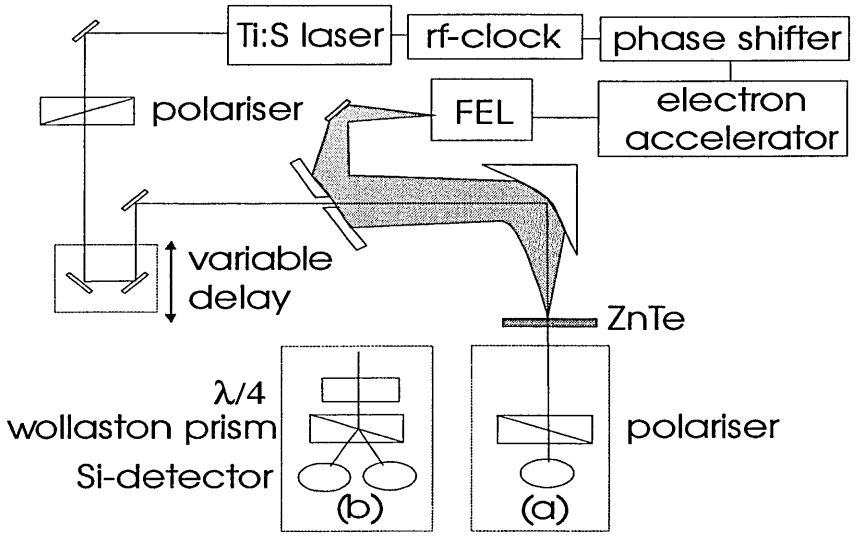

Figure 4-2. *The EO-cross-correlation set-up with two different detectors (a) and (b). In (a) the measured photodiode intensity is proportional to the FEL intensity. In (b) the measured photodiode intensity is proportional to the instantaneous electric field strength of the FEL pulse.*

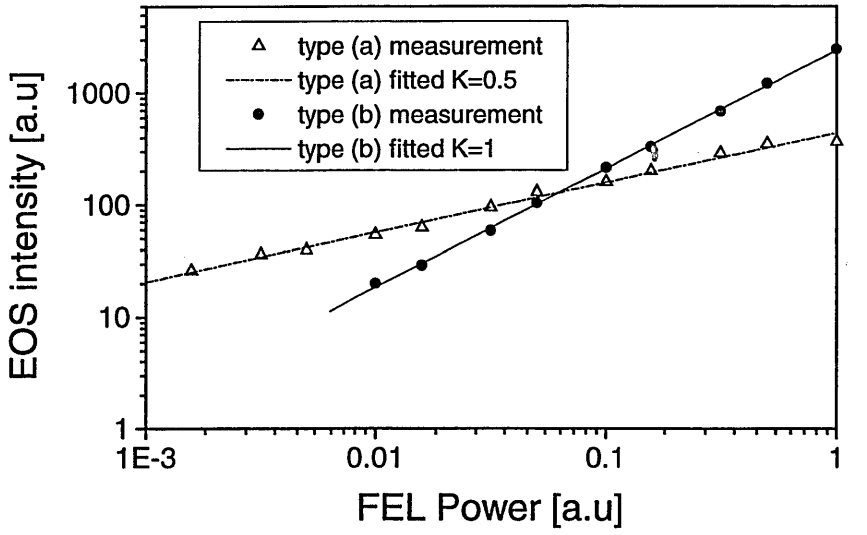

Figure 4-3 *Intensity of electro-optical signals (EOS) measured by type (a) detector is proportional to* ***square*** *of the applied field electric field* E_{Fel} *therefore is proportional to the power of FEL laser (K=1). While the EOS signals at type (b) detector is linearly proportional to the applied electric field* E_{Fel} *or to the square root of the FEL power (K=0.5).*

4.3.2 pulse duration measurements

Using type (a) detector shown in Figure 4-2, we perform a series of electro-optical measurements. Figure 4-4 shows the intensity profiles and power spectra (see insets) of the FEL micropulses at 150 μm wavelength and with cavity detunings ΔL of (a) -100 μm, (b) -300 μm, and (c) –600 μm. These measurements demonstrate that the FEL pulse length and shape are strongly influenced by the value of ΔL, and for large values of ΔL the optical pulse develops a leading edge that can be fitted well with an exponential [17]. Calculation of the time-bandwidth product for different cavity detunings gives values in the range of 0.2-0.3 when the pulse has a clear exponential leading edge, e.g. Figure 4-4 (b) and (c). In case of Figure 4-4 (a) the optical pulse shape is closer to a Gaussian and the time-bandwidth product is 0.6.

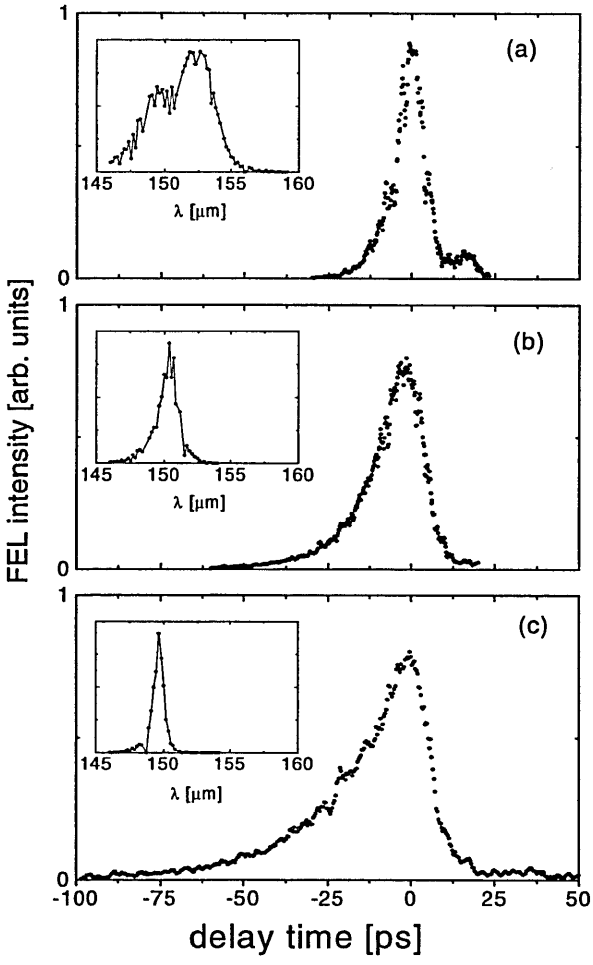

Figure 4-4. *Measured optical pulse shapes (a)-(c) using the EO-cross-correlation technique described in the text, and power spectra (insets) at 150-μm wavelength for ΔL of -100 μm (a), -300 μm (b), and -600 μm (c). The leading edge of the optical pulse (negative delay times) is exponential for large values of ΔL [17]. The time-bandwidth products are 0.59, 0.20 and 0.22 in (a)-(c) respectively.*

4.3.3 Phase sensitive measurements

Using type (b) detector shown in Figure 4-1, the response of the balanced detector is now proportional to the electric field strength instead of the intensity. A typical measurement where the signal from one macropulse of the FEL is taken at a fixed setting of the delay line is shown in Figure 4-5. The jitter between the Ti:S laser and the FEL is negligibly small on this fast time scale (the jitter is about 50 *fs* over a scanning time of 10 μs) and consequently we are dealing with two perfectly synchronised laser systems [18]. The Ti:S repetition frequency is phase-locked to the electron bunch repetition frequency, and therefore also to the FEL pulse

envelope roundtrip frequency (the FEL gain keeps the pulse envelope at the position of the electron bunches). This means that during the macropulse, the Ti:S pulse train samples the envelope of the circulating FEL micropulses at the same position. However, the phase of the FEL carrier wave shifts in each roundtrip with respect to the envelope by $\Delta\phi_{rel} = 2\pi \cdot 2\Delta L/\lambda$, depending on the applied cavity detuning. This relative phase shift leads to the beat signal observed in Figure 4-5, with frequency:

$$f_{beat} = \frac{-2\Delta L}{\lambda}\frac{c}{2L} \qquad \textbf{Equation 4-4}$$

Here L is the length of the cavity (6 m). When $\Delta L = k\lambda/2$ with integer k, the phase advance per roundtrip is just $k \cdot 2\pi$, and is indistinguishable from zero, and so the observed beat frequency is actually $f_{beat} \bmod (c/2L)$. The values of $\Delta L_k = k\lambda/2$ at which the observed beat frequency is zero, can be determined with an accuracy of about 0.5 μm, or a few parts-in-thousand of the laser wavelength. In a dispersionless cavity there is one exact synchronism position ($k = 0$). This position can be found by varying the wavelength, as ΔL_k is independent of λ only when $k = 0$. In our present case, the waveguide introduces noticeable dispersion, and the group velocity synchronism differs from the phase velocity synchronism. Taking this into account, it is still possible to determine the exact cavity length with high precision.

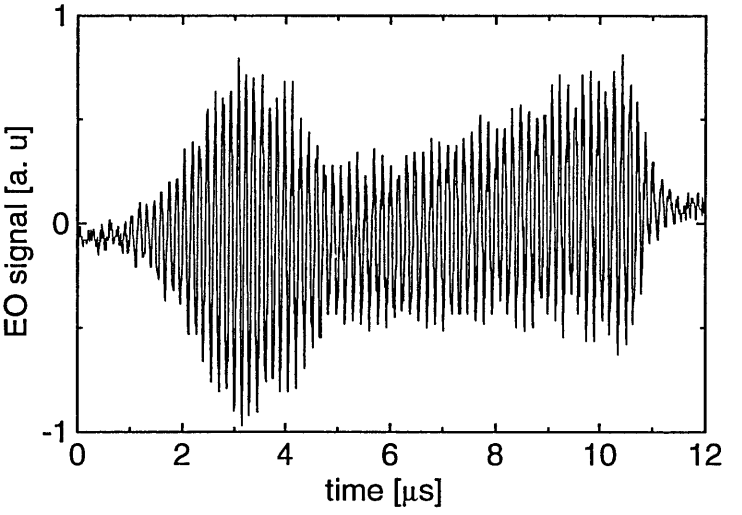

Figure 4-5 *EO-signal recorded during a macropulse with* $\Delta L = -20\mu m$. *The beat signal results from a phase shift per roundtrip* $2\pi \cdot 2\Delta L/\lambda$ *of the FEL carrier wave with respect to the Ti:Sapphire pulse train, causing the Ti:Sapphire pulses to sample different phases of the electric field cycles.*

4.3.4 Rapid scanning technique

The ability to measure the details of the electric field with this EO-detection method opens up the possibility of measuring the complete FEL pulse envelope profile including the individual electric field cycles, thereby completely characterising the optical output. The fact that the jitter between the Ti:S pulse train and the FEL pulse train is extremely small (~ 50 *fs*) during a macropulse also allows a high-temporal resolution measurement, provided that the delay between the Ti:S pulse and the FEL pulse can be scanned far enough during these few microseconds. This can be achieved by a so called rapid scanning technique, operating the FEL at a slightly different frequency from the Ti:S laser by switching the frequency of the rf-clock driving the accelerating structures of the FEL with a voltage-controlled rf-phase shifter. In view of the low duty factor of the FEL it is necessary to start this different frequency just before the FEL macropulse arrives and switching it back after the macropulse has passed. The frequency-switching technique has already been demonstrated in the past as a way of obtaining short and stable optical pulses [19], and is now adapted to rapidly scan the delay between the Ti:S laser pulses and the envelope and carrier wave of the FEL pulse.

The phase of the electron bunch, denoting as Φ, can be changed by the ramping voltage V_{rmp} applied to the rf-phase shifter. As we found in our measurement, if we apply a 10-V ramping-voltage to the rf-system, then the responding phase change of electron bunch is $\Delta\Phi = \pi/2$ at 1 GHz. If we define the ramping voltage as:

$$V_{rmp} = V_0 + S \cdot t \qquad \textbf{Equation 4-5}$$

where V_0 is the bias voltage, S is the ramping slope, and t is the time that ramping voltage is applied on the rf-system. The phase of the electron bunch will be changed as a function of the ramping voltage:

$$\Phi = \Phi_0 + \frac{\pi}{20} \cdot V_{rmp} = \Phi_0 + \frac{\pi}{20} \cdot V_0 + \frac{\pi}{20} \cdot S \cdot t \qquad \textbf{Equation 4-6}$$

As we know that the accelerating field of electron pulses is a cosine wave:

$$Cos(2\pi f \cdot t + \Phi) = Cos(2\pi f \cdot t + \Phi_0 + \frac{\pi}{20} \cdot V_0 + \frac{\pi}{20} \cdot S \cdot t) = Cos(2\pi f' \cdot t + \Phi_0') \qquad \textbf{Equation 4-7}$$

Here $\Phi_0' = \Phi_0 + V_0 \times \pi/20$ and $f' = f + S/40$, therefore we have

$$\Delta f = \frac{S}{40} \qquad \textbf{Equation 4-8}$$

The envelope of FEL micropulses now has the same phase advance as the electron bunch, since the gain keeps it at the same position in the electron bunch. While the Ti:Sapphire laser will not follow the change in its repetition frequency, because its PZT driver has slow mechanical response time of a few milliseconds (see Chapter 2 for detail). Meanwhile, if the carrier wave of the FEL micropulse can run at the same speed as its envelope, then the carrier wave will stand still with respect to its envelope and results in a correct beat frequency of the EO-signal at the detector.

Denoting the "normal" cavity length and the electron bunch repetition frequency as L and f (for which combination the cavity is perfectly synchronised), respectively, we straightforwardly find that the desynchronism ΔL normalised to the normal cavity length L is:

$$\frac{\Delta L}{L} = \frac{\Delta f}{f} \qquad \textbf{Equation 4-9}$$

where ΔL and Δf denote a small deviation from the nominal values. Hence a cavity length desynchronisation ΔL has the same effect as a frequency detuning of the electron bunch arrival rate $\Delta f = f\,\Delta L/L$. By applying a suitable ramping voltage to the rf-system of the FEL, The carrier wave now has the same speed as its envelope, and the FEL is effectively running at a perfect synchronised cavity length. From Eq. 4-8 and Eq. 4-9, we find the slope of the ramping voltage:

$$S = \frac{\Delta L}{L} \cdot 40 f \qquad \textbf{Equation 4-10}$$

For example, when FEL is running at $f = 1\ GHz$, the normal cavity length is 6 m, and the detuning length is $L = 20\mu m$, then the slope of the ramping voltage should be set to S=0.133 V/μs. In the rapid scanning measurement, the FEL cavity length has to be set such that: (1) the cavity detuning has the correct value for the shifted rf-clock frequency, (2) the scanning speed of the FEL micropulse over the Ti:Sapphire pulse is fast enough to obtain the complete profile of the FEL micropulse.

4.3.5 Electric field profile of the FEL pulse

Figure 4-6 shows a measurement of the electric field profile of a micropulse using this rapid-scanning technique. A frequency offset of 3 ppm is applied just before the beginning of the macropulse. This results in a

speed of 0.133 ps/roundtrip, equivalent to 3.3 ps/μs, at which the Ti:S pulse train and the FEL pulse train sweep over each other. Provided that the effective FEL cavity detuning is equal to kλ/2, and under-sampling in the data-acquisition is avoided, the observed beat signal corresponds to the FEL electric field cycles. Therefore, Figure 4-6 is the electric field profile of an FEL micropulse lasing at $\Delta L = 0$ μm. Since the technique acquires the trace within one macropulse, it is only a relevant measurement if the micropulse shape does not change significantly during the macropulse. We have indications that this condition is sufficiently well fulfilled in our case. The observed number of cycles at the fwhm is 26, corresponding to only 18 optical cycles fwhm of the intensity profile.

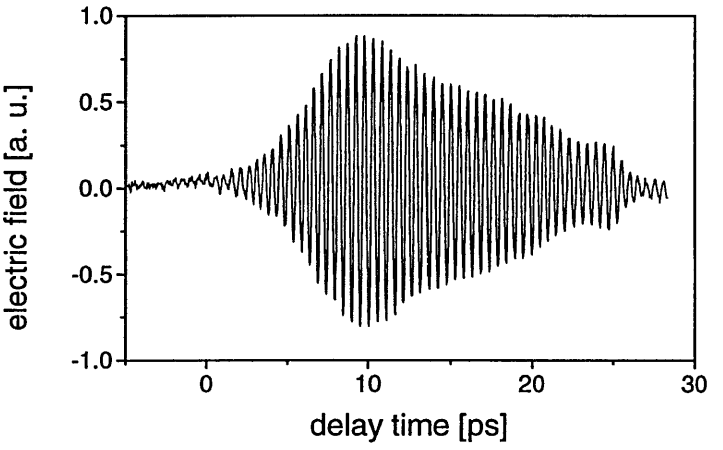

Figure 4-6. *The micropulse electric field profile of the FEL pulse is shown (see text for details).*

4.4 Conclusions

We have generated intense picosecond far-infrared laser pulses from 30-250 μm in a waveguide free-electron laser. The shortest pulses observed at 150-μm have a length of only 18 optical field cycles at the fwhm of the intensity profile. The combination of short pulse duration, high pulse energy, and diffraction-limited beam quality leads to unprecedented power densities of up to 0.1 GW/cm^2, allowing non-linear experiments in a wide range of the far-infrared spectrum. The electric field profile of the optical pulses has been characterised with a rapid-scanning cross-correlation technique with an actively synchronised 10-fs Ti:S laser. This technique allows complete characterisation of the optical output as well as accurate experimental determination of one of the most important parameters for free-electron lasers, the absolute cavity detuning.

4.5 References:

[1] G. Ramian, Nucl. Instrum, & Methods **A318**, 225 (1992).

[2] T.I. Smith et al., Nucl. Instrum. & Methods **A304**, 812 (1992).

[3] K. Imasaki *et al.* Nucl. Instrum. Methods Phys. Res., **A318**, 235 (1992).

[4] R. Prazeres et al., Nucl. Instrum. & Methods **A358**, 212 (1995).

[5] F. Ciocci et al., Phys. Rev. Lett. **70**, 928 (1993).

[6] D. Oepts, A.F.G. van der Meer and P.W. van Amersfoort, Infrared Phys. Technol. **36**, 297 (1995).

[7] W.B. Colson, Nucl. Instrum. Methods Phys. Res., **A429**, 37-40 (1999).

[8] T.Tomimasu et al., Nucl. Instrum. & Methods **B144**, 1 (1998).

[9] D. You et al., Opt. Lett. **18**, 290 (1993).

[10] D. Oepts et al., Infrared. Phys. Technol. **36**, 297(1995).

[11] D.A. Jaroszynski et al., Phys. Rev. Lett. **78**, 1699 (1997).

[12] R.W. Warren et al., Nucl. Instrum. & Methods **A250**, 19 (1986).

[13] L. Lin et al., Rev. Sci. Instrum. **68**, 4342 (1997).

[14] A.E. Siegman, Proceedings SPIE **1224**, 2 (1990).

[15] J.A. Valdmanis et al., Appl. Phys. Lett. **41**, 211 (1982).

[16] G.M.H. Knippels et al., Opt. Lett. **23**, 1754 (1998).

[17] This has been measured previously at the Stanford facility at a much shorter FEL wavelength of 6.3 μm, see C.W. Rella et al., Opt. Commun. **157**, 335 (1998).

[18] A. Poppe et al., IEEE J. Quantum Electron. **4**, 179 (1998).

[19] R.J. Bakker et al., Phys. Rev. E **48**, R3256 (1993).

Chapter 5 Formation of low time-bandwidth product, single-sided exponential optical pulses in free-electron laser oscillators

Abstract

The detailed shape of picosecond optical pulses from a free-electron laser (FEL) oscillator has been studied for various cavity detunings. For large values of the cavity detuning the optical pulse develops an exponential leading edge, with a time constant proportional to the applied cavity detuning and the quality factor of the resonator. This behaviour has been observed at two separate FELs that have completely different resonator layouts and electron beam characteristics, and using different methods of optical pulse length measurement. The optical pulses have a full width at half maximum time-bandwidth product $\Delta t_{FWHM} \cdot \Delta f_{FWHM}$ of 0.2–0.3. The results presented here can be used to predict the optical pulse length and corresponding minimum spectral width that can be generated in a FEL pumped by short electron bunches. This is important for the design of new infrared free-electron laser user facilities, which need to make a balanced choice between short pulses for high temporal resolution and narrow bandwidth for linear and non-linear spectroscopy.

5.1 Introduction

FELs, operating over a large range of wavelengths and optical pulse lengths, have proved to be extremely useful for many experiments, especially in the mid- and far-infrared (3-1000 μm), and several international infrared user facilities have been constructed to exploit this [1,2,3,4,5,6,7,8]. Although competition from solid-state laser systems, such as Ti:Sapphire laser pumped optical parametric generators is strong at the shorter wavelengths, the FEL has the unique capability of allowing the user to select the appropriate optical pulse duration – or spectral width – for the experiment under investigation. This feature, combined with the high optical pulse energy, Fourier-transform limited spectrum, and diffraction-limited beam quality makes the FEL an indispensable tool for linear and non-linear spectroscopy and experiments requiring high temporal resolution. Variable bandwidth pulses from the FELIX laser were used to systematically characterise the dynamics of the

local vibrational modes of hydrogen (H^+) in CaF_2 [9]. First, a narrow laser bandwidth was used to investigate the dynamics (lifetime and dephasing) of the lowest excited state. Then, by increasing the bandwidth, additional states of the enharmonic ladder were included in the excitation, leading to quantum beating between the multiple excited states. Flexibility in the laser bandwidth enabled a clearer picture of the vibrational dynamics.

Previous characterisations of the optical output of FELs operating in the infrared part of the spectrum have been limited to intensity autocorrelation measurements, with the noticeable exceptions of FROG measurements at Stanford [10], and experiments using a novel Rydberg atom based streak camera at (far-)infrared wavelengths [11]. The intensity autocorrelation measurements yield no information on possible asymmetries in the optical pulse, and, indeed, little information about the exact shape of the pulse is obtained: only its duration can be estimated. In this paper we describe results from a series of pulse shape measurements, obtained by cross-correlating the FEL pulse with an ultra-short Ti:Sapphire laser pulse. In these experiments detailed information is obtained about the shape of the pulse, and under certain conditions highly asymmetric optical pulses have been observed.

The experiments described in this chapter consist of two parts: one was performed on the mid-infrared FEL of the Stanford Picosecond Free-Electron Laser Centre [12] *, and one was performed on the long wavelength FEL of the FELIX facility in The Netherlands [13]. Both the infrared FEL facilities in Stanford and the Netherlands were designed to serve an international community of users from a wide range of scientific areas. Although the goals of the two facilities are very similar, there are significant technical differences between the FELs. The laser at Stanford is pumped by an electron beam from a superconducting linear accelerator (linac) and the laser cavity consists of highly reflecting dielectric mirrors, while FELIX uses normal conducting rf-linacs and operates with an intra-undulator waveguide and copper mirrors. It is therefore interesting to make a detailed comparison between the optical outputs of the two lasers. A summary of the relevant machine parameters for the two FELs is given in Table 5-1.

* The author gratefully acknowledges the data provided by the Stanford FEL group.

Table 5-1. *Overview of accelerator and laser parameters for the measurements taken at the two different FELs*

	Stanford mid-IR FEL	**FELIX far-IR FEL**
Accelerator parameters	**super conducting**	**normal conducting**
RF-frequency [MHz]	1300	3000
Electron bunch freq. [MHz]	11.8	1000
Charge per bunch [pC]	17	200
Bunch length (rms) [ps]	1.0	0.7
Beam energy [MeV]	32	13.1
Norm. emittance [10^{-6} π rad]	8	70
Energy spread (rms) [%]	0.1	0.2
Laser parameters		
Wavelength [μm]	6.3	150
Micropulse length (FWHM) [ps]	3-7	1-30
Micropulse energy [μJ]	2	17
Micropulse rep. rate [MHz]	11.8	1000
Macropulse duration [μs]	5000	10
Macropulse rep. rate [Hz]	20	10
Cavity length [m]	12.7	6.0
Cavity roundtrip loss [%]	<1	20
Undulator period [mm]	31	65
Number of periods	72	38

Two main optical pulse length measurement techniques were used: differential optical gating measurements [[14]] (see chapter 2), and electro-optic cross-correlation (see chapter 3). In the following sections, the experiments at Stanford and at FELIX are described. At Stanford, the DOG technique is needed, as the synchronisation between the probing Ti:Sapphire laser and the FEL laser is poor. While the electro-optical sampling technique is adopted at FELIX, since the jitter is only about 400 *fs* (rms) over a scanning time of 2 minutes, the jitter can be even reduced to 50 *fs* by using a rapid scanning technique. We analysed both sets of

data and the experimental data are compared to the results of a 1-D computer model that includes the effects of slippage and short electron bunches [15,16].

5.2 Experiments at the Stanford Mid-IR FEL

The experiments at the Stanford facility were performed at a central laser wavelength of 6.3 μm, where the absence of strong atmospheric absorption ensures that there is no temporal distortion of the optical pulse. The cross-correlation measurements of the FEL intensity using a 60-fs Ti:Sapphire laser (Tsunami, Spectra Physics, Mountain View, CA, USA) were obtained using the differential optical gating technique to enhance the temporal resolution. The details of the technique are described in Ref. 7 (see also chapter 2). Here we will limit ourselves to a short description.

A schematic diagram of the experimental set-up is shown in Figure 5-1. The Ti:Sapphire (gate) beam is split into two arms, one of which is delayed with respect to the other by a known amount δ. In both arms the FEL beam and the gate co-propagate through a $AgGaS_2$ crystal and the corresponding sum-frequency signals are detected by silicon diodes. The essence of the technique is that although the FEL pulses and the Ti:Sapphire gating pulses are imperfectly synchronised (jitter in the system at Stanford has been measured to be of the order of 2 ps [17]) it is possible, by means of an optical delay, to make two closely-spaced cross-correlation measurements separated by a time interval – δ in Figure 5-1– that is well defined. The precise time at which each such pair of measurements is made is, by definition, uncertain; but each pair can be used to provide accurate estimates of both the average value and the time derivative of the pulse shape at the (unknown) time of measurement. By accumulating, in successive pulses, values of the FEL pulse shape and its derivative at different – and still unknown – times throughout the pulse, a phase-space representation of the pulse is obtained from which its form, as a function of time, can be reconstructed.

The normal FEL resonator at Stanford consists of dielectric mirrors on ZnSe substrates, with a high reflector (R>99.5%), and an out-coupler (R=97.5%, 2% out-coupled). For the purpose of this experiment the out-coupler was replaced with another high reflector and measurements were made on the small fraction (<0.5%) out-coupled from it. The reduced losses allow the FEL to operate over a larger range of cavity detunings and allow the formation of longer optical micropulses.

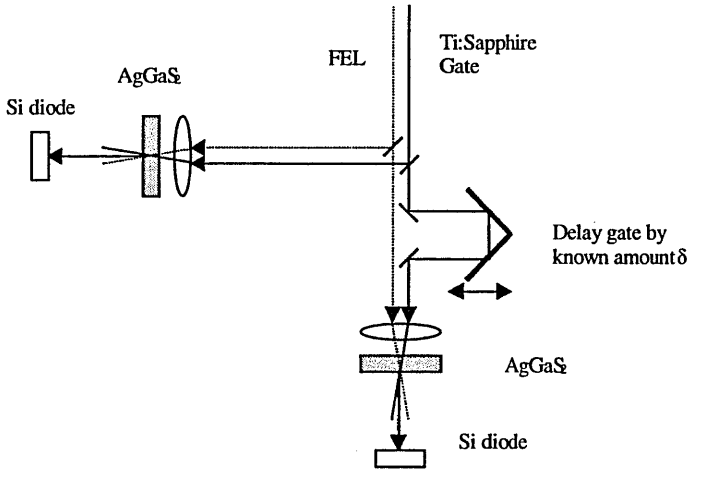

Figure 5-1. *Schematic of the experimental set-up for Differential Optical Gating [14] at a wavelength of 6.3 μm. The Ti:Sapphire (gate) beam is split into two arms, one of which is delayed with respect to the other by a known amount δ. In both arms the FEL beam and the gate beam co-propagate through a $AgGaS_2$ crystal and the corresponding sum-frequency signals are detected by silicon diodes.*

5.3 Experiments at FELIX

For the experiments performed at FELIX, cross-correlation with a 10 fs Ti:Sapphire laser (Femto Source Pro HP, Femto Lasers, Vienna, Austria) was used. Pulse shape measurements were performed at a wavelength of 150 μm in the wave-guide far-IR FEL by means of electro-optic detection [18] in a ZnTe crystal. Since the jitter between the Ti:Sapphire laser and the FELIX FELs is only 400 fs (rms) on a time-scale of several minutes [19] and the optical pulse lengths at 150 μm are several picoseconds, the shape of the micropulses could simply be recorded by scanning the delay between the FEL and the Ti:Sapphire laser pulse trains. A diagram of the experimental setup is shown in Figure 5-2 and the method is described in more detail elsewhere [20]. The optical power spectrum is recorded in the evacuated diagnostic station with a spectrometer equipped with a 48-channel pyro-electric array [21].

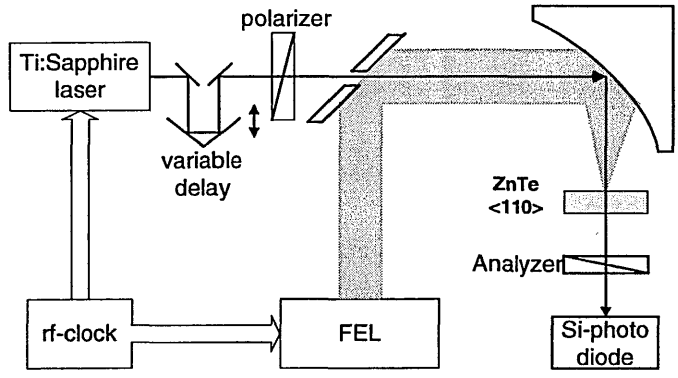

Figure 5-2. *Schematic of the electro-optic cross-correlation set-up. The FEL-induced birefringence in a ZnTe crystal is probed with a synchronised Ti:Sapphire laser. A Si-photodiode measures the Ti:Sapphire intensity passing through a pair of crossed polarisers.*

5.4 Discussion

5.4.1 Exponential rising edge of the optical pulses

Figure 5-3 shows measurements of the optical pulse, taken on the Stanford FEL at a central wavelength of 6.3 μm, and at three different settings of the cavity detuning: ΔL = -7.65 μm (dotted line), -4.9 μm (solid line), and -1.65 μm (dash-dot line). The pulses are clearly asymmetrical and the semi-logarithmic plot of the data at in the inset (for ΔL= -7.65 μm) shows that the rising edge is an exponential with a time constant of 4.45 ps, while the falling edge is a Gaussian with FWHM = 2.3 ps. Data taken at FELIX, at a wavelength of 150 μm and at detunings ΔL= -100 μm (a), -300 μm (b) and -600 μm (c), shown in Figure 5-6, show similar exponential rising edges.

The exponential nature of the edge may be understood as follows. This is in fact the *leading* edge of the optical pulse, propagating in a cavity where the losses, characterised by the constant α, reduce the pulse intensity by a factor $e^{-\alpha}$ in each round trip. In a perfectly synchronised FEL cavity, at saturation, the position of the leading edge of the optical pulse remains fixed with respect to the electron bunches at the start of successive round trips. When the FEL cavity is shortened by an amount ΔL, as in the cases described in this chapter, the optical pulse moves ahead of the electron bunch by a distance $2\Delta L$ in each round trip. The front part of the optical pulse then decays from round trip to round trip because it has lost contact with the gain medium. In one

round trip, the intensity at a point in this part of the pulse is reduced by a factor $e^{-\alpha}$, and in the same round trip the pulse is advanced with respect to the new electron bunch by an amount $\Delta t = \frac{2\Delta L}{c}$, so that a steady state develops in which the pulse profile in this region shows a time dependence $e^{\frac{c\alpha t}{2\Delta L}}$ i.e. with a time constant of $\tau = \frac{2\Delta L}{\alpha c} = \left(\frac{2\lambda}{\alpha c}\right)\frac{\Delta L}{\lambda}$. This effect was previously noted by Colson [15], although there appears to be a factor of two discrepancy with the expression used in this paper.

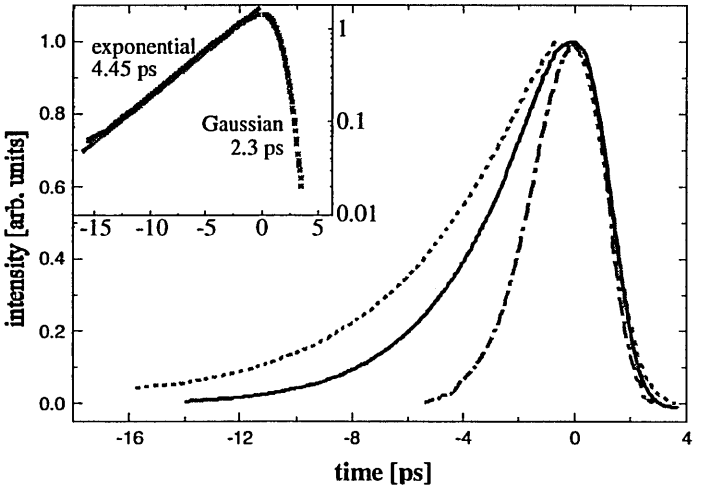

Figure 5-3. *FEL pulse shape as measured at three different settings of the cavity detuning: -7.65 μm (dotted line), -4.9 μm (solid line), and -1.65 μm (dash-dot line). The inset shows the pulse generated at -7.65 μm in a semi-logarithmic format together with a fit to an exponential on the rising edge.*

5.4.2 Cavity desynchronism and exponential time constants of the rising edge of the pulse

The data from both FELs exhibit this behaviour as shown in Figure 5-4, which shows graphs of the measured value of the leading edge time constant, τ, against the normalised cavity detuning, $\Delta L/\lambda$ together with values calculated from simulations of the micropulse evolution. Simulations were performed using a 1-D code [15,16] that, in the case of FELIX only, had been modified to take account of the waveguide in FEL-1. In both cases the simulations used values for the parameter α obtained from independent cavity ring-down measurements. Figure 5-5, which is typical of a comparison between the measured and simulated pulse shapes for FELIX, shows that the 1-D code is able to reproduce the optical pulse shape accurately – in this case at a detuning of -300 μm. The results from Stanford are shown in Figure 5-4(a): the experimental data are plotted as

solid squares that are seen to follow the expected linear relationship; the results of the simulations are shown as a dashed line; and the least squares fit to the experimental data is shown as a solid line with a slope of 4.4 ps ± 10%. The argument presented in the preceding paragraph gives $2\lambda/\alpha c = 4.6\text{ps}$ for $\lambda = 6.3$ μm and $\alpha = 0.0091$ (corresponding to a measured cavity $Q \approx 1/\alpha$ of 110). Figure 5-4(b) presents the FELIX data (solid squares), a best fit line (solid) of slope 4.5 ps ± 6%, and the time constants obtained from the simulations (dashed line). In this case $2\lambda/\alpha c = 4.8\text{ps}$ for $\lambda = 150$ μm and $\alpha = 0.21$ (obtained from independent measurements of the cavity ring-down time) showing that the optical pulses have again evolved an exponential leading edge consistent with the mechanism described above. It is invariably difficult to determine the exact point of zero detuning, however this offset may be deduced from the requirement that the graphs of τ against $\Delta L/\lambda$ pass through the origin: the FELIX data required the addition of 0.6λ to the recorded values; no adjustment was made to the Stanford data.

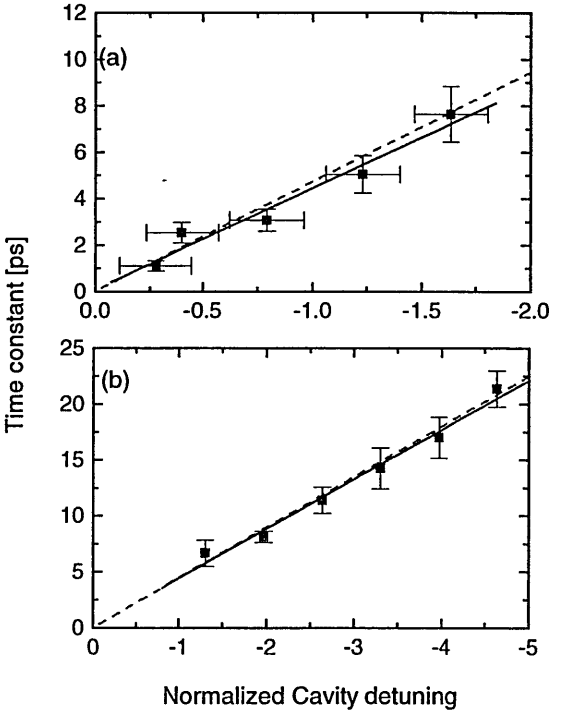

Figure 5-4. *Measured and simulated exponential time constants of the rising edge of the pulse as function of cavity desynchronism. The data at 6.3 μm from Stanford is shown in (a), while the 150 μm wavelength data taken at FELIX is shown in (b). The solid lines are linear fits to these data, the dashed lines show the results from simulations with a 1-D code [15]. See text for details.*

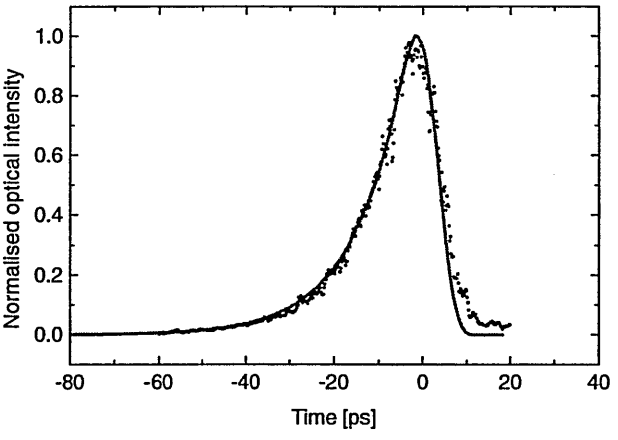

Figure 5-5. *A comparison of the experimental and simulated optical pulse shapes for FELIX operating at a wavelength of 150 μm and at a cavity detuning of -300 μm.*

5.4.3 Time-bandwidth product of FEL pulses

The data from FELIX also include spectral measurements, which illustrate the potential flexibility in selecting pulse and spectral widths in an FEL by selecting an appropriate cavity detuning. A series of measurements at a wavelength of 150 μm and cavity detunings between -100 μm and -600 μm were made. Typical results are shown in Figure 5-6: pulses in the time domain (a-c) with corresponding power spectra (d-f) were measured at FELIX operating at a wavelength of 150 μm and at detunings ΔL = -100 μm (a/d), -300 μm (b/e) and -600 μm (c/f). A summary of the results is presented in Figure 5-7, which shows that the time-bandwidth product $\Delta t_{FWHM}\Delta f_{FWHM}$ remains approximately constant at around 0.2 for normalized cavity detunings in the range -1 to -5, corresponding to pulse durations in the range 2 to 27 ps. This was investigated further by calculating the dependence of the time-bandwidth product of an idealized pulse – with an exponential leading edge and a Gaussian trailing edge, joined at the maximum of the Gaussian – on the time constant of the exponential part. It was found that the value of the time-bandwidth product was relatively insensitive to variations in the width of the Gaussian side over the range of values found in our measurements.

The solid curve in Figure 5-7 was generated by fixing the Gaussian half-width at a value of 12 ps and varying the time constant of the exponential over the range found in our experiments. In spite of the crudeness of the model, good qualitative agreement with experiment is obtained. At small detunings, where the exponential edge is very steep, the time-bandwidth product is dominated by the Gaussian part (the time-bandwidth product

for a Gaussian pulse is $2\ln 2/\pi \approx 0.44$) while for detunings of greater than one wavelength the time-bandwidth product varies slowly, dominated by the effect of the exponential edge and bounded below by the value of $\ln 2/2\pi \approx 0.11$ corresponding to a single-sided exponential.

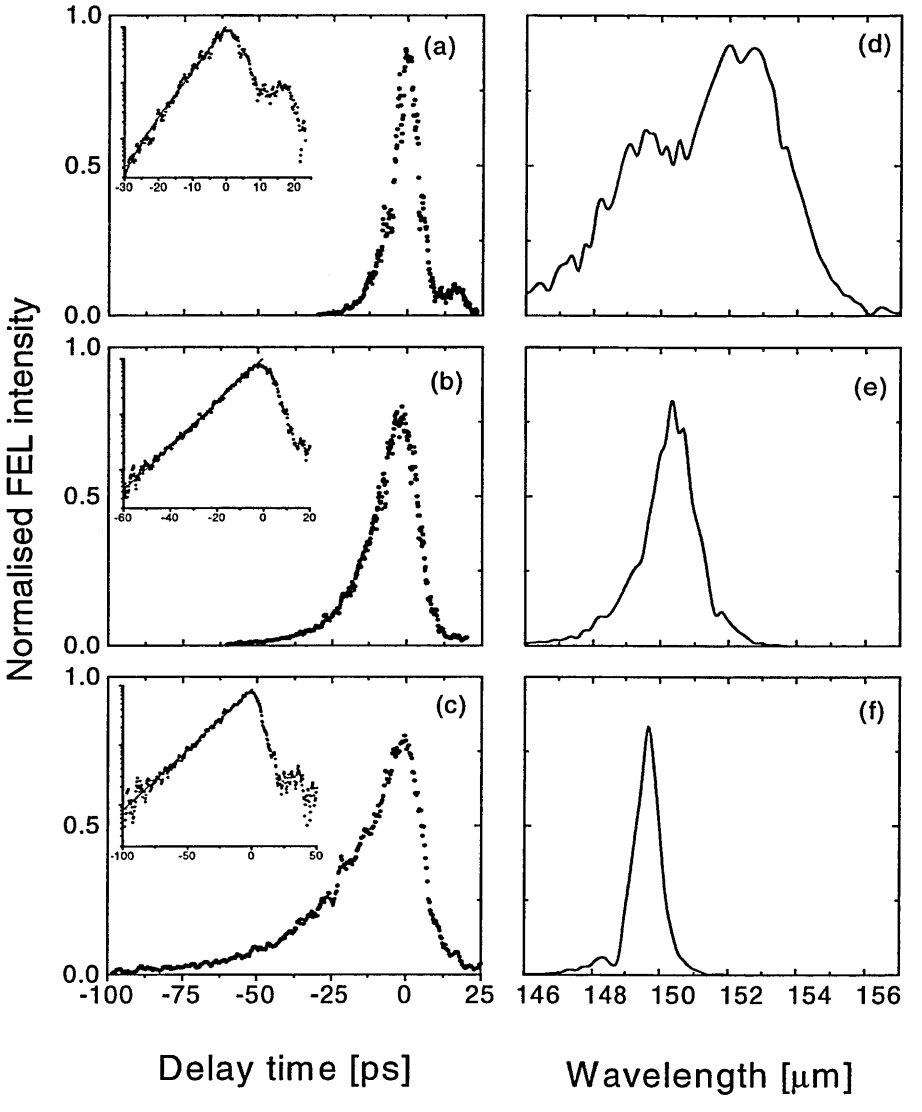

Figure 5-6. *Measured optical pulse shape (a)-(c) using the EO-cross-correlation technique described in the text, and corresponding power spectrum (d)-(f) at a wavelength of 150 μm for different cavity detunings ΔL of (a) -100 μm, (b) -300 μm, and (c) -600 μm. The pulse length is changed from 8.5 ps FWHM (a) to 21 ps FWHM in (c). The solid lines indicate exponential fits to the leading edges.*

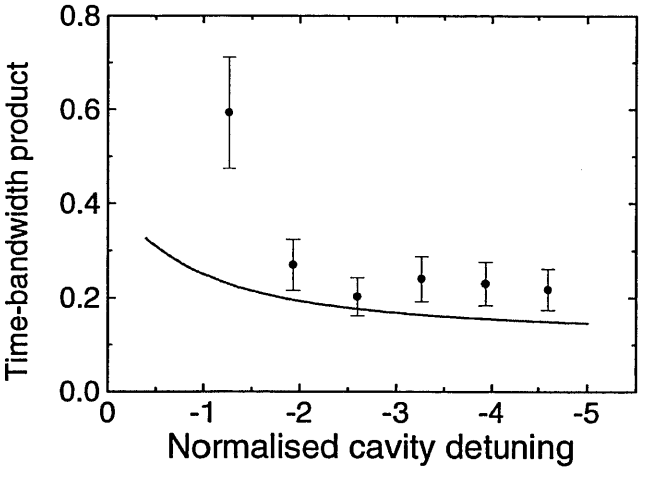

Figure 5-7. *Time-bandwidth product (FWHM) measured for different cavity detunings (solid dots). The product is in the range 0.2-0.3 if the optical pulse has an exponential leading edge. The product grows to 0.6 for pulses with a more Gaussian pulse shape. The solid line shows the calculated time-bandwidth product for pulses with an exponential leading edge and Gaussian trailing edge. See text for details.*

5.5 Conclusion

It has been shown that optical pulses in two very different FELs, operating in different regimes, evolve an exponential leading edge, and that the time constant for this exponential is proportional to the ratio of cavity detuning to the cavity loss parameter, α. A simple model has been presented to explain this effect. It has also been shown that the effect may be adequately modelled by a simple 1-D code and that the values obtained from the simulations are in good agreement with experiment both for the Stanford FEL and for FELIX. It has further been shown experimentally that the time-bandwidth product for pulses in an FEL pumped by short electron bunches remains approximately constant over a range of cavity detunings and indeed that this is in qualitative agreement with calculations made on a simplified pulse shape. This has important consequences for the design of new infrared free-electron laser user facilities that are driven by short electron bunches and that need to make a balanced choice between short pulses for high temporal resolution and narrow bandwidth for linear and non-linear spectroscopy. Users of existing FELs may use this result to enable them to select the pulse width or spectral width most appropriate to the experiment being undertaken by choosing an appropriate cavity detuning.

5.6 References:

[1] G. Ramian, Nucl. Instrum, & Methods **A318**, 225 (1992).

[2] T.I. Smith et al., Nucl. Instrum. & Methods **A304**, 812 (1992).

[3] K. Imasaki *et al.* Nucl. Instrum. Methods Phys. Res., **A318**, 235 (1992).

[4] R. Prazeres et al., Nucl. Instrum. & Methods **A358**, 212 (1995).

[5] F. Ciocci et al., Phys. Rev. Lett. **70**, 928 (1993).

[6] D. Oepts, A.F.G. van der Meer and P.W. van Amersfoort, Infrared Phys. Technol. **36**, 297 (1995).

[7] T.Tomimasu et al., Nucl. Instrum. & Methods **B144**, 1 (1998).

[8] W.B. Colson, Nucl. Instrum. Methods Phys. Res., **A429**, 37-40 (1999).

[9] J-P. R. Wells, C.W. Rella, Phys. Rev. Lett. **84**, 4998-5001 (2000).

[10] R. Trebino *et al.*, Rev. Sci. Instrum. **68**, 3277 (1997); B.A. Richman *et al.*, Opt. Lett. **22**, 721 (1997).

[11] M. Drabbels, G.M. Lankhuijzen, and L.D. Noordam, IEEE J. Quantum Electron. **34**, 2138 (1998).

[12] K.W. Berryman *et al.*, Nucl. Instrum. Methods Phys. Res., **A358**, 300 (1995).

[13] D. Oepts, A.F.G. van der Meer, and P.W. van Amersfoort, Infrared Phys. Technol. **36**, 297-308 (1995).

[14] C.W. Rella, G.M.H. Knippels, D.V. Palanker, and H.A. Schwettman, Opt. Commun. **157**, 335-342 (1998).

[15] W. B. Colson in Laser Handbook, Vol. 6, p117-194, edited by W.B. Colson, C. Pellegrini, and A. Renieri, (North Holland, 1990).

[16] W.B. Colson Proc. SPIE **1045**, p2-9 (1989).

[17] R.J. Stanley, R.I.Swent, and T.I.Smith, Opt. Commun. **115** p87-92 (1995).

[18] Q. Wu and X.C. Zhang, Appl. Phys. Lett. **71** p1285-1286 (1997).

[19] G.M.H. Knippels *et al.*, Opt. Lett. **23**, 1754 (1998).

[20] G.M.H. Knippels *et al.*, Phys. Rev. Lett. 83 1578-1581 (1999).

[21] G.M.H. Knippels and A.F.G. van der Meer, Nucl. Instrum. Methods Phys. Res., **B144** 32-39 (1998).

Chapter 6 Accurate measurement of the cavity synchronism of a far-infrared FEL using an electro-optical sampling technique

Abstract

In this chapter, we study the cavity synchronism of an FEL, which has a waveguide in the undulator. We also present a new method to measure the phase-synchronous cavity length of FEL with a precision of 1 μm. This method is an extended application of the electro-optical sampling technique [1] *developed at FELIX [2].

6.1 Introduction

Free Electron Lasers are versatile laser sources, which can generate tunable, coherent, high-power radiation, and currently span wavelengths from sub-millimeter to UV and potentially into the x-ray region. As we discussed in chapter 4, the FEL can also produce high pulse energies in transform-limited pulses of variable bandwidth, which is very important, for some pump and probe experiments [3]. In an FEL oscillator, successive electron bunches periodically enter the undulator, where they co-propagate with stored optical pulse. By varying the cavity desynchronism between the period of electron beam injection and the round trip time of the optical radiation inside the cavity, it is possible to control the overlap between the electron pulses and the FEL pulses over many round trips. In fact, optical cavity shortening from perfect synchronism is required to compensate the effect of laser lethargy, which causes the group velocity of the optical radiation to be slower than the speed of light in vacuum (see chapter 1). For most of FELs operating at far-infrared spectrum region, it is necessary to employ a waveguide inside the undulator, as a waveguide can reduce diffraction losses at long wavelength and increase the transverse overlap between the optical pulses and the electron beams. In addition it can introduce a better filling factor and therefore a larger gain. However, adding a waveguide will introduce appreciable group velocity dispersion in the optical pulses, and the effective cavity synchronism will be different due to the same group velocity dispersion.

* Details are described in chapter 3 and 4.

FEL cavity synchronism is studied in this chapter. In the present FEL-1 at FELIX, the phrase-synchronous cavity detuning is not linear in the wavelength, as the waveguide introduces noticeable dispersion. The possibility of measuring the individual field cycles of the FEL micropulses with the electro-optical (EO) sampling technique (see chapter 4) is exploited to determine the phase-synchronous length of the FELIX cavity. The absolute value of the cavity detuning length is obtained with a precision of 1 μm. Using a fast detector, we also observed superimposed sinusoidal phase modulation of 25 MHz on the independent micropulses in the optical cavity. At a large detuning length, evolution of a subpulse with an abrupt phase change between the main pulse and the subpulse has been recorded.

6.2 Waveguide FEL

The user facility FELIX currently operates two FELs: with FEL-1 lasing from 30 to 250 μm, and FEL-2 lasing from 5 to 30 μm. The operation range of FELIX has been extended to long wavelength FEL-1 by insertion of a one-dimensional parallel-plate waveguide inside the undulator.

Figure 6-1 shows the waveguide FEL-1 resonator. A parallel-plate waveguide with a narrow gap of 10 mm along the ***B*** field direction (x) of the planar undulator is used to extend the FEL-1 to long wavelength up to 250 μm. The pole faces of the undulator are in the vertical plane (y-z), and the two parallel plates of the waveguide are in the vertical plane as well. In order to leave enough space for necessary diagnostics in the FEL-1 resonator, the waveguide only starts after the second dipole B2 of the bending chicane and extends all the way to the downstream mirror. Due to the abruptly terminated waveguide, a special configuration of the upstream and downstream mirrors has been arranged such that a single mode operation can be obtained with small diffraction losses. The mirrors have been chosen as follows. In the vertical plane, the optical beam is a simple Gaussian beam, therefore the downstream mirror is a cylindrical mirror with a radius of curvature of 4 m, while the upstream mirror is an ellipsoidal mirror, also with a radius of curvature of 4 m. In the horizontal plane (guided direction), the radius of the upstream mirror has to match the wave front of the optical wave originating from the waveguide so that no higher order modes are excited when the optical wave is reflected back to the waveguide. In practice a few inter-changeable upstream mirrors are used for phase matching over different wavelengths. It has been verified that single mode (lowest mode) operation can be achieved over the wavelength range of 40-250 μm by using this configuration of the FEL resonator [4].

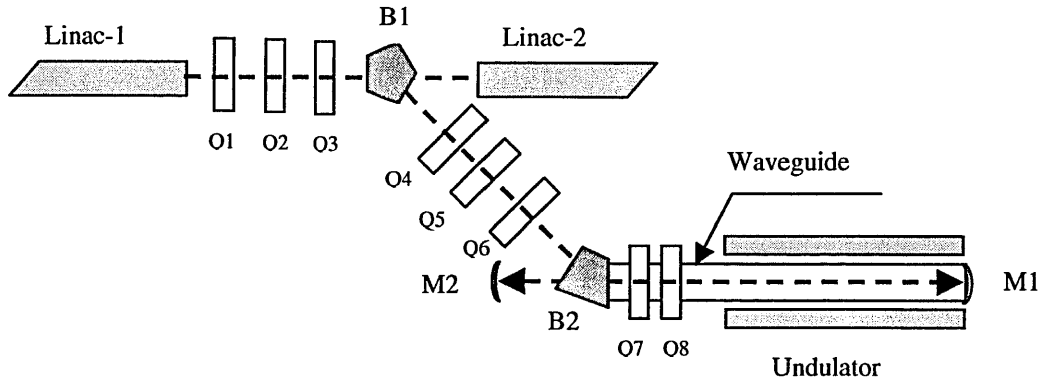

Figure 6-1 *Schematic of the FELIX long wavelength FEL resonator with a parallel-plate waveguide inside the planar undulator.*

In the dispersionless case ($k_z = k_0 = \omega_0 / c$), we define a synchronous cavity length L_0 such that the round-trip time of the optical pulse is an integer multiple of the repetition time T_0 of the electron pulses: $2L_0 = mT_0 c$. For FEL-1 operating at 1 GHz, $m = 40$, while at 25 MHz, $m = 1; L_0 = 6\,\text{m}$. The phase difference between successive optical pulses is then equal to $\Delta\Phi = \omega_0 m T_0 - 2k_z L_c$, where L_c is the actual (or effective) cavity length. Therefore, when we have $\Delta\Phi = 2n\pi$ (n=0, ±1, ...), and $L_c = L_0 - \Delta L$, the phase-synchronous detunings are proportional to the wavelength: $\Delta L = n\lambda/2$. In the case of dispersion, either due to the cavity configuration or the interaction with the electrons, the dependence of the phase-synchronous detunings on the wavelength is different. For this discussion, we neglect the effect of the electrons.

The round-trip phase change in an actual resonator depends on the cavity modes under consideration. For the different longitudinal modes, the phase difference between successive modes is just 2π, therefore the cavity synchronism is independent of the longitudinal modes. For the different transverse modes (either Gauss-Hermite or Gauss-Laguerre modes), the round-trip phase is defined as:

$$\Delta\Phi = \omega_0 m T_0 - 2k_z L_c + \Delta\Phi_G \qquad \textbf{Equation 6-1}$$

where $\Delta\Phi_G$ is the Guoy phase [5], and for Gauss-Hermite modes (p,q-order)

$$\Delta\Phi_G = 2(p+q+1)[\arctan(L_1/L_R) + \arctan(L_2/L_R)] \qquad \textbf{Equation 6-2}$$

or for the Gauss-Laguerre (axisymmetric p-order)

$$\Delta\Phi_G = 2(2p+1)[\arctan(L_1/L_R)+\arctan(L_2/L_R)] \qquad \textbf{Equation 6-3}$$

where L_1, L_2 are the distance from the mirrors to the waist position, and L_R is the Rayleigh length. For a cavity much longer than twice the Rayleigh length and with a waist more or less at the center of the cavity, $\Delta\Phi_G = 2n\pi$, where n is an integer number. Therefore it has no visible influence on the cavity synchronism.

In FELIX FEL-2, without the waveguide, the Rayleigth length is about 1m, and the cavity length is about 6 m. These give $\Delta\Phi_G \approx 0.8 \cdot 2\pi$ for the lowest order mode. The Rayleigh length, as well as the Gouy phase $\Delta\Phi_G$, does not depend on the wavelength. The corresponding exact phase synchronous cavity length (n=0) is about one half wavelength longer than L_0 defined above. The phase-synchronous cavity length of a FEL without waveguide is proportional to the wavelength of the optical radiation in the cavity.

$$L = L_0 + (\Delta\Phi_G/2\pi - n)\frac{\lambda}{2} \qquad \textbf{Equation 6-4}$$

In the present FEL-1, the phase-synchronous cavity detuning is not linear in wavelength, as the waveguide introduces noticeable dispersion [6]. We will discuss the successive round-trip phase difference in three parts, and only the lowest order mode (p=q=0) will be take into account. Firstly, phase change over the waveguide with length of L_w, $\Delta\Phi_W = -2k_z L_w = -\frac{2\pi}{\lambda}(1-\frac{\lambda^2}{8g^2})2L_w$, where g is the width of the waveguide, and $g >> \lambda$ [4]. Secondly, in the vertical (unguided) direction, the beam is still a Gaussian with a Rayleigh length determined by the mirror curvature, we have L_R=1.73m and the Guoy phase shift $\Delta\Phi_{GV} = 2\pi/3$. Finally, we need to consider the phase change over the part of cavity without waveguide. We have in the horizontal direction $\Delta\Phi_X = -2k_0(L_c - L_w) + \Delta\Phi_{GX}$, where $\Delta\Phi_{GX}$ is the Guoy phase shift in the horizontal direction on this part of the cavity and $L_c - L_w$ is a constant because the change of the cavity length is made inside the waveguide. As the beam is not Gaussian in this direction, we numerically compute the one-dimensional Huygens integrals (in the Fresnel approximation) for the profile of optical field propagating from the waveguide exit to the upstream mirror and back to the waveguide. It is found that the Guoy phase shift is approximately proportional to $1/\lambda$ and

$\Delta\Phi_{GX} = a + b/\lambda$. In order to obtain single mode operation, a few inter-changeable mirrors are used for different wavelength ranges [4] and the coefficients a and b are different for each mirror.

The total round-trip phase shift is $\Delta\Phi = \omega_0 m T_0 - \Delta\Phi_w - \Delta\Phi_X + \Delta\Phi_{GV}$. When $\Delta\Phi = 2n\pi$, we find out that the corresponding phase-synchronous cavity-detuning length is:

$$\Delta L_n(\lambda) = \frac{\lambda}{2}\left[\, n + \frac{L_w \lambda}{4g^2} + \frac{(a\lambda + b)}{2\pi\lambda} + \frac{1}{3} \,\right] \qquad \textbf{Equation 6-5}$$

Where the second term is caused by the dispersion of the waveguide, L_w is the length of the waveguide (4.345m), and g is the gap of the waveguide (10mm). The third term is caused by the Gouy phase shift in the horizontal direction in between the end of the waveguide and the upstream mirror. The last term is from the Gouy phase shift in the vertical direction, and corresponds to a phase shift of $2\pi/3$ in our case.

6.3 Experiment

Figure 6-2 schematically shows the experimental setup of the electro-optical detection method, which is a cross-correlation measurement, based on the Pockels effect [7]. Using the electro-optical detector one can sample the electric field of an FEL micropulse. The Ti:Sapphire pulse repetition frequency is phase-locked to the electron pulse repetition frequency and therefore also to the FEL micropulse at saturation, when the pulse shape has become stationary. So, at a fixed setting of the optical delay line, the Ti:Sapphire pulses sample the FEL output at a fixed position in the micropulse. However, this is only true with regard to the envelope of FEL micropulse. The phase of the FEL carrier wave shifts in each round-trip with respect to the envelope by an amount $\Delta\Phi = 2\pi(2\Delta L/\lambda)$, due to the applied cavity detuning ΔL, where λ is the wavelength of the FEL optical pulse. This phase shift leads to a beat oscillation in the observed signal (see Figure 6-3) with $f_{beat} = -c\Delta L/\lambda L_0$ [1] (see chapter 4, page 4-8), where L_0 is the FEL cavity length (6 m). The phase of the beat signal varies from macropulse to macropulse, because the optical field develops from spontaneous emission and its phase is not fixed to the Ti:Sapphire pulses.

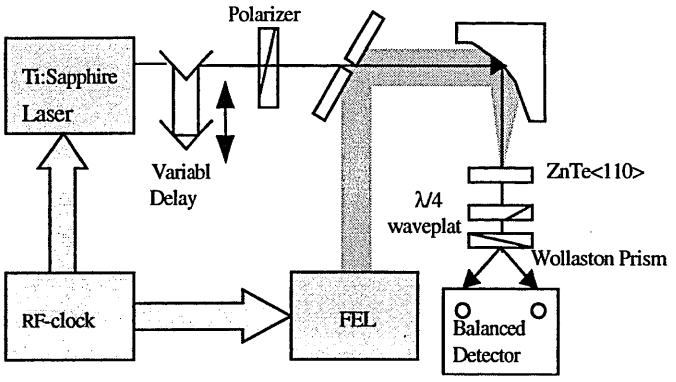

Figure 6-2. *The experimental setup of phase sensitive electro-optic measurements of the FEL optical pulses.*

The possibility of measuring individual field cycles of the FEL micropulses is used to determine the phase-synchronous length of the FELIX cavity. When $\Delta L_n = n\lambda/2$ $(n = 0,\pm1,...)$, the phase advance per round-trip is just $2n\pi$, and therefore indistinguishable from zero, and the beat-frequency modulation of the measured signal will be absent. So the observed beat frequency is actually $f_{beat} \bmod(c/2L)$. The wavelength dependence of the phase-synchronous condition allows the determination of the integer number k and therefore the exact cavity detuning length. In a dispersionless cavity there is an exact zero detuning cavity length (synchronism position) for all wavelengths ($n = 0$), as ΔL_n is independent of λ only when $n = 0$. In our present situation, the waveguide in FEL-1 introduces appreciable dispersion. Taking the dispersion of the waveguide and the effect of the Gouy phase shift in the FEL cavity into account, the phase-synchronous lengths can be approximated by Equation 6-5. The solid curves in Figure 6-4 show the calculated results for different n values, while the data points indicate the experimental results of the phase-synchronous cavity length for a large range of wavelengths in the waveguide FEL. The integer number n for the experimental cavity detuning length has been determined by fitting the vertical position of the measured data to the theoretical curves. In this way, the absolute value of the cavity detuning length is obtained with a precision of ~1μm.

Due to the well-known lethargy effect (see chapter 1,section 1.3.2), the group velocity of the FEL pulse is reduced during build-up but it will recover to c (its vacuum value) as the FEL pulse reaches saturation. In the waveguide, the group velocity of the FEL pulse is reduced to $c(1-\lambda^2/8g^2)$ [4]. In order to achieve effective small-signal gain, the FEL has to start up at a sufficiently negative cavity detuning length. As illustrated in Figure 6-4 by the dashed line, the zero detuning length for the pulse envelope at saturation is obtained at $\Delta L_e = -L_w\lambda^2/8g^2$.

Indeed, one can see that the FEL can only run at cavity detunings below the dashed curve. It is not clear yet why at long wavelengths no lasing could be obtained at small detunings.

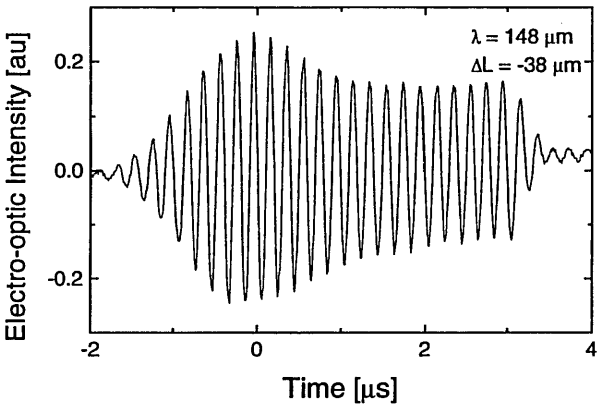

Figure 6-3. *The electro-optic signal recorded during a FEL macropulse with λ=148μm and $\Delta L = 38 + n \times \lambda / 2 (n = 0, \pm 1, \ldots)$ μm. The observed beat results from a phase shift per round-trip of $2\pi \times 2\Delta L/\lambda$ of the FEL carrier wave with respect to the Ti:Sapphire pulse train, causing the Ti:Sapphire pulse train to sample different phases of the electric-field cycles, so the expected oscillation frequency is 5 MHz.*

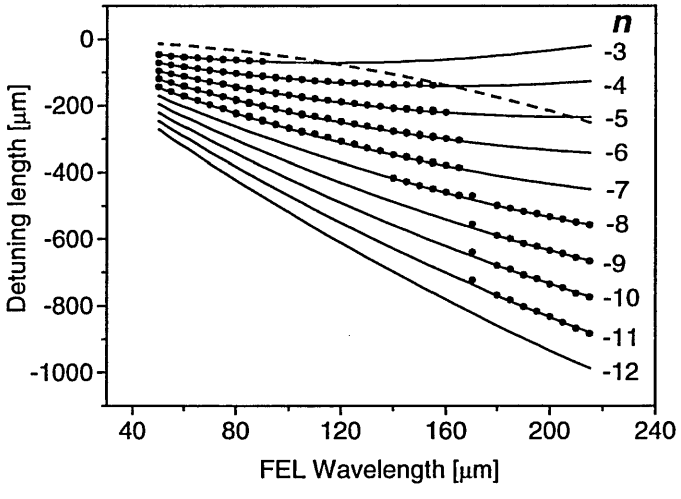

Figure 6-4. *Phase-synchronous cavity detuning lengths for different wavelengths in FEL-1. The data points are the experimental results. The solid lines are the calculated results for different integer numbers n as marked at the right side of this figure. The dashed line is the effective zero-detuning length for the FEL pulse envelope at saturation, and gives the upper limit for the cavity detuning lengths at which the FEL will lase.*

Electro-optical detection of individual field cycles of FEL micropulses is also performed with a fast detector, using the experimental setup in Figure 6-2. In this experiment, the probing pulses from the ultra-short Ti:Sapphire laser is generated at frequency of 100 MHz, while the FEL is running at 1GHz repetition rate by seeding 40 independent optical radiation pulses at one time in its 6-m long optical cavity. The Ti:Sapphire pulse was therefore synchronised with every 10^{th} of successive FEL pulses. Using a fast detector, one can see clearly that the experimental data shown in Figure 6-5 consist of 4 sets of traces, which correspond to 4 independent optical pulses probed by the Ti:Sapphire laser. It is clearly seen that those independent micropulses intend to develop their phases to be close to their neighbouring pulses. In Figure 6-5, micropulse #1 has a closer phase to micropulse #31(notice that number 41 is just the replica of micropulse #1), while micropulse #21 has a similar phase to micropulse #31. In another words, the optical cavity somehow constraints the phase of those micropulses, which might be expected to have a random initial phase due to the independence of the gain medium of freshly injected electron pulses. It is not difficult to understand that those pulses apart by 40 ns (repetition rate=25 MHz) should have the same phase, as they are just replicas of themselves after a round-trip in the optical cavity. For the results shown in Figure 6-5, we hypothesise that there is an internal superimposed sinusoidal phase modulation of 25 MHz, but it is still unclear where comes the 25 MHz modulation, and why the phase difference among those independent micropulses becomes smaller as the macropulse reaches saturation.

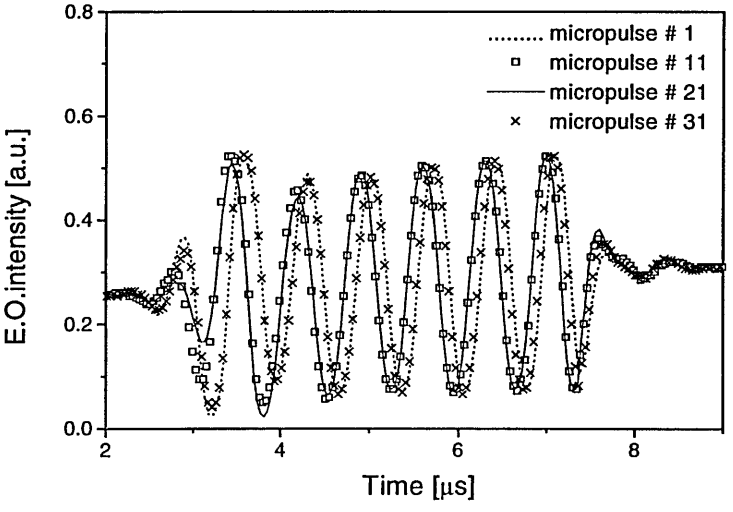

Figure 6-5 *Four independent micropulses inside the FEL cavity have an internal phase relation with their neighbouring pulses, which indicates a superimposed sinusoidal phase modulation of 25 MHz on these pulses when the FEL is running at 1 GHz.*

Figure 6-6(a) shows the electric field of the micropulse at an intermediate cavity detuning length, where a dynamic balance between the laser lethargy and saturation of optical power is reached. At this stage, the micropulses consist of sets of successively growing and decaying subpulses [8]. The evolution of subpulse is clearly presented here. Abrupt phase change is recorded in this graph, and this result is consistent with the optical power spectrum shown in Figure 6-6(b), where asymmetric sidebands are seen due to a sudden phase change in the time domain of the optical pulse.

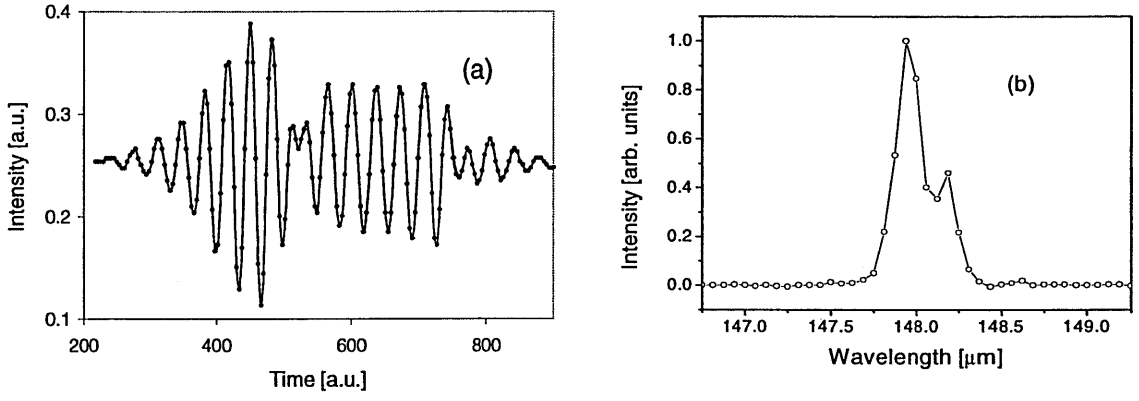

Figure 6-6 (a) *Evolution of subpulses at large cavity detuning length. One can see clearly an abrupt phase change (180^0) between the main pulse and the subpulse. (b)* Asymmetric sidebands are seen in the optical power spectrum due to a sudden phase change in the time domain of the optical pulse.

6.4 Conclusion

Accurately measuring the desynchronism of FEL cavity becomes more important, as in a recent work [9,10,11], it was found that modulating the desynchronism provides a new method of controlling the pulse length and the output power of an FEL. However, adding a waveguide inside the undulator of a long wavelength FEL introduces noticeable dispersion, therefore the dependence of the phase-synchronous cavity length on the wavelength is not linear any more. We have studied the cavity synchronism theoretically and verified this with experimental data. Using the electro-optical sampling technique, we have obtained the phase-synchronous cavity length of FEL-1 at FELIX with a precision of 1 μm.

Using a fast detector, we have further studied the internal phase relation among independent micropulses in the FEL optical cavity. It was found that the phases of optical radiation pulses exhibit an internal sinusoidal modulation of 25 MHz, in spite of the fact that those optical pulses are derived from independent freshly injected electron pulses.

An abrupt (180^0) phase change between the main pulse and the subpulse of the optical radiation was also observed at a larger detuning length. This phenomenon explains the asymmetric sidebands seen in its spectral measurement.

6.5 References

[1] G.M.H. Knippels, X. Yan and A.M. MacLeod, W.A. Gillespie, M. Yasumoto, D. Oepts, A.F.G. van der Meer, Phys. Rev. Lett. **83**, p. 1578-1581 (1999).

[2] D. Oepts, et al.,, Infrared Phys. Technol. **36**, p. 297 (1995).

[3] C.D. Bezant, M.M. Chamberlain, H.P.M. Pellemans, B.N. Murdin, W. Betty, M. Henini. Semicond. Sci. & Techn., 14 (1999) L25.

[4] L.Y. Lin and A.F.G. van der Meer, Rev. Sci. Instrum. **68**, p. 4342 (1997).

[5] A.E. Siegman, *Lasers* (University Science Books, Mill Valley, California, 1986), p. 682-685.

[6] L. Elias and J. Gallardo, Appl. Phys. B **31**, (1983).

[7] C.C. Davis, *Lasers and Electro-optics: Fundamentals and Engineering* (Cambridge University Press, Cambridge, England, 1996), p. 472.

[8] D.A. Jaroszynski et al. Phys. Rev. Lett. **70**, 3412 (1993)

[9] O.G. Calderson, T. Kimura and T.I. Smith, Phys. Rev. ST Accel. Beams **3**, 90 701 (2000)

[10] O.G. Calderson, T. Kimura and T.I. Smith, Phys. Rev. E, Vol. **65**, 016504 (2001)

[11] N. Nishimori et al. Phys. Rev. Lett. VOL. **56**, 5707 (2001)

Chapter 7 Sub-picosecond electro-optic measurement of relativistic electron pulses

Abstract

Time resolved measurements of the transverse electrical field associated with relativistic electron bunches are presented. Using a modification of the rapid scanning technique described early in chapter 4 and an ultra-fast electro-optical sensor close to the electron beam, the longitudinal profile of the electric field was measured with sub-picosecond time resolution and without time reversal ambiguity. Results are shown for two cases: inside the vacuum beam line in the presence of weak fields, and in air behind a beryllium window, effectively probing the near-field transition radiation. Reconstruction of the longitudinal electron bunch shape is straightforward, especially in the latter case.

7.1 Introduction

Many applications based on relativistic electron bunches require an accurate measurement of the peak current. For this, the duration and possibly the shape of the electron bunch have to be measured. Free Electron Lasers (FELs) are important devices that use high-peak current electron bunches and are well-established tuneable radiation sources in the (far)-infrared part of the spectrum. Considerable effort has been made, notably at DESY [1] and SLAC [2], to extend the operating wavelength range into the XUV and soft x-ray part of the spectrum. Crucial for the success of these projects is the demonstration of self-amplified spontaneous emission (SASE) at short wavelengths. In the SASE mode of operation, an ultra-short, high-peak current, relativistic electron bunch is used to amplify its own spontaneous emission radiation to saturation in one pass through the undulator. Important parameters in these experiments are of course the length and shape of the driving electron bunch, which, together with the total charge in the bunch, yield the current profile. For example, for the DESY project [1], a 25 GeV electron beam with a fwhm bunch length of about 180 fs with 1nC charge per bunch is planned.

While there are a large number of excellent diagnostics available to measure the shape and duration of ultra-short laser pulses, few measurement techniques exist for short electron pulses. A streak camera system

detecting the light pulses generated by the electrons at a target screen was shown to have a limiting resolution of 1.6 ps fwhm [3]. Recently, an off-phase rf-acceleration method has been demonstrated to measure the longitudinal density profile of relativistic electron bunches with sub-picosecond time resolution [4], but this approach requires magnetic longitudinal dispersion, an off-phase rf-accelerator section, and an energy spectrometer. In addition, it interferes with normal beam operation and can only measure the beam profile at one particular position in the beam line. Most other diagnostics available to characterize short electron bunches have employed a method that was first described in references [5] and [6]. In this approach the electron beam is passed through a thin foil, and then the electron bunch profile is reconstructed by measuring the spectrum of the coherent part of the emitted transition radiation (usually in the THz-frequency range), and Fourier-transforming this to the time-domain. The method relies on the use of the Kramers-Kronig relations for the reconstruction process and requires an extrapolation of the measured spectrum to zero frequency. Furthermore, although an asymmetric pulse shape can be obtained, the method cannot distinguish between the leading edge and trailing edge of the pulse. In this chapter we present measurements based on a completely different approach which avoids these limitations and does not disturb the electron beam. The method is based on the Pockels effect [7] (see also chapter 3). By rapid scanning the delay between the electron pulse train and the synchronised Ti:Sapphire pulse train the electric field profile, including its sign, is measured (assuming all the pulses are identical, see chapter 4 for details). In the relativistic limit, the measured electric field profile is directly proportional to the longitudinal density distribution of the electron bunch.

7.2 Coulomb field of a relativistic electron beam

The Coulomb field of a relativistic electron beam moving in a straight line is concentrated in the direction perpendicular to its trajectory, within an angle of the order of $2/\gamma$ [8], where γ is the Lorentz factor. An electro-optic sensor, placed close enough to the beam so that the field of different parts of the electron bunch can be distinguished, is used to sample the Coulomb field of passing electron bunches. The time resolution, τ, when probing the field at a distance of R from the centre of the electron beam, can be estimated as $\tau \approx 2R/\gamma c$ (where c is the speed of light in vacuum) [9]. As an example, with R=6 mm and γ=90, corresponding to a beam energy of about 46 MeV, one has τ=0.44 ps, and the resolution clearly improves at higher energies. When the probe pulse and the electron field pulse traverse the sampling crystal at the same speed, the magnitude of the electro-optic effect is proportional to the crystal length. However, in reality, there is a velocity mismatch due to the dispersion

in the material, which limits the maximum length at a fixed time resolution. A more important aspect of the dispersion is the response time of the sample's electric polarization. ZnTe has a TO-phonon resonance at 5.3 THz, which means that an electric field pulse shorter than about 200 fs will be distorted and attenuated. It has been shown, however, that frequencies up to 37 THz can still be measured with ZnTe [10] and the effects of the dispersion and absorption can be modelled accurately [11]. An alternative electro-optic sensor material suitable for shorter pulses appears to be GaP, which has its fundamental TO-phonon resonance at 8.7 THz.

7.3 Experimental setup

Figure 7-1 shows the experimental setup used for the electro-optic sampling of the relativistic electron pulses, which are produced by the radio-frequency linear accelerator at the FELIX FEL facility in the Netherlands [12]. Relevant beam parameters are given in Table 1. The electron bunch profile is measured at two positions: at the entrance of the undulator (position (a)) and behind the exit of a Beryllium window (position (b)). A mode-locked Ti:Sapphire laser producing a 12-fs pulse at 800 nm with a repetition rate of 100 MHz is employed as a probe beam, and is actively synchronised to the accelerator rf-clock [13]. A 0.5mm thick <110> oriented ZnTe crystal (Ingcrys, U.K.) is used as an electro-optic sensor and is placed perpendicularly to the propagation direction of the electron beam. The polarisation direction of the laser probe pulse is set to be parallel to the <001> axis of the ZnTe crystal for optimal electro-optic modulation. The repetition rate of the electron bunch can be changed electronically via a rf-phase shifter which sweeps the electron pulse train over the Ti:Sapphire pulse train at a speed of a few picoseconds per microsecond (see also chapter 4), and the complete electric field profile is thereby measured within a few microseconds. An additional advantage of this rapid scanning technique is that on a time scale of a few microseconds there is a negligibly low jitter of approximately 50 fs between the Ti:Sapphire pulse train and the electron pulse train [14].

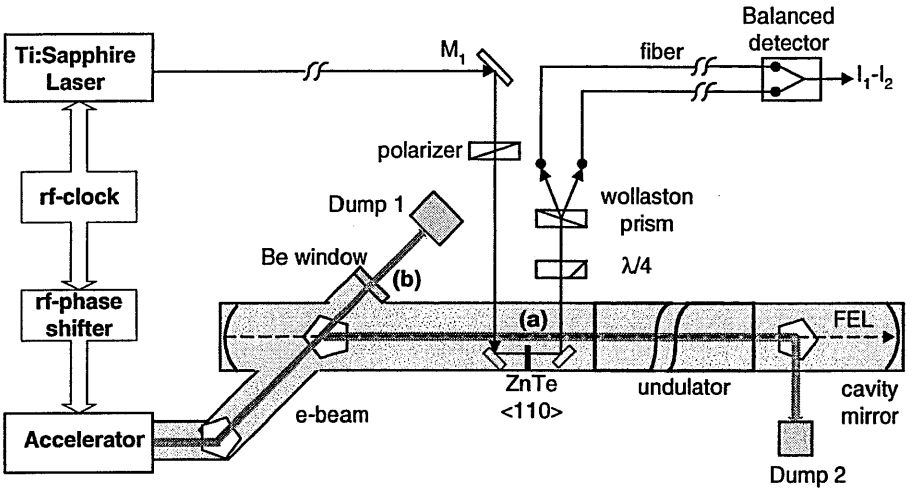

Figure 7-1. *Experimental setup of the electro-optic measurement of the shape of relativistic electron bunches. The electron bunch profile is measured by using an electro-optic crystal of ZnTe at two positions: (a) at the entrance of the undulator inside the vacuum pipe; (b) in ambient air, between the Beryllium window and the current dump (Ti:Sapphire beam path and the crystal are not shown). The shaded parts indicate the vacuum housing for the electron beam.*

Table 7-1 *Parameters of the electron beam used for the electro-optic measurements at FELIX.*

Beam energy	46 MeV
Energy spread (rms)	0.2%
Normalised emittance	50π mm mrad
Bunch charge	200 pC
Micropulse spacing	1 ns
Macropulse duration	≤ 8 μs

7.3.1 Non-intercepting Method— Measuring Wake Fields Of The Electron Beam

In the setup at (a) in Figure 7-1, the electric field is measured at the entrance of the undulator inside the vacuum pipe, while the FEL is lasing properly. The electron beam has a diameter of approximately 1 mm at this position and the crystal is located 6 mm from the centre of the electron beam. The probe laser pulses propagate in the electron beam direction passing through entrance and exit glass (Kodial) windows, which maintain the polarization state of the probe laser pulse. Figure 7-2 shows measurements of the observed electric field profile. In the case of Figure 7-2(a), the large peak (marked by an arrow) represents the direct field of the electron bunch. It is known that the electron beam at FELIX consists of well-defined bunches of length ~ 2 ps separated in time by 1 ns. The electric field of the bunch at the crystal will always have the same sign, and the other parts of the signal that have both positive and negative signs are therefore attributed to the wake fields excited by the electron bunches, due to unavoidable discontinuities in the beam pipe [[15]] and in the measurement system itself. We have also performed measurements with a 40 ns interval between the electron bunches and in that case there was no measurable signal preceding the main peak. This shows that the oscillations are excited by the passing electron bunch and have not completely disappeared after 1 ns. The ability to measure wake fields in situ with high temporal resolution may prove useful in cases where these fields give rise to degradation of the beam quality. The shortest electron bunch we have measured is about 1.7±0.2 ps fwhm, as illustrated in Figure 7-2(b), and the time resolution (estimated as $\tau \approx 2R/\gamma c$ [[9]]) is about 0.44 ps in this configuration. The electric field strength at the ZnTe crystal position can be calculated as $E=Q/2\pi\varepsilon_0 RL_b$, where Q is the total charge of the electron bunch and L_b is its effective length [[9]]. In our case, the electric field strength is approximately 12 kV/cm at the crystal, leading to a sensitivity of our technique of around 1 kV/cm for a S/N=1. The accelerator settings used to drive the FEL at FELIX result in a clearly asymmetric pulse shape. The steep rising edge of the electron bunch is consistent with the observed enhancement of the coherent spontaneous emission, which can considerably facilitate the startup of a short-pulse FEL at longer wavelengths [[16]], and is consistent with simulations [[17]] based on a general particle tracking code [[18]].

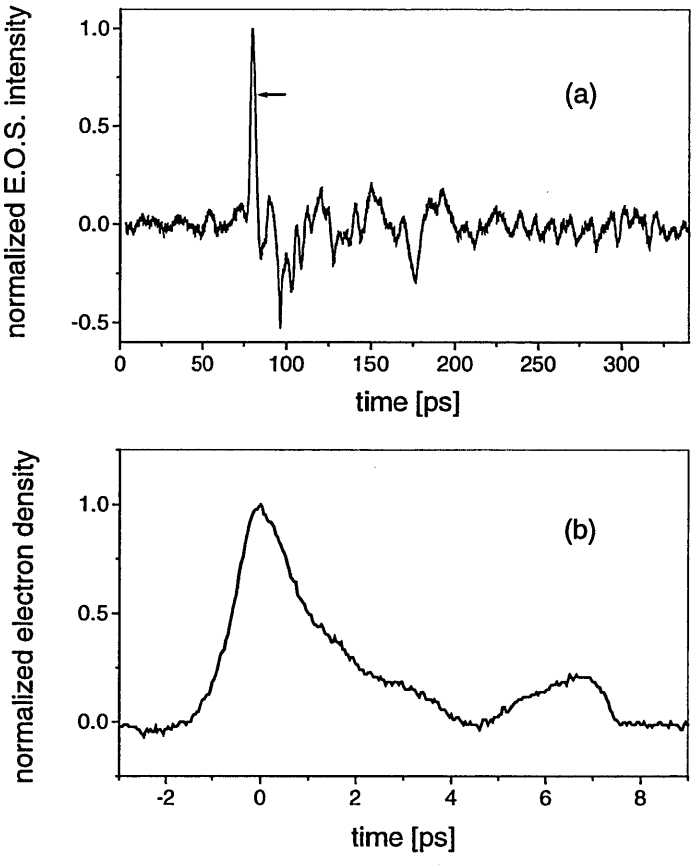

Figure 7-2. *The electric field profiles measured at the entrance of the undulator inside the vacuum pipe, while the FEL is running properly. (a) Electric field profile measured over several hundred picoseconds, the large positive peak marked by an arrow is the direct field of the passing electron bunch, while the other parts of the signal are attributed to the effects of the wake fields excited by the electron bunches in the beam pipe. (b) The electron bunch profile measured inside the vacuum pipe has a clearly asymmetric pulse shape and the shortest pulse length measured is about 1.7±0.2 ps fwhm.*

Figure 7-3 illustrates the measured duration of the electron bunches as a function of the phase setting of the prebuncher input RF-field. In normal use at FELIX, the prebuncher is used to apply a decelerating field to the leading part of the electron bunch and an accelerating field to the trailing edge of the bunch. It gives a ramp in the energy of electrons with respect to the longitudinal distribution in the bunch. In the drift space between the prebuncher and the buncher, the modulation of the energy of the electron bunch results in a substantial compression of the electron bunch. Indeed, from Figure 7-3, it can be seen that the electron bunch profile is quite sensitive to the setting of prebuncher and the fwhm length may be varied between 1.7 ps and 4.1 ps.

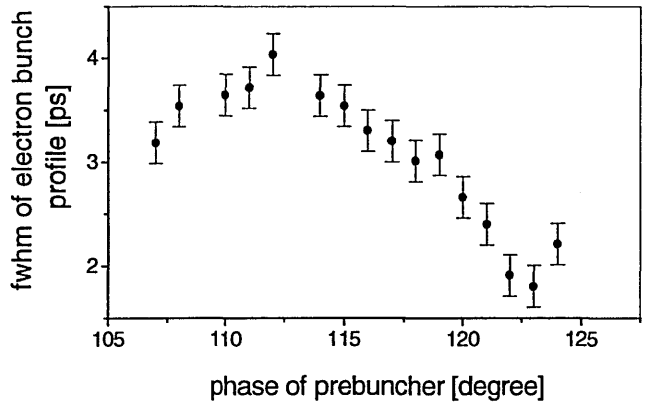

Figure 7-3. *Measured duration of electron bunches as a function of the phase settings of the prebuncher input RF-field.*

7.3.2 Intercepting Method----Probing The Near-Field Transition Radiation

In a second experiment, the electric field profile is measured at the position shown at (b) in Figure 7-1, where the beam propagates in air after passing through a Beryllium window and before being dumped. The beam diameter is about 3 mm at the Be window. The field is probed at a distance of about 6 mm from the centre of the electron beam and 120 mm from the Be window. Figure 7-4 shows experimental results, where the solid line represents the electric field profile with the accelerator settings normally used for running the FEL, and the dotted line is obtained by slightly adjusting the phase of the prebuncher. From the steep rising edges and the 830 fs fwhm pulse duration of the dotted curve, it is seen that a sub-picosecond time resolution can be achieved with this electro-optic sampling technique. Note that at this position, the electron beam is dispersed in the horizontal plane. Therefore, for the dotted line, an energy ramp over the bunch causes the probe laser beam to sample only part of the dispersed bunch, leading to a smaller signal and a narrower time profile. In these experiments, there are no surrounding conductive walls, and indeed, no observable wake field effects. In order to minimize the beam spreading after the Be window, the measurement is performed at a relatively short distance of about 120 mm behind the window. At such a distance, the field of the electron bunch has not yet recovered its normal free space configuration at 6 mm from the beam line. Instead of the undisturbed Coulomb field, what is detected can be considered to be the near field of the transition radiation generated by the Be window [19]. However, in the present case, the resulting signal should still give an accurate representation of the longitudinal charge density. The time resolution of our measurement in this configuration is not determined by the spreading of the Coulomb

field anymore, but by the finite spot size of the electron beam at the Be window. This finite spot size causes the transition radiation from different parts of the spot to arrive at different times at the sampling crystal. Given the spot size of the electron beam and crystal position, a resolution of 0.5 ps is estimated.

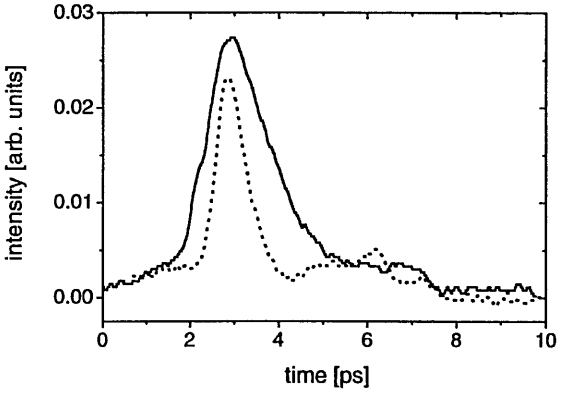

Figure 7-4. *Near-field profile of the transition radiation generated by the electron bunch at the exit of a Beryllium window measured with sub-ps time resolution. Solid line: accelerator settings normally used for running the FEL optimally. Dotted line: phase of the accelerator prebuncher shifted by about 10 degrees at 1 GHz.*

7.4 Conclusion

Time-resolved measurements of the transverse electric field associated with relativistic electron bunches are presented. Using an ultra-fast electro-optic sensor close to the electron beam, the longitudinal profile of the electric field was measured with sub-picosecond time resolution and without time-reversal ambiguity. Results are shown for two cases: inside the vacuum beam line in the presence of wake fields, and in air behind a Beryllium window, effectively probing the near-field transition radiation. Reconstruction of the longitudinal electron bunch shape is straightforward, especially in the later case.

Although we have demonstrated a non-intercepting approach for relativistic electron bunches based on the electro-optical detection, which can measure the electron bunch profile within one macropulse using the rapid scanning technique, it requires constant micropulses during the measurement. In order to study bunch to bunch fluctuations, it is necessary to measure the length and pulse shape of individual electron bunches. Therefore a real-time single shot measurement is proposed at FELIX [20], and this technique will be introduced in chapter 8.

7.5 References

[1] B. Faatz, J. Pflüger, J. Rossbach, et al, Nucl. Instr. Meth. A, **407**, 302-306 (1998).

[2] E.L. Saldin, E.A. Schneidmiller, M.V. Yurkov, Nucl. Instr. Meth. A, **429**, 197-201 (1999).

[3] A.H. Lumpkin et al., Nucl. Instr. Meth. A, **429**, 336 (1999).

[4] K.N. Ricci, T.I. Smith, Physical Review Special Topics – Accelerators and Beams, **3**, 032801 (2000).

[5] W. Barry, Proc. of the Workshop on Advanced Beam Instrumentation, **1**, (KEK Proc. 91-2), 224-235 (1991).

[6] P. Kung et al., Phys. Rev. Lett., **73**, 967 (1994).

[7] C.C. Davis, in "Lasers and electro-optics: fundamentals and engineering", Cambridge University Press 1996, p. 472.

[8] J.D. Jackson, in "Classical Electrodynamics", Wiley, New York, 2nd edition 1975, p. 555.

[9] D. Oepts, G.M.H. Knippels, Pro. 20th Int. FEL conference, Williamburg, Abstract 45 (1998).

[10] Q. Wu and X.-C. Zhang, Appl. Phys. Lett., **71**, 1285 (1997).

[11] H.J. Bakker et al., J. Opt. Soc. Am. B., **15**, 1795-1801 (1998).

[12] D. Oepts et al., Infrared Phys. Tech., **36**, 297 (1995).

[13] G.M.H. Knippels et al., Opt. Lett., **23**, 1754 (1998).

[14] G.M.H. Knippels, X. Yan, A.M. MacLeod, W.A. Gillespie, M. Yasumoto, D. Oepts and A.F.G. van der Meer, Phys. Rev. Lett., **83**, 1578-1581 (1999).

[15] M.J. Fitch et al., Proc. 1999 Part. Acc. Conference, New York, 2181-2183 (1999); M.J. Fitch et al., Internal report, FERMILAB-TM-2096.

[16] D.A. Jaroszynski et al., Phys. Rev. Lett., **71**, 3798-3801 (1993).

[17] H.H. Weits, C.A.J. van der Geer, D. Oepts, A.F.G. van der Meer, Nucl. Instr. Meth. A, **434**, 205-217 (1999).

[18] M.J. de Loos et al., Proc. 5th Eur. Part. Acc. Conf., Sitges, 1241, (1996).

[19] T.I. Smith, Proc. 21st Int. FEL conference, Hamburg (1999)

[20] I. Wilke, A.M. MacLeod et al., Phys. Rev. Lett., **88**, 124801(2001).

Chapter 8 Closing Remarks

8.1 Achievements

In this thesis, we have discussed ultra-fast diagnostic techniques for both optical pulses and electron pulses at FELIX FEL facility in the Netherlands. In order to measure pulses shorter than the response time of a conventional detector, a non-linear optical gating technique has been employed. The most common and easy method is to use the optical pulse itself as the gating pulse. Autocorrelation can provide a clean measurement of optical pulse length, but it can not provide information on asymmetric pulse shape. Using cross-correlation of the source pulses with ultra-short laser pulses (such as ultra-short Ti:Sapphire laser), it is possible to obtain both the length and shape of the source pulses with a sub-picosecond time resolution.

This first cross-correlation measurement of the FEL optical pulses was done by using the differential optical gating technique with a 10-fs unsynchronised Ti:Sapphire laser and a sum-frequency generation in a $AgGaS_2$ crystal as the gating mechanism. By employing a differential technique to simultaneously measure the intensity of the infrared optical pulse and its time derivative, we have reconstructed the pulse shape with a time resolution of the order of 100-fs. In the DOG measurements, the jitter between two lasers is not an issue, in fact, it is an advantage here, because it helps the probe laser (Ti:Sapphire) to sample the FEL pulse at different positions, therefore one can accumulate the complete map of the intensity and its derivative of the FEL pulse. The DOG technique has also several disadvantages. Firstly, it requires a constant micropulse shape during the measurement, while the measurement itself might require many minutes in order to accumulate enough data points in the intensity-derivative map. Secondly, there is a difficulty in bridging the leading edge and trailing edge of the measured pulse, as there is uncertainty at the peak of the pulse where its derivative is zero. Further study of synchronisation between the Ti:Sapphire laser and the FEL at FELIX encouraged us to use other diagnostic techniques, as the jitter measured in our experiment was only about 400 fs rms over a scanning time of 2 minutes, by using an optical delay line, and the jitter can be further reduced to <100 fs (~50 fs) over a scanning time of 10 μs, by using a rapid scanning technique.

Theoretical and practical investigations of electro-optical detection technique, based on the Pockels effect, have been undertaken following the successful DOG measurements. Two types of configuration of

detection have been demonstrated. This technique is particularly sensitive because the Pockels effect is linear in the applied electric field, and also the detection can be done in the visible, where excellent detectors and polarisers are available. By using a configuration of a balanced detector in the experimental setup, it is possible to obtain not only the intensity profile of the source pulse, but also the individual electrical cycles under its envelope.

Using electro-optical detection technique as a powerful diagnostic tool for sub-picosecond optical pulses and electron bunches, we were able to study the FEL physics systematically. The FELIX user facilities can generate intense picosecond far-infrared laser pulses from 30-250 μm in a waveguide free-electron laser. The electric field profile of the FEL optical pulses has been characterised with a rapid-scanning cross-correlation technique with an actively synchronised 10-fs Ti:S laser. This technique allows complete characterisation of the optical output as well as accurate experimental determination of one of the most important parameters for free-electron lasers, the absolute cavity detuning with a high precision of 1 μm. The shortest pulses observed at 150-μm have a length of only 18 optical field cycles at the fwhm of the intensity profile. The combination of short pulse duration, high pulse energy, and diffraction-limited beam quality leads to unprecedented power densities of up to 0.1 GW/cm^2, allowing non-linear experiments in a wide range of the far-infrared spectrum.

The detailed shape of picosecond optical pulses from a free-electron laser (FEL) oscillator has been studied for various cavity-detunings. For large values of the cavity detuning the optical pulse develops an exponential leading edge, with a time constant proportional to the applied cavity detuning and the quality factor of the resonator. This behaviour has been observed at two separate FELs that have completely different resonator layouts and electron beam characteristics, and using different methods of optical pulse length measurement. The optical pulses have a full width at half maximum time-bandwidth product $t_{FWHM} \cdot f_{FWHM}$ of 0.2–0.3. The results obtained here can be used to predict the optical pulse length and corresponding minimum spectral width that can be generated in a FEL pumped by short electron bunches. This is important for the design of new infrared free-electron laser user facilities, which need to make a balanced choice between short pulses for high temporal resolution and narrow bandwidth for linear and non-linear spectroscopy.

Although a range of electron bunch diagnostics is available to measure the transverse spatial profile of a relativistic electron beam, few exist for measuring the longitudinal profile. The most common technique is based on spectral measurements of the coherent millimetre-wave transition radiation [1], but such methods suffer from

inaccurate low frequency spectral content. We have demonstrated a new method, which is a non-destructive approach based on the electro-optic sampling of the electric field generated by the electron beam when it passes close to a non-linear crystal such as ZnTe. The electric field is probed via the Pockels effect by observing the polarisation rotation of a Ti:Sapphire laser beam passing through the crystal. Again, by using the rapid scanning technique, the longitudinal profile of the electric field of electron pulse was measured with sub-picosecond time resolution and without time reversal ambiguity. By changing the delay between Ti:Sapphire laser and the electron beam, we also detected the wake fields travelling together with the electron pulses. Wake fields are electric fields which are caused by the interaction of the electric field of the electron bunches with the geometry of the resistive wall of the accelerator beam pipe. In linear accelerators with a high electron bunch charge, characterisation and control of wake field effects are important in order to minimise energy spread and emittance growth. The knowledge about the accurate profile of the electron bunch itself and its wake field will contribute to further improvement of the FEL at FELIX.

8.2 Plans for future work

Dense, relativistic, sub-picosecond electron bunches are essential for the success of the advanced accelerators employed in new TeV linear electron-positron colliders for high energy physics, as well as the next generation of FEL based on self amplified spontaneous emission (SASE) within one bunch. Examples of such projects are, the TeV Super-conducting Linear Accelerator (TESLA) at DESY with its integrated SASE FEL [2], and the Next Linear Collider, or SASE-type Linac Coherent Light Source at SLAC [3]. The principles of SASE have been intensively studied theoretically, and tuneable X-ray lasers are being designed on the basis of SASE. Recently, the onset of SASE has been observed experimentally at longer infrared wavelengths, which is an important step forward, but progress is hindered because little experimental information is available on the detailed characteristics of the electron bunch length and shape.

Although we have demonstrated a non-intercepting approach based on the electro-optical detection, which can measure the electron bunch profile within one macropulse using the rapid scanning technique, it requires constant micropulses during the measurement [4]. However, it has been known that pulse-to-pulse variations of electron beam parameters contribute to unwanted fluctuations of the energy in the SASE-FEL photon radiation pulses. In order to study bunch to bunch fluctuations it is necessary to measure the length of individual electron bunches. The measurement of the individual electron bunch profile will allow the

investigation of the origin of the fluctuation of electron bunch profiles along the bunch train, their correlation with accelerator parameters, and will contribute to an improved performance of the FEL. After my experimental work was over, a precise single-shot measurement of the electron bunch profile was obtained by the FELIX team. The following parts of this chapter will briefly describe the method and some experimental results [5].

8.3 Single-shot electron bunch measurements

The new method is based on the solid ground of our previous electro-optical sampling technique to sense the Coulomb field travelling with the electron bunch using an electro-optical crystal [4]. Instead of using a synchronised ultra-short Ti:Sapphire laser pulse to scan the electron bunch profile rapidly in the time domain, the new method employs a chirped laser pulse to encode the longitudinal electron-bunch shape electro-optically on to its spectrum. The birefringence induced by the passing electron bunch is probed by monitoring the change of polarisation of the wavelength components of the chirped, synchronised Ti:Sapphire laser pulse. The electron-bunch length is determined by analysing individual laser-pulse spectra obtained with and without the presence of an electron bunch. Since the length of the chirped laser pulse can be easily changed, the electron bunch can be visualised on different time scales. This single-shot imaging technique is a promising method for real-time electron-bunch diagnostics.

Figure 8-1 shows the experimental setup used for the single-shot measurements of the relativistic electron pulses, which is produced by the rf linear accelerator at the FELIX FEL facility. The electron beam has energy of 46 MeV and its charge per bunch is around 200 pC. The repetition rate of micropulse is 25 MHz, while the macropulse is about 8 μs long and repeats at a rate of 1 KHz. The Ti:Sapphire laser amplifier producing 30 fs FWHM pulses at 800 nm with a repetition rate of 1 KHz is used as a probe beam. The 30 fs Ti:Sapphire laser pulses are chirped to up to 20 ps FWHM duration , using an optical stretcher which consists of a grating, a lens and a plane mirror. The electron bunch is measured at the same position as described in chapter 7. The incoming chirped laser is linearly polarised, the outgoing chirped laser is then split into two beams: a signal beam analysed by a second crossed polarizer and a reference beam used for monitoring possible fluctuation of the laser power. The spectra of the chirped laser pulses are dispersed with a grating spectrometer and then detected by a CCD camera equipped with a intensifier, which acts as a nanosecond shutter with a gating period of 100 ns. The electron pulse, Ti:Sapphire pulse and the gate of the CCD camera are all synchronised, therefore only one chirped laser pulse can be recorded at the CCD camera at a time (within one macropulse).

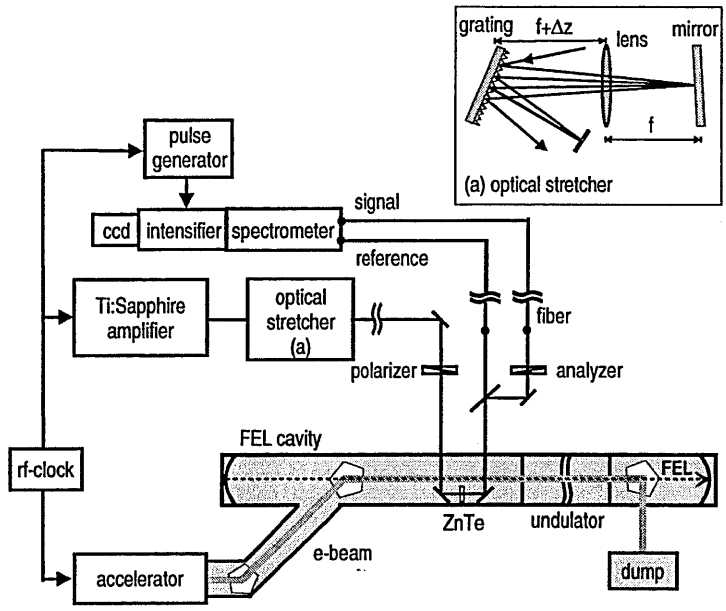

Figure 8-1. *Experimental set-up for electron bunch length measurements by electro-optic sampling with chirped optical pulses. The electron bunch length is measured by using a ZnTe crystal placed inside the vacuum pipe at the entrance of the undulator. The inset (a) exhibits a simplified two-dimensional schematic of the optical stretcher. The lens and flat mirror are mounted on a linear translation stage (not shown). The focal length f of the lens is 200 mm.*

8.4 Preliminary results

Figure 8-2 shows measurements of the chirped laser pulse spectra with and without a co-propagating electron bunch. The signal spectra are labelled by S and S', respectively. The strong change of the spectrum shown in S is attributed to the wavelength dependent change in polarisation of the chirped laser pulse due to the electric field of the electron bunch. The length and shape of the electron bunch is obtained by subtracting the spectrum without temporal overlap between and electron bunch and the chirped laser pulse. All signals have been corrected for the laser power fluctuation by using the reference spectra signal of the laser.

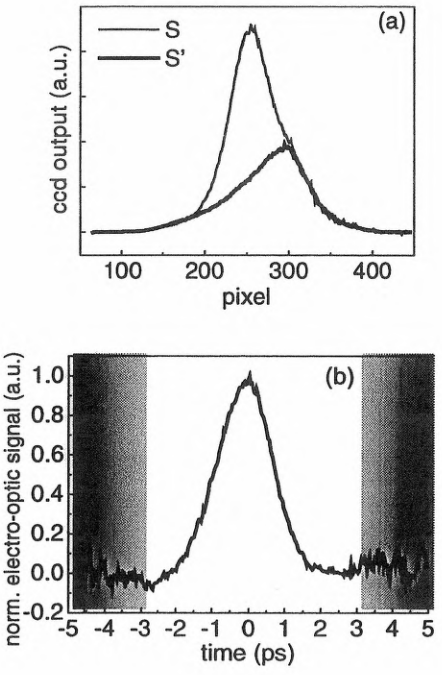

Figure 8-2 *Single-shot measurements of the electric field of individual electron bunch. (a) Raw data, single-shot chirped laser pulse spectra S and S'. The large peak (thin solid line) is detected when the electron bunch and the chirped laser pulse overlap in time. The bold solid line indicates the spectrum that is measured when the laser pulse is 50 ps earlier than the electron bunch. (b) Electron bunch length and shape obtained from the spectra as displayed in (a). The electron bunch width is (1.72±0.05) ps (FWHM). The leading edge of the electron bunch is to the right. The shaded areas indicate the regions of increased noise introduced by the subtraction of the spectra and corrections for laser power fluctuations and wavelength dependent variations in intensity of the spectrum.*

The temporal overlap between the electron bunch and the chirped laser pulse is controlled by an electronic delay. By shifting the synchronised chirped laser pulse with respect to the electron bunch in time, one can measure the electric field as well as its wake fields (see Figure 8-3). The time resolution of the single shot measurement is determined by the chirp and the bandwidth of the probing laser pulse, the distance between the electron beam and the probe beam at the electro-optical crystal, and the resolution of the spectrometer. By using a high resolution spectrometer and an ultra-short (5 fs) Ti:Sapphire laser, it is possible to achieve a time

resolution of 70 fs, which is mainly limited by the shortest distance (here is 1 mm in the experimental configuration) acceptable between the electron beam and the probing laser beam.

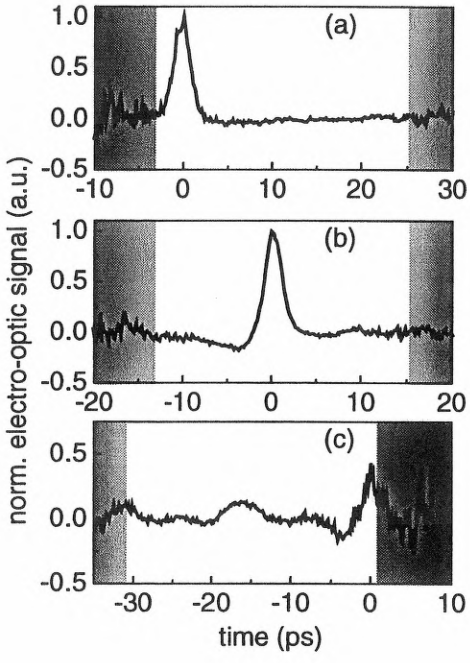

Figure 8-3 *Single-shot Wakefield measurements over several tens of picoseconds are performed by choosing a chirp of 18.65 ps FWHM and shifting the synchronised chirped laser pulse with respect to the electron bunch in time. Experimental conditions: (a) Measurements start with electron bunch visible in the time window at 0 ps. (b) The laser pulse has been shifted by 15 ps. Laser pulse and electron bunch now overlap in the centre of the time window. (c) Laser pulse shifted again by 15 ps. The signal following the electron bunch is attributed to wakefields excited by the electron bunch in the beam pipe.*

8.5 Reference:

[1] R. Lai, U. Happek, A.J. Sievers, *Phys. Rev. E* **50**, R4294 (1994).

[2] J. Andruszkow et al., Phys. Rev. Lett. **85**, 3825 (2000).

[3] E. L. Saldin, E. A. Schneidmiller, and M.V. Yurkov, Nucl. Instrum. Meth. Phys. Res., Sect. A **429**, 197 (1998).

[4] X. Yan et al., Phys. Rev. Lett. **85**, 3404 (2000).

[5] I. Wilke, A.M. MacLeod et al., Phys. Rev. Lett., **88**, 124801 (2001).

Appendix 1. FEL tables *

==========EXISTING==========

FELs	λ(μm)	σ_z	E(MeV)	I(A)	N	λ_0(cm)	K(rms)	Acc.,	Type & [Ref.]
ANL (APSFEL)	0.385	0.65ps	354	184	648	3.3	2.2	RF	S[40]
Beijing (IHEP)	10	4ps	30	14	50	3	1	RF	O[14]
BNL (ATF)	0.5	6ps	50	100	70	0.88	0.4	RF	O[24]
BNL (HGHG)	5.3	6ps	40	120	60	3.3	1.44	RF	A[16]
Bruyeres (ELSA)	20	30ps	18	100	30	3	0.8	RF	O[7]
Darmstadt (IR-FEL)	6~8	2ps	25~50	2.7	80	3.2	1	RF	O[15]
Dartmouth (FEL)	200	CW	0.04	0.001	50	300	-	SP	O[2]
DESY (TTF1)	0.109	0.5ps	233	300	492	2.73	1.17	RF	S[42]
Dortmund (FELICITAI)	0.47	50ps	450	90	17	25	2	SR	O[25]
Duke (MarkIII)	3	3ps	44	20	47	2.3	1	RF	O[19]
Duke (OK-4)	0.1947	1.6ps	800	35	2x33	10	0~4	SR	O[30]
Himeji (LEENA)	65~75	10ps	5.4	10	50	1.6	0.5	RF	O[3]
Italy (ELETTRA)	0.2~0.4	28ps	1000	150	2x19	10	4.2	SR	O[38]
Korea (KAERI-FEL)	97~150	25ps	6.5	0.5	80	2.5	1.6	RF	O[47]
LANL (RAFEL)	15.5	15ps	17	300	200	2	0.9	RF	O[10]
Maryland (MIRFEL)	12~21	5ps	9~14	100	73	1.4	0.2	RF	O[13]
Nieuwegein (FELIX)	4~200	1ps	50	50	38	6.5	1.8	RF	O[18]

* Reference location: http://www.physics.nps.navy.mil/table1.pdf and http://sbfel3.ucsb.edu/www/fel_table.html.

FELs	λ(μm)	σ_z	E(MeV)	I(A)	N	λ_0(cm)	K(rms)	Acc.,	Type & [Ref.]
Okazaki (UVSOR)	0.24	6ps	607	10	2x9	11	2	SR	O[28]
Orsay (CLIO)	3~53	0.1~3ps	21~50	80	38	5	1.4	RF	O[22]
Orsay (Super-ACO)	0.3~0.6	15ps	800	0.1	2x10	13	4.5	SR	O[26]
Osaka (FELI1)	5.5	10ps	33.2	42	58	3.4	1	RF	O[17]
Osaka (FELI2)	1.88	10ps	68	42	78	3.8	1	RF	O[17]
Osaka (FELI3)	0.3~0.7	5ps	155	60	67	4	1.4	RF	O[27]
Osaka (FELI4)	18~40	10ps	33	40	30	8	1.3~1.7	RF	O[8]
Osaka (ILE/ILT)	47	3ps	8	50	50	2	0.5	RF	O[4]
Osaka (ISIR)	40	30ps	17	50	32	6	1	RF	O[5]
Stanford (FIREFLY)	15~65	1~5ps	15~32	14	25	6	1	RF	O[11]
Stanford (SCAFEL)	3~13	0.5~12ps	22~45	10	72	3.1	0.8	RF	O[21]
TJNAF (FEL)	1~6	0.4ps	48	60	41	2.7	0.9	RF	O[20]
Tokai (JAERI-FEL)	22	5ps	16.5	100	52	3.3	0.7	RF	O[6]
Tokyo(FEL-SUT)	5~16	2.5ps	32	0.2	40	3.2	0.7~2.5	RF	O[48]
Tsukuba(NIJI-IV)	0.2~0.6	160ps	310	5	2x42	7.2	2	SR	O[29]
UCLA-Kurchatov	16	3ps	13.5	80	40	1.5	1	RF	A[9]
UCLA-Kurchatov-LANL	12	5ps	18	170	100	2	0.7	RF	A[12]
UCSB(FIR FEL)	60	25μs	6	2	150	2	0.1	EA	O[1]
UCSB(mm FEL)	340	25μs	6	2	42	7.1	0.7	EA	O[1]
Vanderbilt(FELI)	2.0~9.8	0.7ps	43	50	52	2.3	1	RF	O[23]

==========PROPOSED==========

FELs	λ(μm)	σ_z	E(MeV)	I(A)	N	λ_0(cm)	K(rms)	Acc.,	Type & [Ref.]
ANL(APSFEL)	0.12	1ps	440	150	864	3.3	3.1	RF	S[40]
BNL(DUVFEL)	0.1	6ps	230	1000	256	2.89	1.2	RF	A[39]
DESY(TESLA)	0.0001	0.08ps	35000	5000	1200	5	4.2	RF	S[46]
DESY(TTF2)	0.006	0.17ps	1000	2500	981	2.73	0.9	RF	S[44]
Duke(VUV)	0.01~1	1ps	1000	50	4x32	12	3	SR	O[43]
Florida(CREOL)	355	8μs	1.3	0.13	185	0.8	0.1	EA	O[31]
Frascati(COSA)	0.08	10ps	215	200	400	1.4	1	RF	O[41]
Harima(SUBARU)	0.2~10	26ps	1500	50	33,65	16,32	8	SR	O[37]
Moscow(Lebedev)	100	20ps	30	0.25	35	3.2	0.8	MA	O[34]
Netherlands(TEUFEL)	180	20ps	6	350	50	2.5	1	RF	O[32]
Novosibirsk(RTM)	2~11	20ps	98	100	4x36	9	1.6	RF	O[35]
Rocketdyne/Hawaii(FEL)	0.3~3	2ps	100	500	84	2.4	1.2	RF	O[36]
Rutgers(IRFEL)	140	25ps	38	1.4	50	20	1	MA	O[33]
SLAC(LCLS)	0.00015	0.07ps	14350	3400	3328	3	3.7	RF	S[45]
TJNAF(UVFEL)	0.16~1	0.2ps	160	270	72	3.3	1.3	RF	O[20]

RF	RF Linac Acceleration	**O**	FEL Oscillator
SR	Electron Storage Ring	**S**	SASE FEL
SP	Smith-Purcell Oscillator	**A**	FEL Amplifier
MA	Microtron Accelerator		
EA	Electrostatic Accelerator		

▪ References

[1] G. Ramian, Nucl. Inst. and Meth. **A318**, 225-229 (1992).

[2] J. Urata et. al., Physical Review Letters **80**, 516-519 (1998).

[3] T. Mochizuki et. al., Nucl. Inst. and Meth. **A393**, II-47 (1997); S. Miyamoto and T. Mochizuki, J. Japan Society of Infrared Science and Technology, 7, 73-78 (1997).

[4] N. Ohigashi et. al., Nucl. Inst. and Meth. **A375**, 469 (1996).

[5] S. Okuda et. al., Nucl. Inst. and Meth. **A341**, 59 (1994).

[6] N. Nishimori et. al., Nucl. Inst. and Meth. **A445**, 432-436 (2000).

[7] P. Guimbal et. al., Nucl. Inst. and Meth. **A341**, 43 (1994).

[8] T. Takii et. al., Nucl. Inst. and Meth. **A407**, 21-25 (1998).

[9] M. Hogan et. al., Physical Review Letters **80**, 289 (1998).

[10] D. C. Nguyen et. al., Nucl. Inst. and Meth. **A429**, 125-130 (1999).

[11] K. W. Berryman and T. I. Smith, Nucl. Inst. and Meth. **A375**, 6 (1996).

[12] M. Hogan et. al., Physical Review Letters, **81**, 4867 (1998).

[13] I. S. Lehrman et. al., Nucl. Inst. and Meth. **A393**, 178 (1997).

[14] J. Xie et. al., Nucl. Inst. and Meth. **A341**, 34 (1994).

[15] J. Auerhammer et. al., Nucl. Inst. and Meth. **A341**, 63 (1994).

[16] I. Ben-Zvi et. al., Nucl. Inst. and Meth. **A318**, 208 (1992).

[17] A. Kobayashi, et. al., Nucl. Inst. and Meth. **A375**, 317, (1996).

[18] D. Oepts et. al., Infrared Phys. Technol. **36**, 297 (1995).

[19] S.V. Benson et. al., Nucl. Inst. and Meth. **A250**, 39 (1986).

[20] S. Benson et. al., Nucl. Inst. and Meth. **A429**, 27-32 (1999).

[21] H. A. Schwettman et. al., Nucl. Inst. and Meth. **A375**, 662 (1996).

[22] J. M. Ortega et. al., Nucl. Inst. and Meth. **A375**, 618 (1996).

[23] C. Brau, Nucl. Inst. and Meth. **A318**, 38 (1992).

[24] K. Batchelor et. al., Nucl. Inst. and Meth. **A318**, 159 (1992).

[25] D. Nolle et. al., Nucl. Inst. and Meth. **A341**, ABS7 (1994); Schmidt et. al., Nucl. Inst. and Meth. **A341**, ABS9 (1994).

[26] M. E. Couprie et. al., Nucl. Inst. and Meth. **A407**, 215-220 (1998).

[27] T. Tomimasu et. al., Nucl. Inst. and Meth. **A393**, 188-192 (1997).

[28] H. Hama et. al., Nucl. Inst. and Meth. **A341**, 12 (1994).

[29] T. Yamazaki et. al., Nucl. Inst. and Meth. **A341**, ABS3 (1994).

[30] V. N. Litvinenko et. al., Nucl. Inst. and Meth. **A407**, 8-15 (1998).

[31] M. Tecimer et. al., Nucl. Inst. and Meth. **A341**, A126 (1994).

[32] J. I. M. Botman et. al., Nucl. Inst. and Meth. **A341**, 402 (1994).

[33] E. D. Shaw et. al., Nucl. Inst. and Meth. **A318**, 47 (1992).

[34] K. A. Belovintsev et. al., Nucl. Inst. and Meth. **A341**, ABS45 (1994).

[35] N. G. Gavrilov et. al., Status of Novosibirsk High Power FEL Project, SPIE Proceedings, vol. 2988, 23 (1997); N. A. Vinokurov et. al., Nucl. Inst. and Meth. **A331**, 3 (1993).

[36] R. J. Burke et al, Proc. SPIE: Laser Power Beaming, Los Angeles, Jan. 27-28, 1994, Vol 2121.

[37] S. Miyamoto et. al., Report of the Spring-8 International Workshop on 30 m Long Straight Sections, Kobe, Japan (August 9, 1997).

[38] R. P. Walker et. al., Nucl. Inst. and Meth. **A429**, 179-184 (1999); Twenty-Second International Free Electron Laser Conference, Duke University, Durham, NC.

[39] E. D. Johnson, Nucl. Inst. and Meth. **A393**, II-12 (1997).

[40] S. V. Milton et. al., Nucl. Inst. and Meth. **A407**, 210-214 (1998); Twenty-Second International Free Electron Laser Conference, Duke University, Durham, NC.

[41] F. Ciocci et. al., A. Torre, IEEE J.Q.E. **31**, 1242 (1995).

[42] W. Brefeld et. al., Nucl. Inst. and Meth. **A393**, 119 (1997).

Appendix 2. Complete list of publications

Appendix 2 contains details of all my publications and conference contributions that are associated with the work described in this thesis. The four most fundamental publications are marked with an asterisk and are reprinted in full.

✧ List of publications

1. W.A. Gillespie, A.M. MacLeod, X. Yan, G.M.H. Knippels, A.F.G. van der Meer, C.W. Rella. **Electron and optical pulse shape measurements on a far-infrared free-electron laser using differential optical gating.** *Proceedings of CLEO/Europe-EQEC'98, Glasgow, Scotland, United Kingdom, 13-18th September 1998.*

2. X. Yan, A.M. MacLeod, W.A. Gillespie, G.M.H. Knippels, et al. **FEL pulse shape measurements with 100-fs temporal resolution using a 10-fs Ti:Sapphire laser and differential optical gating.** *Proceedings of 20th Int. FEL Conf., Williamsburg, VA, USA 16-21th August 1998." Nucl. Instrum. & Methods A429, II-97 (1999).*

3. A.M. MacLeod, W.A. Gillespie, X. Yan, G. M. H. Knippels. **Measurement of optical and electron beam pulse profiles in a free-electron laser .** *Proceedings of Northern Vacuum Electronics Conference, CLRC Daresbury, Darsbury, March 1998.*

4. * G.M.H. Knippels, X. Yan, A.M. MacLeod, W.A. Gillespie, M. Yasumoto, D. Oepts, A.F.G. van der Meer. **Generation and complete electric-field characterization of intense ultra-short tunable far-infrared laser pulses.** *Phys. Rev. Lett. 83, 1578-1581 (1999).*

5. D. Oepts, G.M.H. Knippels, X. Yan, A.M. MacLeod, W.A. Gillespie, A.F.G. van der Meer. **Picosecond electron-bunch length measurements using an electro-optic sensor.** *Proceedings of 21th Int. FEL Conf., Hamburg, Germany 23-28th August 1999. Nucl. Instrum. & Methods A416 (1999).*

6. G.M.H. Knippels, D. Oepts, A.F.G. van der Meer, X. Yan, A.M. MacLeod, W.A. Gillespie. **Optical pulse characterization in the infrared.** *Proceedings of 21th Int. FEL Conf., Hamburg, Germany 23-28th August 1999. Nucl. Instrum. & Methods A416 (1999).*

7. * A.M. MacLeod, X. Yan, W.A. Gillespie, G.M.H. Knippels, D. Oepts, A.F.G. van der Meer, C.W. Rella, T.I. Smith, H.A. Schwettman. **Formation of low time-bandwidth product, single-sided exponential optical pulses in free-electron laser oscillators.** *Phys. Rev. E 62, 4216-4220 (2000).*

8. * X. Yan, A.M. MacLeod, W.A. Gillespie, G.M.H. Knippels, D. Oepts, A.F.G. van der Meer, W. Seidel. **Sub-picosecond electro-optic measurement of relativistic electron pulses.** *Phys. Rev. Lett. 85, 3404-3407 (2000).*

9. * X. Yan, A.M. MacLeod, W.A. Gillespie, G.M.H. Knippels, D. Oepts, A.F.G. van der Meer. **Application of electro-optic sampling in FEL diagnostics.** *Proceedings of 22nd Int. FEL Conf., Durham, U.S.A. 13-18 August 2000. Nucl. Instrum. & Methods A475 (2001) pp. 504-508.*

10. X. Yan, G.M.H. Knippels, D. Oepts. **Unexpected angular dependence in ZnTe electro-optic sampling.***Proceedings of CLEO/IQEC Europe 2000, September 10-15, Nice, France.*

11. X. Yan, A.M. MacLeod, W.A. Gillespie, G.M.H. Knippels, et al. **FEL pulse shape measurements with 100-fs temporal resolution using a 10-fs Ti:sapphire laser and differential optical gating.** *Proceedings of Najaarsvergadering van de sectie Atoomfysica en Quantumelektronica, De Blije Werelt, Lunteren, The Netherlands, 5-6th November 1998.*

12. X. Yan, G.M.H. Knippels, D. Oepts. **Unexpected angular dependence in ZnTe electro-optic sampling.** *Proceedings of Najaarsvergadering van de sectie Atoomfysica en Quantum electronica, De Blije Werelt, Lunteren, The Netherlands, November 16-17th, 2000.*

✧ Oral contributions

1. G.M.H. Knippels, A.F.G. van der Meer, M.J. van de Pol, X. Yan, A.M. MacLeod, W.A. Gillespie, C.W. Rella. **FEL pulse shape measurements with 100-fs temporal resolution using a 10-fs Ti:sapphire laser and differential optical gating.** *Oral contribution on the 19th of August at the 20th International Free-Electron Laser Conference, 16-21th august 1998, Williamsburg, VA, USA*

2. G.M.H. Knippels, D. Oepts, A.F.G. van der Meer, X. Yan, A.M. MacLeod, W.A. Gillespie. **Optical pulse characterization in the infrared.** *Oral contribution contribution on the 27th of August at the 21th International Free-Electron Laser Conference, 23-28th august 1999, Hamburg, Germany.*

3. G.M.H. Knippels, M.J. van de Pol, T. Ram, D. Oepts, A.F.G. van der Meer, X. Yan, A.M. MacLeod, W.A. Gillespie. **Synchronization of external lasers to FELIX.** *Invited oral contribution at the Workshop on Research with IR radiation, August 30-31th 1999, Rossendorf, Germany.*

4. X.Yan, A.M. MacLeod, W.A. Gillespie, G.M.H. Knippels, D. Oepts, A.F.G. van der Meer. **Generation and characterization of intense ultrashort tunable far-infrared (30-250 μm) laser pulses.** *Oral contribution at the CLEO/QELS 2000, San Francisco, USA, May 7-12th 2000. Oral contribution at the CLEO/IQEC Europe 2000, September 10-15, Nice, France*

5. G.M.H. Knippels, D. Oepts, A.F.G. van der Meer, X. Yan, A.M. MacLeod, W.A. Gillespie. **FELIX: a versatile source for non-linear time-resolved experiments.** *Invited oral contribution at the far-infrared coherent radiation workshop, 5-6th Nov. 2000, DESY, Hamburg, Germany*

6. X. Yan, G.M.H. Knippels, D. Oepts. **Unexpected angular dependence in ZnTe electro-optic sampling.** *Invited oral contribution at the Najaarsvergadering van de sectie Atoomfysica en Quantum electronica, De Blije Werelt, Lunteren, The Netherlands, November 16-17th, 2000*

The four published articles cited below have been removed from the e-thesis due to copyright restrictions:

G.M.H. Knippels, X. Yan, A.M. MacLeod, W.A. Gillespie, M. Yasumoto, D. Oepts, A.F.G. van der Meer. Generation and complete electric-field characterization of intense ultra-short tunable far-infrared laser pulses. Phys. Rev. Lett. 83, 1578-1581 (1999).

A.M. MacLeod, X. Yan, W.A. Gillespie, G.M.H. Knippels, D. Oepts, A.F.G. van der Meer, C.W. Rella, T.I. Smith, H.A. Schwettman. Formation of low time-bandwidth product, single-sided exponential optical pulses in free-electron laser oscillators. Phys. Rev. E 62, 4216-4220 (2000).

X. Yan, A.M. MacLeod, W.A. Gillespie, G.M.H. Knippels, D. Oepts, A.F.G. van der Meer, W. Seidel. Sub-picosecond electro-optic measurement of relativistic electron pulses. Phys. Rev. Lett. 85, 3404-3407 (2000).

X. Yan, A.M. MacLeod, W.A. Gillespie, G.M.H. Knippels, D. Oepts, A.F.G. van der Meer. Application of electro-optic sampling in FEL diagnostics. Proceedings of 22nd Int. FEL Conf, Durham, U.S.A. 13 -18 August 2000. Nucl. Instrum. & Methods A 475 (2001), 504-508.